DOCTORAL DISSERTATION SERIES

Publication No.: 8412

AUTHOR: Richard Erick Slattery, Ph. D., 1954

University of Michigan

TITLE: DESIGN AND CONSTRUCTION OF A THIN LENS COINCIDENCE SPECTROMETER WITH APPLICATIONS TO THE DECAY OF Eu^{152} AND Eu^{154}

University Microfilms, Ann Arbor, Michigan

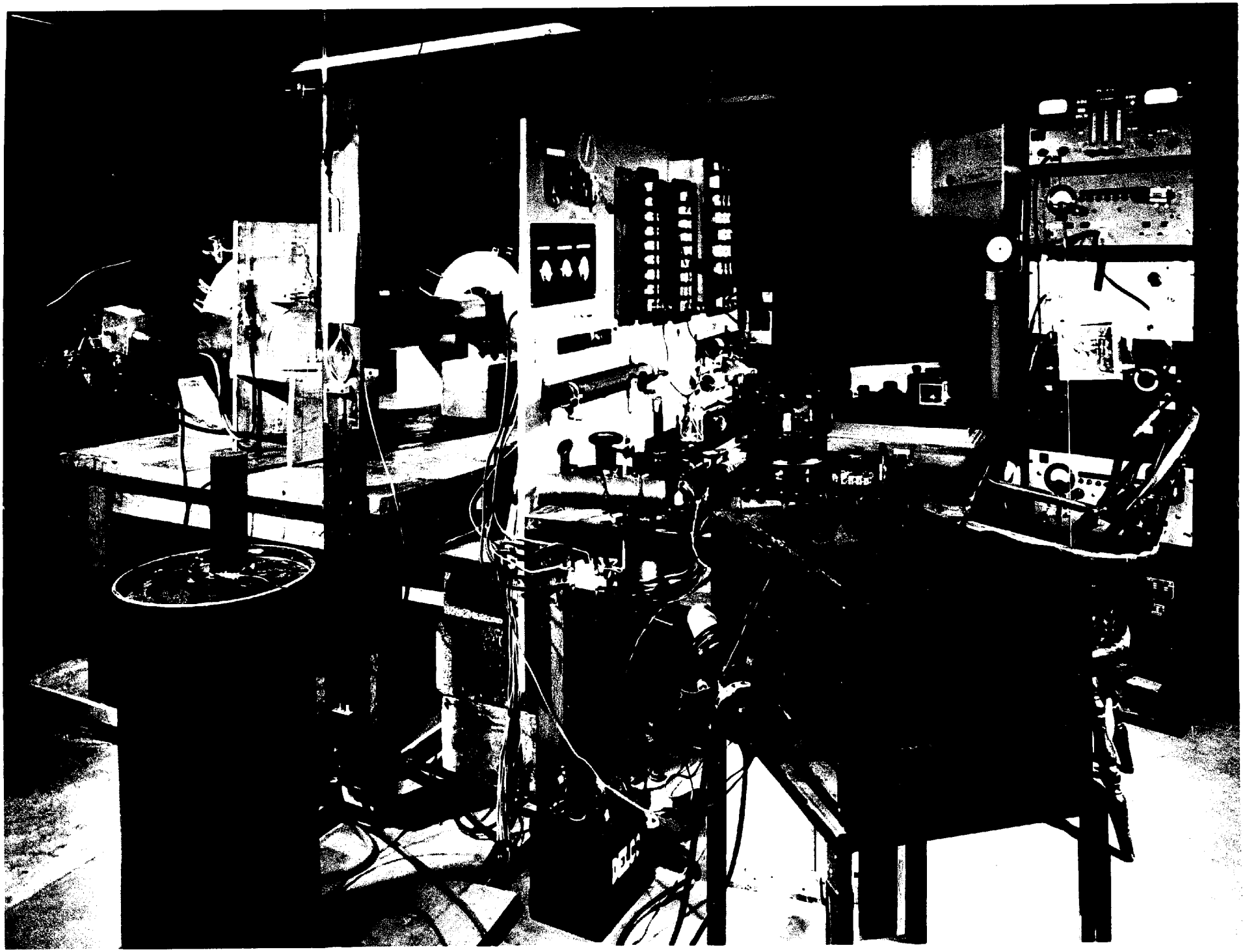
DESIGN AND CONSTRUCTION OF A THIN LENS COINCIDENCE SPECTROMETER WITH APPLICATIONS TO THE DECAY OF Eu^{152} AND Eu^{154}

by
Richard Erick Slattery

A dissertation submitted in partial fulfillment
of the requirements for the degree of
Doctor of Philosophy in the
University of Michigan
1954

Committee in charge:

Associate Professor Marcellus L. Wiedenbeck, Chairman
Professor Ruel V. Churchill
Professor James M. Cork
Professor Otto Laporte
Professor George E. Uhlenbeck



DESIGN AND CONSTRUCTION OF A THIN LENS COINCIDENCE SPECTROMETER WITH APPLICATIONS TO THE DECAY OF Eu^{152} AND Eu^{154}

By Richard Erick Slattery

A coincidence arrangement between two thin lens beta spectrometers has been designed and constructed. The spectrometers are mounted at 180° with respect to each other on a common tube. The indivdual halves of the instrument are of conventional design, utilize ring focusing, and are capable of resolutions of about two percent. Coupling between coils when both are carrying current is less than one percent, and is easily compensated. The coincidence spectrometer is mounted north-south to reduce effects due to the horizontal component of the earth's field. The vertical component is cancelled by means of large Helmholtz type coils. Geiger tube detectors were used, and coincidences were measured by means of both Rossi and Garwin circuits on different occasions, with resolving times of 0.38 and 0.28 microseconds respectively.

A characteristic of this instrument is the narrowing of conversion lines (i.e., improved resolution) when coincidence spectra are plotted. The cause of this narrowing is discussed, with examples drawn from the decay of Hf^{181}.

Using the component thin lens spectrometers, normal beta spectra and conversion coefficients can be measured. By means of the coincidence arrangement, coincidences between conversion lines and between conversion lines and beta spectra can also be determined. It is demonstrated how the conversion coefficients of obscured peaks can be established. The advantages and disadvantages of the coincidence spectrometer are discussed.

The radioactivity of $Eu^{152,154}$ was examined by means of this instrument. The beta spectrum was complex, consisting of components with end-points at 1.45 ± 0.09 Mev, 0.70 ± 0.03 Mev, and 0.33 ± 0.10 Mev. The last mentioned end-point is doubtful due to the presence of conversion lines with accompanying scattering. Coincidences were noted between the conversion lines due to the 122 or 123 (unresolved) and 244 kev transitions. No coincidences were noted between the 122 and 123 kev conversion lines, the 344 and 244 kev conversion lines, or between the 122 or 123 and 344 kev conversion lines. Coincidences were noted between the 344 kev transition and the beta spectrum with 0.70 Mev end-point. The coincidence beta spectrum was plotted. No other coincidences between conversion lines and beta spectra were found.

This information, combined with other data from a crystal summing spectrometer allowed the decay schemes of Eu^{152} and Eu^{154} to be established.

To
L. J. S.
and
H. M. W.

ACKNOWLEDGEMENT

The author wishes to express his grateful recognition of the aid and guidance given to him throughout the course of this work by Professor Marcellus L. Wiedenbeck.

Professors J. M. Cork and W. W. Meinke were helpful and generous in the procuring of sources. The spectrometer proper was constructed by Mr. A. Buchholz of the Physics Instrument Shop, under the direction of its foreman, M. H. Roemer.

The crystal summing data on $Eu^{152,154}$ were taken by Mr. D. C. Lu and is used with his permission. To Mr. Lu is extended the author's recognition of many helpful discussions.

The author's wife and mother were a constant source of encouragement throughout the vicissitudes of this work, and his wife, Nancy Raisbeck Slattery, aided in the preparation of the manuscript.

TABLE OF CONTENTS

Chapter		Page
I.	INTRODUCTION	1
	Historical Review	1
	Beta Decay	4
	Kurie Plots of Allowed and Forbidden Shapes	6
	Isomerism, Gamma Emission and Internal Conversion	8
	Experimental Methods Now in Use	13
	Statement of the Present Research	17
II.	CONSTRUCTION OF THE SPECTROMETER	19
	The Spectrometer Tube	19
	Source and Source Holder	22
	Baffles	22
	Focusing Coils	24
	Coil Power Supply	27
	Corrections for Earth's Magnetic Field	29
	Vacuum Equipment	29
	Detectors	30
III.	THE ELECTRONICS	32
	Introduction	32
	First Electronics System	34
	Second Electronics System	38
IV.	PROPERTIES AND CALIBRATION OF THE THIN LENS SPECTROMETER	44
	Ring Focus	44
	Alignment and Resolution	47
	Calibration of the Beta Spectrometers	51
	Correction Factors	53
V.	THE THIN LENS COINCIDENCE SPECTROMETER	59
	Coupling	59
	Coincidence Resolution	59
	Coincidence Data and Corrections	67
	Limitations of the Thin Lens Coincidence Spectrometer	68
	Uses	70
VI.	THE DECAY OF Eu^{152} AND Eu^{154}	72
	Source Preparation	73
	Beta Spectrum	77
	Coincidences between the Beta Spectrum and the Conversion Lines	78
	Coincidences between Conversion Peaks	80

Chapter Page

The Gamma-Gamma Coincidences 83
Isotopic Assignments 87
Decay Scheme of Eu^{152} 88
Decay Scheme of Eu^{154} 88
Results 91

BIBLIOGRAPHY 92

LIST OF ILLUSTRATIONS

Figure — Page

FRONTISPIECE

1.1 A Hypothetical Level Scheme 9

2.1 Sketch of the Thin Lens Coincidence Spectrometer 20

2.2 Source Holder 21

2.3 Schematic Drawing of Baffle Arrangement 23

2.4 Detail of Coil Tilting Mechanism 25

2.5 Assembly Detail of Focusing Coil 26

2.6 Current Supply to Focusing Coils 28

2.7 Sketch of Geiger Tube 31

3.1 First Electronic System 35

3.2 Rossi Circuit 37

3.3 Modified Al Output 39

3.4 Garwin Circuit 41

3.5 Second Electronic System 42

4.1 Effect of Baffle Spacing On Resolution 49

4.2 Momentum Spectrum of Cs^{137} 54

4.3 Kurie Plot for Cs^{137} 55

5.1 Beta Spectrum of Hf^{181} 61

5.2 K, K Coincidence Peaks 62

5.3 K, L Coincidence Peaks 63

5.4 Influence of Source Size on Resolution 65

6.1 Conversion Lines of $Eu^{152,154}$ 74

6.2 Conversion Lines of $Eu^{152,154}$ 75

6.3 Beta Spectrum of $Eu^{152,154}$ 76

6.4 Kurie Plot for $Eu^{152,154}$ 79

6.5 Coincidence Momentum Spectrum, $Eu^{152,154}$ 81

Figure Page

6.6 Kurie Plot of Coincidence Beta Spectrum..... 82

6.7 Crystal Summing Data for $Eu^{152,154}$ 86

6.8 Decay Scheme of Eu^{152} 89

6.9 Decay Scheme of Eu^{154} 90

LIST OF TABLES

Table		Page
I.	Selection Rules for Beta Decay	7
II.	Selection Rules for Radiative Transition	10
III.	Calibration Constants of the Thin Lens Spectrometers	53
IV.	Half-Life Measurements for Eu^{152} and Eu^{154}	72

CHAPTER I

INTRODUCTION

The history of beta decay and nuclear isomerism is nearly as old as that of nuclear physics itself. The discovery of radioactivity was announced in 1896 (1), and shortly thereafter, the resolution of the radiation into two components termed alpha and beta was accomplished (2) (3). This separation was done by deflecting the beta type particles in a magnetic field. Using stronger fields, Rutherford (4) was able to accomplish the final resolution of the radiation from natural sources into its basic components, which he designated alpha, beta, and gamma. These names are still in use.

The so-called alpha radiation consists of helium nuclei with discrete kinetic energies. Its history and properties form a study unto themselves and shall not concern us further; rather let us examine the beta and gamma components which are the objects of this research.

Historical Review

The beta particles were very early identified as electrons by a whole series of workers, while the gamma radiations were found to be electro-magnetic in character. The beta emission process was not clearly understood at first, and as time progressed, considerable difficulty was encountered in explaining the continuous energy spectrum which they exhibited. In fact in 1924, Bohr and several others (5) suggested the possibility of abandoning the conservation of energy for the process of beta decay. The classical work of Ellis and Wooster (6) seemed to show that if beta decay were considered a two body problem, the measured energy was not conserved. Similar anomalies existed for angular momentum and statis-

tics. A way around this paramount difficulty was suggested by Pauli (7), who postulated the existence of an almost massless body called the neutrino, which carried away a portion of the energy and angular momentum. A particle of this nature would be almost impossible to detect, but a whole generation of investigators (8) (9) (10) have accumulated an impressive body of evidence for its existence; however, no clear cut proof yet exists. In 1934, Fermi (11), assuming the existence of a massless neutrino, developed a theory of beta decay, which, in its improved form, the accumulation of evidence seems to sustain. At present, this theory has reached a degree of perfection sufficient to explain almost all aspects of the beta decay.

Complementary to the beta decay is the emission of the positron. Positrons are positively charged electrons (12), emitted by nuclei in a continuous energy spectrum. They were first discovered in cosmic rays (13), though a theory existed, unrecognized, which predicted their existence (14). Not long after their discovery, positrons were found to be emitted by many of the low A artificial isotopes.

The result of positron emission is the change of a nucleus from $_{z}N^{A}$ to $_{z-1}N^{A}$. In 1936, Yukawa and Sakata (15) pointed out that a competing process might exist in the nuclear absorption of an orbital electron. This is called the K-capture, since the probability of occurrence is greatest for an electron in the K shell. Alvarez (16) discovered this effect experimentally by detecting the K X-rays from Ti^{49} following the K-capture in Va^{49}.

So far we have discussed the transmutation of a nucleus by means of electron emission or related effects, without regard to the final state of the nucleus. It is very common, indeed, for the product nucleus to be in an excited state. By this is meant a nucleus possessing an energy

above that of its ground state. Such a nucleus is called isomeric and will reach its ground state by the emission of a photon (gamma ray), or several photons (cascading through a series of progressively lower excited states).

Nuclear isomerism is characterized by the existence of nuclei identical in mass and charge, but differing from each other in energy and possibly spin and parity. Their existence was predicted by Soddy (17) as early as 1917 and first found in Pa^{234} by Hahn (18). For many years this stood alone as an example of isomerism, but just before World War II, the isomerism of Br^{80} (preceding, not following a beta decay) was found (19) (20). The post war period in this field has been characterized by the discovery and tabulation of hundreds of cases of nuclear isomerism.

The isomeric decay has been characterized by photon emission in the preceding paragraph. There is, in some cases, a competing process called internal conversion. This is the ejection of an orbital electron of discrete energy equal to the difference of the available gamma energy and the orbital binding energy. Such phenomena were predicted by Rutherford at an early date (21) and found several years later by Ellis (22). In the study of beta decay, these discrete energy electrons often appear superimposed upon the continuous beta spectrum, and, indeed, confused earlier workers in this field (23).

The above historical resumé has shown that, to our present knowledge, a nucleus of charge Z may transmute to a nucleus of charge $Z \pm 1$ by means of positron or electron emission or by K-capture. Quite often the product nucleus is left in an excited energy state, from which it descends to its ground level by photon (gamma ray) emission or by internal conversion.

In the following sections, a few of the details of these processes and the methods used to measure them will be discussed.

Beta Decay

The following types of interaction,

$$p \longrightarrow n + e^+ + \nu$$

$$n \longrightarrow p + e^- + \nu$$

$$p + e^- \longrightarrow n + \nu$$

$$(n + e^+ \longrightarrow p + \nu)$$

between fermions (particles of spin 1/2) are usually considered together in the theory of beta decay and represent successively electron emission, positron emission, K-capture (i.e. orbital electron absorption), and positron capture. The last interaction is hypothetical, but is included for symmetry.

Interactions of this type constitute a rearranging of the nucleus in order to reach a state of lower energy. The presence of a neutrino, ν, must be postulated (7) in order to conserve energy, angular momentum, and statistics for the processes. It might be pointed out here that the competition between positron emission and orbital capture occurs only when the transition energy is greater than two electron masses. Below this value, positron emission can not occur, and capture is the only possible mode of decay available to the proton rich nucleus.

The beta decay transition may be expressed as

$$d\lambda = \frac{2\pi}{\hbar} \left| H_{if} \right|^2 d\rho_F \qquad (1.1)$$

where $d\lambda$ is the number of transitions per second, H_{if} is the nuclear matrix element, and $d\rho_F$ is the density of final states available to the electron and neutrino system between the energies W and W + dW. Since the probability of transition to a volume of phase space is proportional to the volume, one may express

$$d\rho_F = \frac{p_c^2 \, dp_e \, d\omega_e \, p_\nu^2 \, dp_\nu \, d\omega_\nu}{(2\pi\hbar)^6} \qquad (1.2)$$

in units of $h = 2\pi\hbar$, where P_e is the electron momentum corresponding to an energy W, and P_ν is a neutrino momentum corresponding to an energy $cP_\nu = W_o - W = W_\nu$. If we assume that the neutrino has zero rest mass and that $W_o = W + W_\nu$, where W_o is total energy, when we integrate over $d\omega_e d\omega_\nu$,

$$d\rho_F = \frac{p_e^2 (W_o - W)^2 dp_e}{4\pi^4 \hbar^6 c^3} \qquad (1.3)$$

This is sometimes called the "statistical factor". The term (1.3) in (1.1) will dominate the gross shape of the spectrum.

The term H_{if} in Equation (1) is dependent upon the wave functions of the electron, neutrino, proton, and neutron in a complicated fashion. A complete derivation would be out of place here, but, in general, two considerations determine the exact form of H_{if}. These are the variations of the neutrino and electron wave functions across the nucleus and the correction for relativistic effects.

The former is resolved by expanding the essentially plane wave functions for the electron and the neutrino. This leads to a series of terms in the probability of transition differing from each other by $(R/\lambda\!\!\!^{-})^2 \approx (1/137)^2$, where R is of the order of the nuclear radius, and $\lambda\!\!\!^{-}$ the wave length of the electron or neutrino. The leading term corresponds to the probability of an allowed transition, while successive terms represent the varying degrees of forbiddenness of the emission. Due to the rapid convergence of successive terms in this expansion, forbidden terms come into play only when the selection rules for transition from initial to final state preclude occurrence of the more allowed ones.

Fermi chose to express the electron and neutrino wave functions as a bilinear combination of the four Dirac components. When the condition of relativistic invariance is imposed upon that of bilinear combination, certain ambiguities result. Five permissable bilinear combinations are

possible with no a priori choice between them. These are: 1) the scalar, 2) polar vector, 3) tensor, 4) axial vector, and 5) pseudoscalar. According to the theory, any one or combination of these interactions may occur; the choice of correct terms is to be made experimentally. In certain cases of forbidden decay, the shape of the spectrum and information concerning selection rules force particular combinations of SVTAP to be dropped. A thorough examination of evidence available to this date leads Konopinski and his co-workers (24) to the conclusion that an STP combination is the correct one. It is perhaps a little too early to say with certainty.

The final form of Equation (1) with $|H_{if}|^2$ correctly substituted according to the Fermi theory covers the cases of electron and positron decay. The qualitative effect of nuclear charge is to repel positrons and attract electrons, so that the lower energy end of a positron spectrum is shifted to higher energies and vice versa. (In fact, most of the contribution to the positron spectrum near $W = 0$ is due to barrier penetration.) The case of orbital capture is very similar, the major difference being in the statistical factor. (The electrons are monoenergetic in this case.)

Table I shows the selection rules for the various type interactions through second forbidden. The forbiddenness is not strictly according to powers of r (the plane wave expansion) here since certain of the operators resulting from the use of relativistic quantum mechanics introduce factors of of v/c, where v is the nucleon velocity. In this case, $v/c \sim 1/10$ and leads to the grouping of certain terms as first forbidden, which would be allowed if only powers of r were considered.

Kurie Plots of Allowed and Forbidden Shapes

The allowed spectra may be expressed as

$$\frac{d\lambda}{dp_e} = N(p) = C(W_o - W)^2 p_e^2 F(Z,W) \qquad (1.4)$$

TABLE I

SELECTION RULES FOR BETA DECAY

Order	Parity Change	Occurring for Interaction Type	Selection Rules on Nuclear Spin I
Allowed	No	S,V	$\Delta I=0$
		T,A	$\Delta I = 0, \pm 1$ (not $0 \rightarrow 0$)
Once Forbidden	Yes	P,A	$\Delta I = 0$
		S,V V,T T,A	$\Delta I = 0, \pm 1$ (not $0 \rightarrow 0$)
		T,A	$\Delta I = 0$
		T,A	$\Delta I = 0, \pm 1, \pm 2$ (not $0 \rightarrow 0, \frac{1}{2} \rightarrow \frac{1}{2}$, $0 \leftrightarrow 1$)
Twice Forbidden	No	P,A	$\Delta I = 0, \pm 1$ (not $0 \rightarrow 0$)
		S,V V,T T,A	$\Delta I = 0, \pm 1, \pm 2$ (not $0 \rightarrow 0, \frac{1}{2} \rightarrow \frac{1}{2}$, $0 \leftrightarrow 1$)
		V,T	$\Delta L = 0$
		V,T	$\Delta I = 0, \pm 1$ (not $0 \rightarrow 0$)
		T,A	$\Delta I = 0, \pm 1, \pm 2, \pm 3$ (not $0 \rightarrow 0, \frac{1}{2} \rightarrow \frac{1}{2}, \frac{1}{2} \leftrightarrow \frac{3}{2}$ $1 \rightarrow 1$, $0 \leftrightarrow 1$, $0 \leftrightarrow 2$)

where N(p) is the number of emissions per second into a unit momentum range, C is a constant, and F(Z,W) is a correction term for the coulombic charge of the nucleus. It will be noted that N(p) in Equation (1.4) is dominated by the statistical factor. The allowed spectra are the same for any choice of interaction and give no information along this line. From Equation (1.4), it is apparent that

$$(W_o - W) \sim \left[\frac{N(p)}{p^2 F(Z,W)}\right]^{1/2} \qquad (1.5)$$

which is a linear relationship. Data plotted according to Equation (1.5) is called a Kurie plot (25), and if a straight line results, the data are identified as representing an allowed transition (or certain forbidden spectra with constant correction term, see below). Forbidden spectra may be expressed from the Fermi theory as multiplicative correction terms to Equation (1.4). By utilizing these correction terms, it is possible to identify the forbiddenness of an unknown spectrum, which does not give a straight Kurie plot. They are simply applied to Equation (1.5) until the plot is linearized.

Since the forbiddenness and form of interaction in beta decay are determined by the relative spin and parity of the initial and final nuclear states, it is sometimes possible to draw conclusions about these quantities from the shape of the beta spectrum. Such information is of interest to shell theory. Conversely from shell theory, one can sometimes predict the degree of forbiddenness to be expected.

Isomerism, Gamma Emission and Internal Conversion.

1. Isomerism

Nuclear isomerism is a term describing states of a nucleus which are energetically above the stable state and which can differ from the stable state in spin and parity. Strictly speaking, isomerism refers only to

those excited states which have a measurable lifetime; however, this definition merely states the limit of present technique and is subject to change as techniques improve. In this work, all excited nuclear levels shall be called isomeric, as is becoming the general practice. We shall only be interested in those cases of isomerism which follow a beta type decay (i.e. electron emission, positron emission, or K-capture). Shown below is a hypothetical case of isomerism following electron emission.

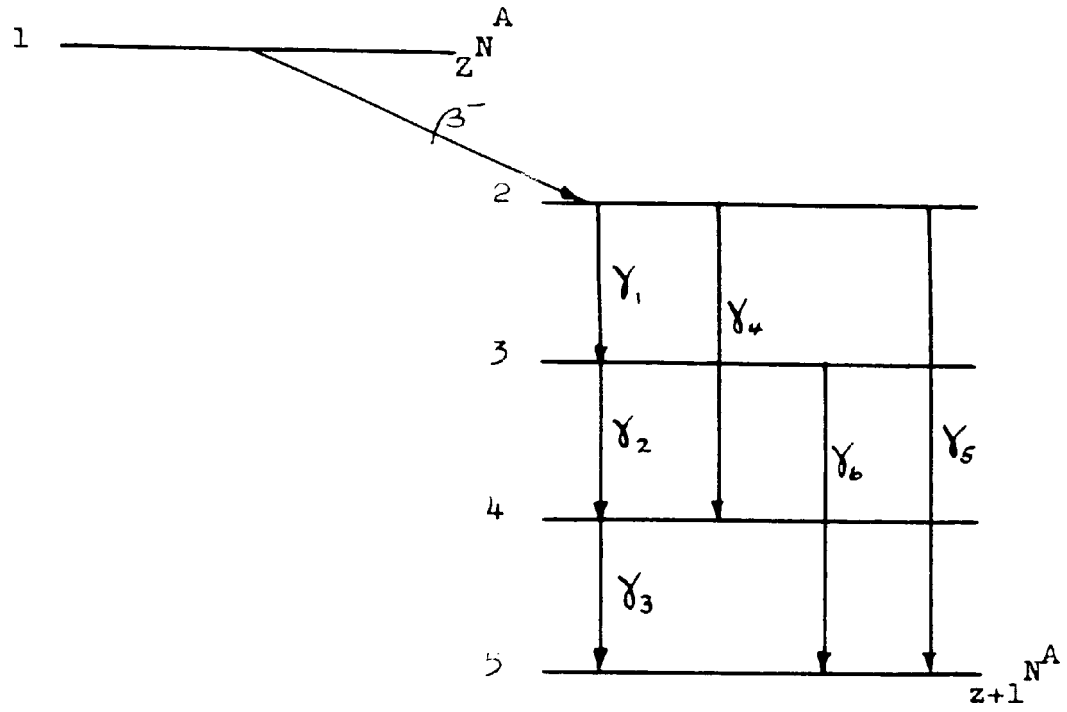


FIGURE 1.1

A Hypothetical Level Scheme

The electron emission by nucleus $_{Z}N^{A}$ leaves the nucleus $_{Z+1}N^{A}$ in the isomeric level 2. From level 2, the nucleus could decay to the ground state by gamma emission through a number of paths as shown. In doing so, the nucleus $_{Z+1}N^{A}$ would emit photons or conversion electrons. Not all of the paths shown are equally likely, and selection rules can operate, which effectively prohibit all but one alternate. On the other hand, many nuclei

exhibit what is known as branching. Using the decay scheme above to illustrate this, suppose that $\gamma 4$ and $\gamma 5$ are prohibited by selection rules so that level 2 can only decay to level 3. If the alternate paths $3 \rightarrow 5$ and $3 \rightarrow 4 \rightarrow 5$ are not prohibited, the relative probability of the two modes is referred to as the branching ratio.

At the present time, the assignment of levels according to energy spin and parity is of crucial interest, and considerable effort is being expended in their study (26) (27). The sorting out of level schemes will form the main topic of this research.

2. Gamma Emission and Transition Probability

The lifetime of an excited level ($\sim \frac{1}{\text{transition probability}}$) with respect to gamma emission will depend on the selection rules governing the emission of a photon and can vary from 10^{-12} seconds to several years.

TABLE II

SELECTION RULES FOR RADIATIVE TRANSITION

Power of x/λ in intensity	2	4	6	8	10
Electric Radiation	dipole	quadr.	oct.	16-pole	32-pole
$\lvert I + I' \rvert \geq$ $\lvert I - I' \rvert \leq$	1	2	3	4	5
Change in Parity	yes	no	yes	no	yes
Magnetic Radiation	--	dipole	quadr.	oct.	16-pole
$\lvert I + I' \rvert \geq$ $\lvert I - I' \rvert \geq$	--	1	2	3	4
Change in Parity	--	no	yes	no	yes

Radiation from a nucleus may be expressed as a series of terms corresponding to dipole, quadrupole, etc., where the intensity of succeeding terms in the multipole expansion differ from each other by $(x/\lambda\!\!\!^{-})^2$. Here x is the order of nuclear dimensions, and $\lambda\!\!\!^{-} = \frac{\text{wave length of the radiation}}{2\pi}$. At 100 kev, $x/\lambda\!\!\!^{-}$ is 1/300; hence, the intensity of quadrapole is 10^5 times smaller than dipole radiation and correspondingly for succeeding terms. The transition probability will vary with the multipolarity, and each term of the multipole expansion has different selection rules. The selection rules for multipole radiation are given in Table II, where I and I' are the angular momentum vectors for the levels between which the radiative transition takes place. Note that electric 2^ℓ pole radiation is grouped with magnetic $2^{\ell-1}$ radiation, due to their similar intensities.

From these selection rules, one would be able to set limits to the spin and parity changes merely from a knowledge of isomeric lifetimes, provided the exact relation between multipolarity and lifetime were known. Unfortunately, none of the theories of radiative transition agree too well with experiment, and more work will have to be done in this field (28). The main difficulty is the evaluation of nuclear matrix elements. Fortunately there are sometimes alternate means of determining the multipolarity of radiation between nuclear levels, such as internal conversion and angular correlation.

3. Internal Conversion

One can most conveniently express the degree of internal conversion in terms of a coefficient. The partial internal conversion coefficient for electrons from the K orbit is expressed as

$$\alpha_K = \frac{N_K}{N_\gamma} \qquad (1.6)$$

where N_K is the number of K orbit conversion electrons emitted, and N_γ is the number of photons. Similar expressions hold for $\alpha_L, \alpha_M, \alpha_N$, etc.

The total conversion coefficient is

$$\alpha = \alpha_K + \alpha_L + \alpha_M + \ldots = \frac{N_e}{N_\gamma} \qquad (1.7)$$

An older definition, still used occasionally, defines α as $N_e/(N_e+N_\gamma)$, the number of electrons ejected per nuclear transition.

Internal conversion can be thought of, and calculated, as a form of photoelectric effect taking place within the atom, the nucleus emitting a photon, which in turn ejects an orbital electron. Actually no photon emission takes place; the interaction occurs purely between the nucleus and the K electron. The problem in these calculations is to determine the probability of transition of orbital electrons to states of the continuum under the influence of perturbing electromagnetic fields of a multipole located at the origin. These calculations are quite complicated and tedious, but depend only on a knowledge of atomic structure and electrodynamics. They have been carried out and tabulated recently by Rose et al (29).

The expressions which one obtains for the internal conversion coefficients are too complicated to be listed here, but an example of the type of result obtained is the expression below, for a non-relativistic treatment, in the case where the orbital binding $\ll$ energy of the conversion electron. This is the K conversion for a multipole of order ℓ (30).

$$\alpha_K^\ell = Z^3 \alpha^4 \frac{\ell}{\ell+1} \left(\frac{2}{\nu}\right)^{\ell+5/2} \qquad (1.8)$$

where Z is the nuclear charge, α the fine structure constant, and ν the gamma ray energy in mc^2 units. The general features of this expression remain unchanged for more exact computations. That is to say, conversion increases rapidly with atomic number and multipolarity and decreases with gamma ray energy. Another useful quantity, more easily measured experimentally and which can also be calculated, is the ratio of conversion

coefficients from the various orbits. Thus, from experimental measurements of α or $^{\alpha}K/\alpha_L$, one can, in principle, determine the multipolarity of the radiation; from this, one knows the limits of spin change between the levels involved in the transition, and also if parity change occurs.

When internal conversion takes place, the lifetime of the level from which the transition occurs is decreased. The half-life of the excited state becomes

$$\tau = \frac{0.69}{\lambda_e + \lambda_\gamma} = \frac{0.69}{\lambda_\gamma(1 + \alpha)} \qquad (1.9)$$

where λ_γ is the decay constant for gamma emission of a nucleus stripped of its electron, λ_e is the decay constant for the transition induced by the orbital electrons, and α is the total internal conversion coefficient as defined in Equation (1.7). An interesting case is when both levels between which transition takes place have I = 0 and the same parity. All radiative transitions are strictly forbidden, and transition can only go by internal conversion. The 1.426 Mev gamma ray in RaC is thought to belong in this category.

Experimental Methods Now in Use

In order to draw a complete level scheme for a decay of the type $_ZN^A \rightarrow {}_{Z\pm1}N^A$, it is necessary to measure experimentally the following quantities: end point and shape of any continuous electron or positron spectra, energy involved in all transitions between excited levels, the spin of all levels, and the parity of all levels involved.

1. Measurements of Beta Spectra and W_o

The most satisfactory method of examining continuous beta spectra is by means of the deflection of the electrons in a magnetic field. For this purpose, an instrument is needed, capable of focusing electrons onto a detector in such a fashion that the relationship between counting at various

energies and instrument settings is known and is simple. Lens spectrometers fulfill this purpose quite well, as do double focusing spectrometers, but simple 180° magnetic spectrometers present difficulties due to the variation of detection with resolution and the non-linear relations between coil current and the momentum of focused electrons. Once the spectrum is known, W_o can be found from the end point of the Kurie plot (Equation (1.5)).

The use of scintillation spectrometers has also been suggested for beta rays, but an unexplained counting rate catastrophe occurs at energies below 200 kev (31).

End point energies can be determined by the use of absorbers, using the method of Feather (32). However, measurements of this type are not as precise as those found from the Kurie intercept.

2. Measurements of Gamma Rays

Many methods exist for the measurement of gamma ray energies. Below 400 kev, modified optical methods utilizing a bent crystal spectrometer (33) give extremely accurate results. Unfortunately, the method is inapplicable to higher energies. At the high end of the energy scale, it is possible to analyze the energy content of electron-positron pairs created by the photon and determine the gamma ray energy in this fashion (34). Many methods of various value are used in the middle energy range, and some are described below.

Gamma sources with a radiator covering them produce photo-electric peaks, which allow analysis by beta spectroscopy, as does the case of internal conversion. When conversion occurs, the peak energies may be measured quite accurately. These peak energies may be added to the known binding energies for the various shells, until, by trial and error, the actual gamma energy is determined. This depends upon the fact that if the binding erergies are added, the resulting gamma energy will be equal for

all orbits.

One of the earliest techniques for gamma measurements is the use of absorbers, utilizing the known dependence of absorption coefficient upon energy. This method is still used to some extent, but isn't too accurate.

Recently the energy dependence of the response of a scintillating crystal and photo tube has allowed entire gamma spectra to be measured by pulse height analysis. This method is not too well suited to precise measurements, due to the poor resolution ($\sim 8\%$), but is excellent for other purposes as shall be shown.

3. Level Schemes: Energy Matching and Coincidence Techniques

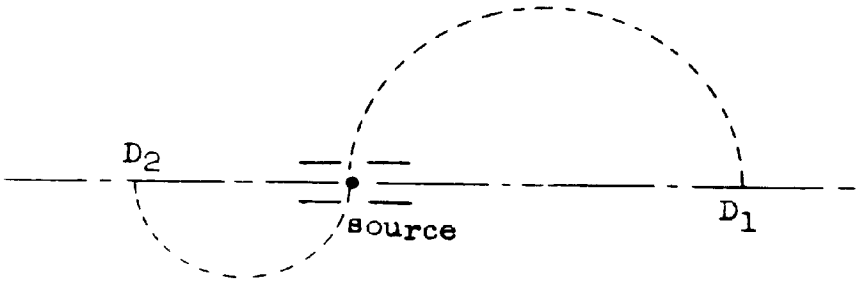
It is sometimes possible to infer the arrangement of nuclear levels from a knowledge of the gamma ray energies between them. This is especially true when branching occurs; in that case, the sum of the energies of the cascade transitions must equal that of the cross over transition. (In Figure 1.1, as an example, $E_6 = E_2 + E_3$.) This can be ambiguous, however, especially if two or more gamma rays have about the same energy. Nor can this system show which transitions lie higher or lower than others. Any scheme proposed, however, must check energywise.

Coincidence techniques are extensively used at present to establish the gamma rays taking part in cascades. The simplest and least satisfactory technique is simply to set up two detectors at 180° with respect to each other and with the source between them. A certain amount of energy selection can be done by placing absorbers in front of one or both detectors, but if there are many gamma rays, or if the energies are close to each other, the interpretation can be extremely difficult.

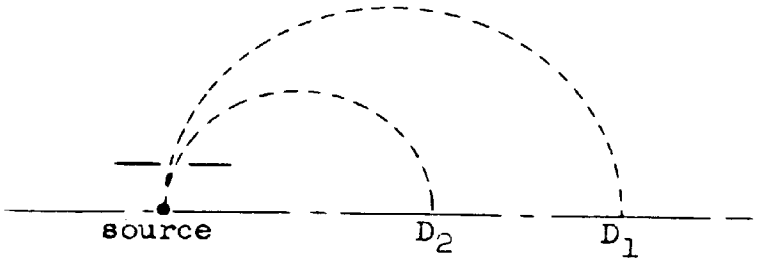
The ideal technique is one where the gamma ray entering the detector is completely selectable.

At present, four methods are in use which allow coincidence techniques

to be used with good enough energy resolution at the detectors to allow for relatively unambiguous interpretation. The first two methods are variations of each other, utilizing the simple 180° magnetic spectrometer in a homogenious magnetic field. Feather (35) arranged two spectrometers about a common source as shown below.



The dotted lines are trajectories for electrons of a given momentum focused into the detectors D_1 and D_2. Coincidences are measured between D_1 and D_2. A similar system used by Fowler (36) and Shreffler (37), and Katz (38) using essentially only one spectrometer is shown below.



Energy selection can also be done by means of scintillation gamma detectors connected in coincidence. The fourth and last method is the crystal summing technique of Wiedenbeck and Lu (39), which will be described in more detail in Chapter VI.

4. Spin and Parity Measurements

When internal conversion occurs, a careful measurement of the partial conversion coefficients and/or their ratio allows an assignment of multipolarity to be made for the radiation involved. Knowing the multipolarity of the radiation, one can set limits to the change of parity and angular

momentum. This does not give a unique assignment to the level, but it is sometimes possible to infer the spin and parity of the levels involved. In order to do this, one generally needs to know at least one level from other means. In the case where the radiation is of mixed origin (electric and magnetic), entirely wrong interpretations can be made; nor does simple shell theory help much.

The exact spin of many ground levels and long-lived isomeric levels have been measured by means of the inhomogenious magnetic field method of Breit and Rabi (40). This method is not applicable to the short-lived states being studied here, but it allows direct measurement of spins.

At the present time, angular correlation (41) (42) between successive gamma rays seems to be the most promising method of making spin assignments to short-lived levels. One can theoretically predict the variation of counting rate between two detectors in coincidence, as the angle between detectors is varied. The theoretical correlation curve is a function of multipolarity and the spin of the levels. Comparing the experimental and theoretical curves allows spin assignments to be made. This type of experiment gives no information about the parity of the levels, and to determine this, so-called polarization correlation must be done. The latter is extremely difficult. In fact, correlation work in general is difficult, due to the necessarily high counting rates and the sensitivity of the shape of the curve to the effect of mixtures and chemical effects.

The severest limitation upon correlation work is that it presumes a knowledge of the levels (spacing, order, and branching). This information is often non-existent or uncertain.

Statement of the Present Research

As outlined in the previous section, one of the main difficulties encountered in studies of isomerism and beta decay is the exact assignment of

level schemes. In order to approach this problem experimentally, it was decided to construct a coincidence arrangement between two thin lens beta spectrometers. Using thin lens spectrometers in this way, unambiguous coincidence work could be done between any gamma emissions which were sufficiently converted, and also between conversion electrons and the continuous beta spectrum. In addition, the individual spectrometers could be used, if needed, to measure the shapes of spectra and conversion coefficients.

In the present research, an instrument of this type was designed and constructed, and its properties studied. The instrument was then used to study the gamma-gamma and beta-gamma coincidences from $Eu^{152,154}$. $Eu^{152,154}$ is a mixture of two artificial radioactive isotopes, which was known to emit many gamma rays, several beta spectra, and to internally convert. With the aid of the coincidence spectrometer, the ordering of the Eu^{152} and Eu^{154} decay schemes was possible.

CHAPTER II

CONSTRUCTION OF THE SPECTROMETER

The instrument used in this work consists essentially of two thin lens beta spectrometers, horizontally mounted at an angle of 180° to each other on a common spectrometer tube and with a mutual source. A schematic representation of the entire instrument is shown in Figure 1.1.

In designing this instrument, it was desired to have available as high a resolution thin lens spectrometer as possible, in addition to having an instrument adapted to coincidence work. With this in mind, the individual halves of the instrument were built to resemble the design of the highly successful thin lens spectrometer already existing in this laboratory (43) (44). Thus, each half of this instrument is a spectrometer with variable resolution and with as fine an ultimate resolution as could be conveniently constructed. In practice, the north instrument has a best resolution of the order of 2.5%, while the south one has a best resolution of ~ 2.0% (where resolution is henceforth defined as $\Delta p/p$ for a single conversion line; where p is momentum and Δp is width at half maximum). Since 2% is generally accepted as a rough lower limit for instruments of this type, further refinement seemed unwarranted, especially since it would only result in greatly decreased luminosity. Resolutions of this order give good representations of continuous beta-spectra and resolve conversion lines well enough for most purposes.

The Spectrometer Tube

The main body of the spectrometers is fabricated from seven inch i.d., one-sixteenth inch thick brass tubing, eight feet long and flanged at both ends to permit the removal of the entire baffle rod and detector systems. An additional flanged joint was constructed at about three feet

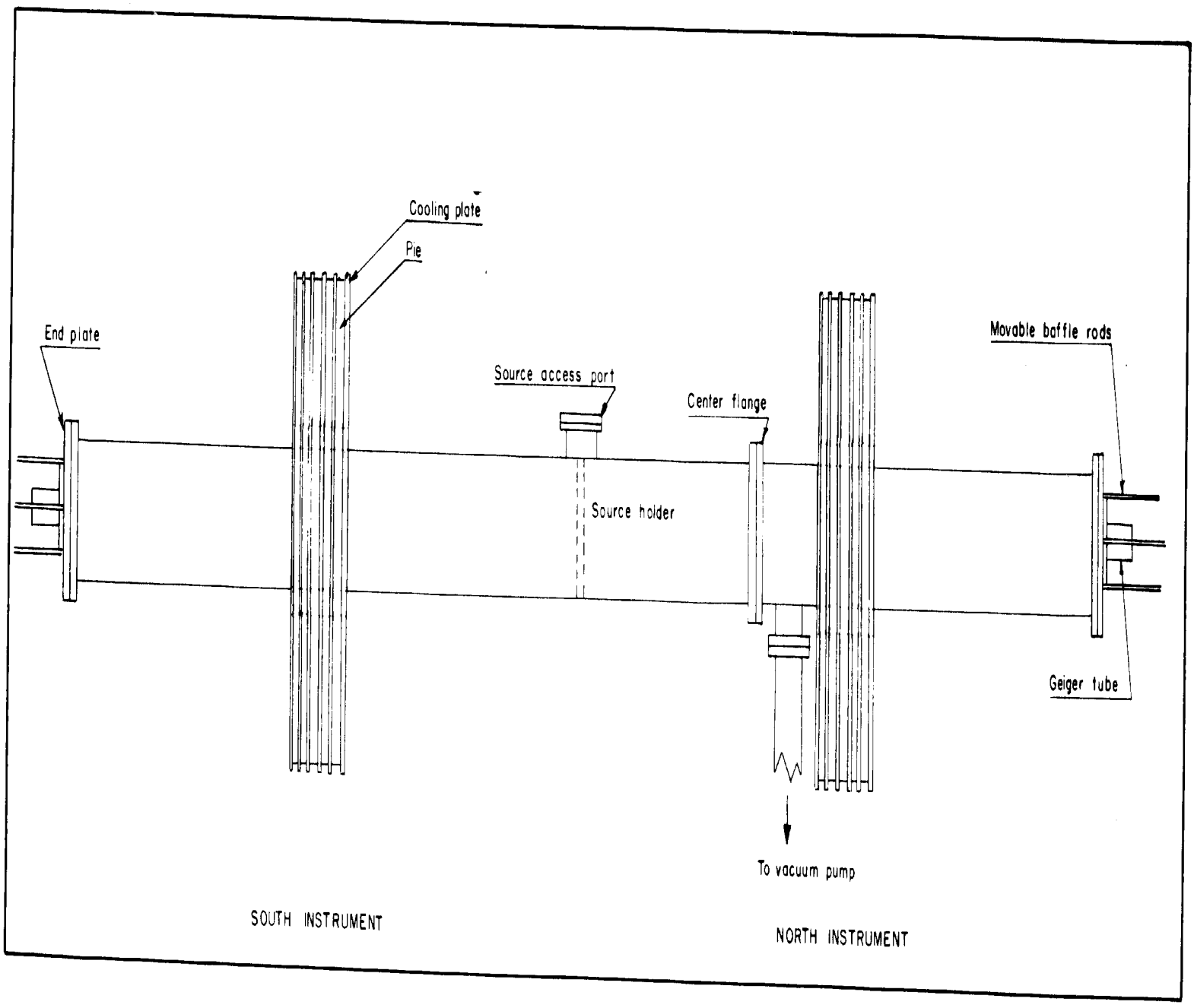


FIGURE 2.1 SKETCH OF THIN LENS COINCIDENCE SPECTROMETER

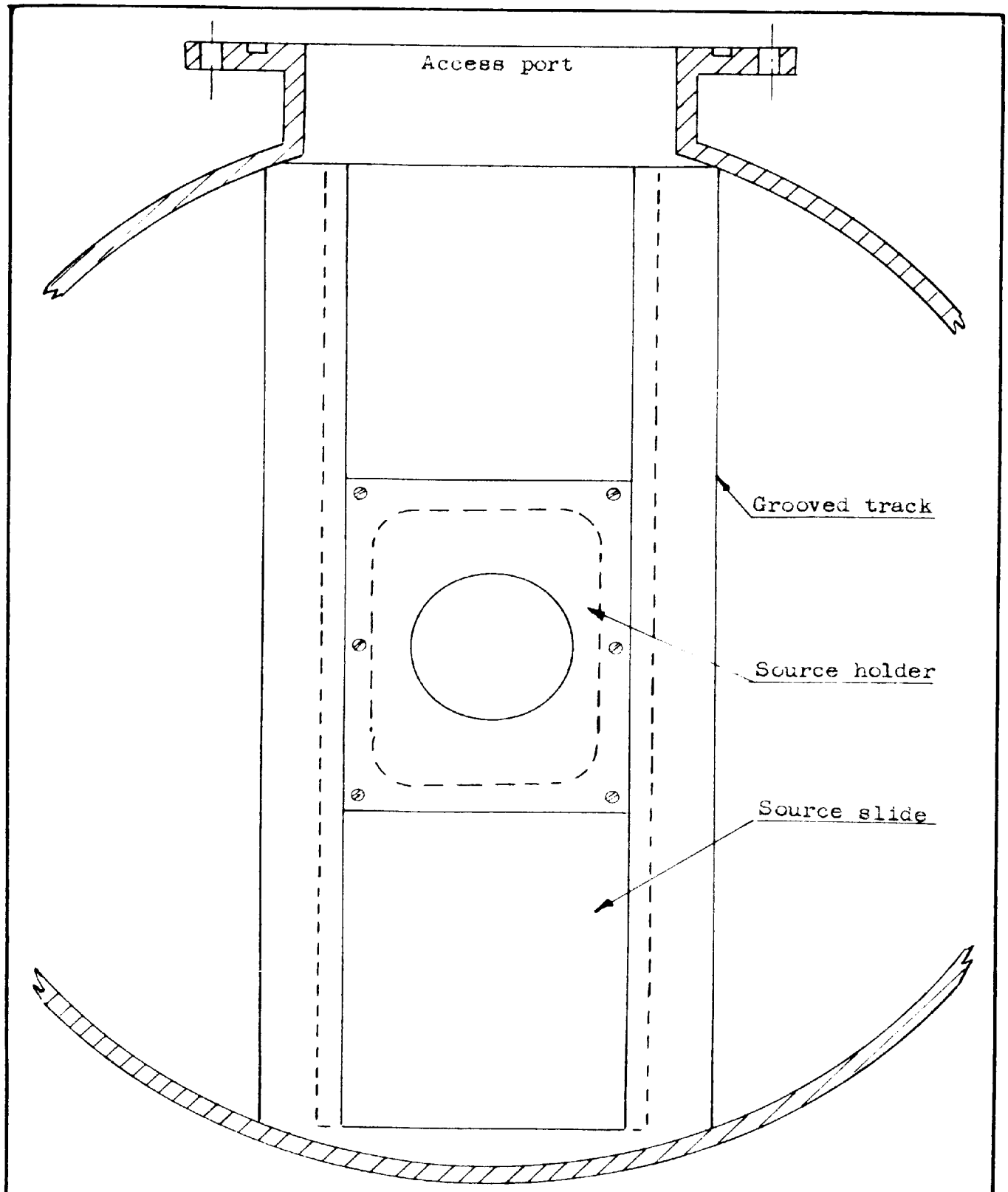


FIGURE 2.2 SOURCE HOLDER

from one end in order to give access to the source holding system and permit placing of certain of the baffles (see below). This arrangement also permitted much easier assembly of the coils. In all cases, these flanges were vacuum sealed by means of three-eighths-inch square cross section rubber gaskets placed in rectangular gasket grooves, and were held in place by twelve 1/4-20 bolts.

Non-ferrous construction was used throughout, and the only ferrous metal near the system was the diffusion pump, which was placed three feet from the spectrometer.

Source and Source Holder

A grooved track is located in the center of the tube permitting a source to be slid in and out of the spectrometers through an access port. Details of the source holder, source slide, track, etc., are shown in Figure 2.2. The entire system is self-centering, and if the source is prepared so as to rest in the center of the circular hole in the source holder, the holder and slide may be centered merely by pushing the slide down the track. The access port is covered by a half-inch thick circular lucite plate. Thus, at all times, the source is open to visual inspection without disturbing the vacuum.

Baffles

Identical baffle arrangements were used in each spectrometer, and a single baffle system is shown in Figure 2.3. Baffle no.1 is fixed in position and defines the physical solid angle of the source. Baffles no.3 and no.4 are used to define ring focusing, and the setting of these baffles determines the resolution of the instrument. They may be moved along the axis as a unit, or with respect to each other, by means of quarter-inch diameter brass rods, which emerge from the end plates through Wilson seals. This enables them to be adjusted externally without disturbing the vacuum.

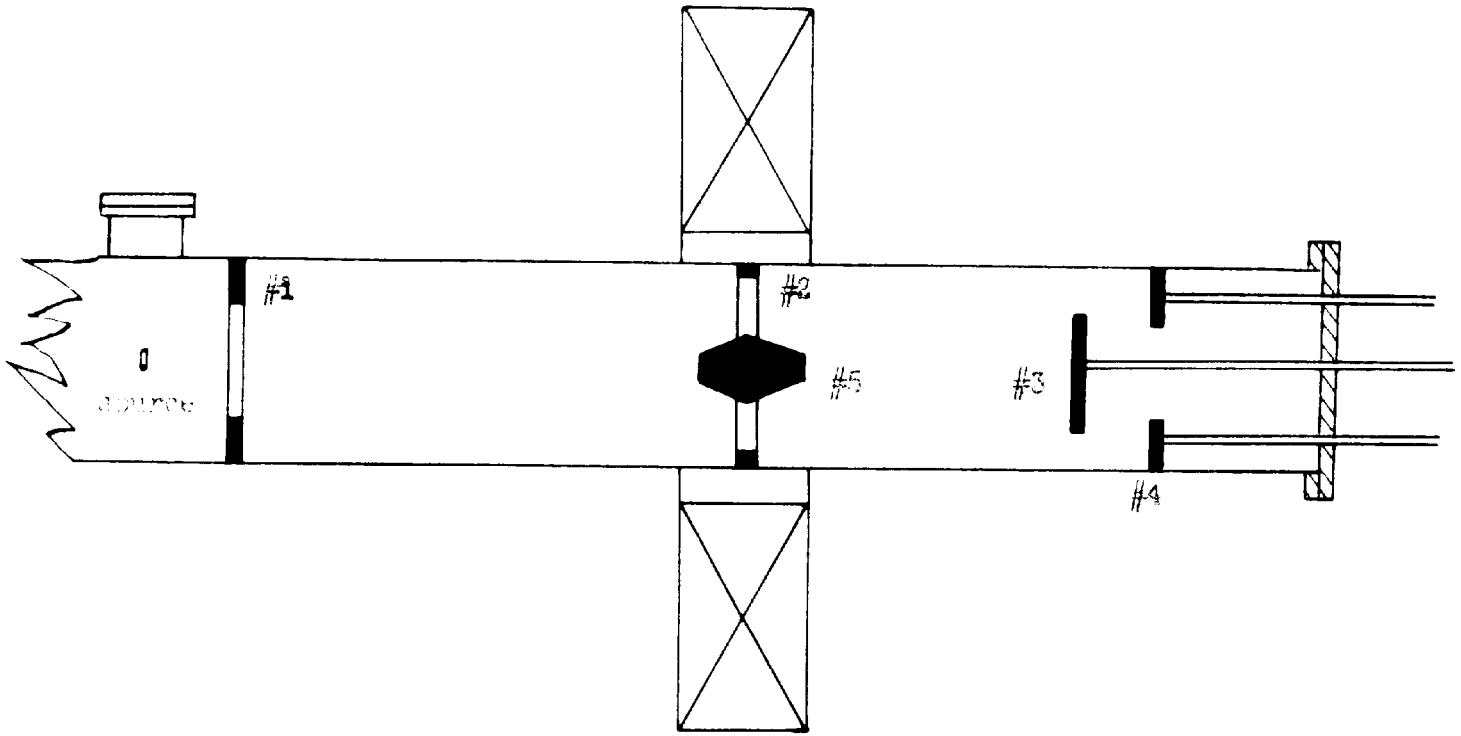


FIGURE 2.3 SCHEMATIC DRAWING OF BAFFLE ARRANGEMENT

Baffle no.5, a lead plug three inches long and one and three-fourths inches in diameter, shields the detector from direct gamma rays from the source and is held in position by three one-quarter inch diameter brass rods arranged symmetrically. Baffle no.2 is also fixed and serves to reduce small angle scattering into the detector. (Some later work of Hutchinson (44), using the Michigan thin lens spectrometer mentioned previously, showed that about ninety percent of the focused electrons pass through an area much smaller than that defined by baffles no. 2 and no.5, so that baffle no.2 could actually have been larger than it is.)

Focusing Coils

The focusing coils in these instruments consist of seven hundred and fifty turns of one-half inch by one-thirty-second inch copper strip, arranged in five "pies" of one hundred and fifty turns each and connected in series. External connections were made at equal angles around the axis of the coil in order to give the greatest electrical symmetry. Paper insulation was used between strips, and the individual "pies" were painted with insulating enamel and baked. Before baking, each coil was tested for shorts by placing it across a 110 V line. The coil itself would heat up slowly, but any shorted sections would heat up rapidly. Thus, one had only to run his fingers along the coil to detect "hot spots", and any shorts would be located. Since there were one hundred and fifty turns, no danger existed from the potential between individual turns of the copper. Baking was accomplished in a similar fashion. Three "pies" were connected in series across a 220 V AC line, and the I^2R heat was sufficient to bake the enamel. The "pies" are separated by means of three-sixteenths-inch aluminum plates, to which copper tubing for water cooling has been soldered along the periphery. The "pies" are insulated from these cooling plates by Fish Paper and Empire Cloth. No water cooling is provided on the outer surfaces

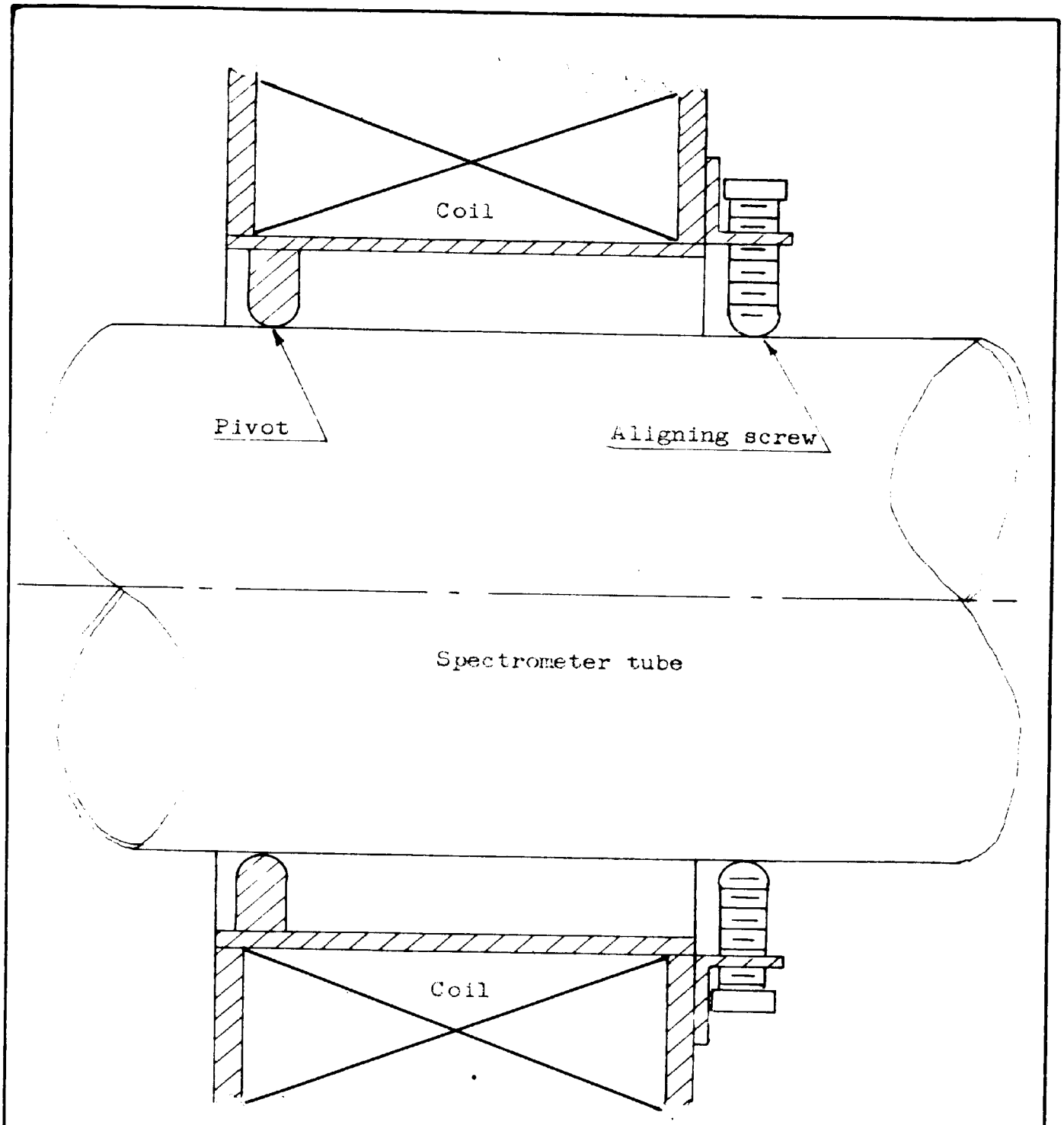


FIGURE 2.4 DETAIL OF COIL TILTING MECHANISM

of the assembled coil; one-quarter inch aluminum plates serve both to hold the coil together and conduct the heat away. The coils were assembled upon the two sections of the spectrometer tube held vertically, and then the entire structure was put in place. A photograph of one of the coils, taken during its assembly, is shown below.

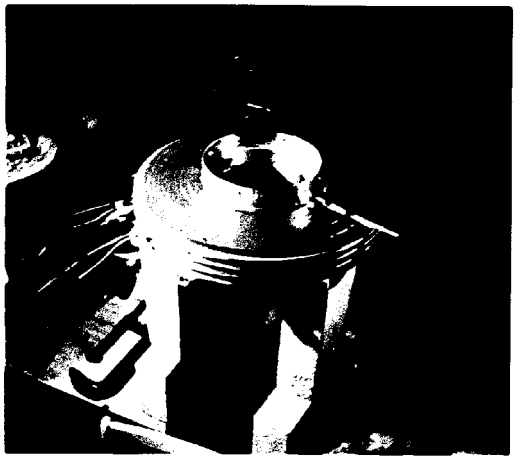


FIGURE 2.5

ASSEMBLY DETAIL OF FOCUSING COIL

A one hundred and fifty turn, enameled "pie" is in position on top of the fish paper separating it from the cooling plate on which it rests. The cooling plates with their water coils are also visible. Four turnbuckles hold the coils, cooling plate, and end plates together. Details of the coil spool and the means of adjusting its position relative to the spectrometer axis are shown in Figure 2.4. The coils are geometrically centered along the axis of the spectrometer tube at one end by means of brass pivots. The other end of the coil spool contacts the spectrometer tube by means of four 1/4-20 brass aligning screws. By manipulating these screws, it is possible to tilt the entire coil assembly with respect to the spectrometer axis, and having done so, to fix the assembly rigidly in place. Small adjustments of these screws have a marked effect upon the counting rate of the detector and serve as a sensitive means of aligning the

spectrometers.

Coil Power Supply

The power supply system for the focusing coils is shown schematically in Figure 2.5. Current is supplied by means of two L-2 aircraft type Leece-Neville 28V generators, each driven by 2 H.P. three phase Master Motors, Inc. electric motors. For the purpose of noise and vibration suppression, the motor generator sets are mounted on rubberized glass wool in a concrete block housing. In parallel with each generator are a 4000 microfarad condenser bank and an adjustable voltage battery bank which serve as regulators. The generator output voltage can be varied by the slide wire potentiometer in the field coil until the batteries draw "zero" current. In theory, these batteries should draw or generate no average current, but, in practice, up to three amperes will have no effect on their regulating properties. In order to draw a particular current, the batteries are connected to give the nearest voltage to that required, and then the field of the generator is varied to adjust its output voltage to the battery. The resultant regulated power (available at two volt intervals) is then adjusted to the exact value desired by means of the variable voltage-dropping resistors. In series with each of the spectrometer coils are individual shunts, in parallel with which is a type K potentiometer. The potentiometer serves both to measure the current and to monitor any slow drifts.

A common battery bank is used to supply both generators. In practice, this method of battery regulation allows a short term variation of $\sim 0.25\%$ as measured by an oscilloscope. Slow drift of the system requires that constant manual corrections be made during operation. Since the measured best resolution is less than 2%, and in coincidence work is generally about 10%, it is apparent that these variations in the supply system are negligible. The various rheostats, potentiometers, galvanometers, and other controlling

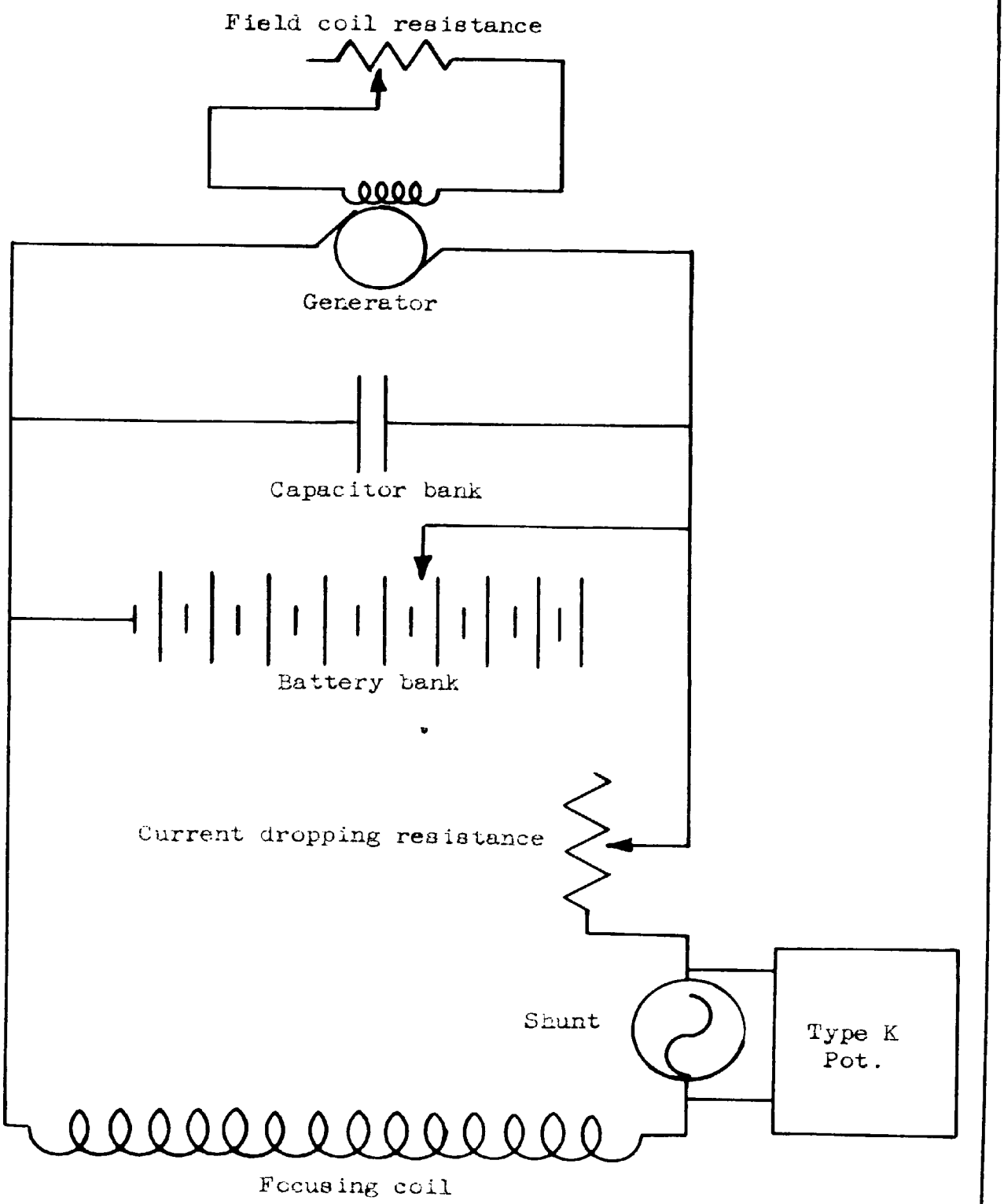


FIGURE 2.6 CURRENT SUPPLY TO FOCUSING COILS

devices are located at a control panel, as shown in the photograph on the frontispiece.

With seven storage batteries (one hundred and twenty ampere-hour, six volt) in the battery bank, it is possible to focus electrons of about 2.0 Mev. However, at these high currents, the coils heat up rapidly, despite the water cooling, and can not be operated for any length of time (i.e. over twenty minutes). For lengthy operation, a practical upper limit of about 1.75 Mev exists.

Corrections for Earth's Magnetic Field

The spectrometers are horizontally mounted in a north-south direction to minimize effects due to the horizontal component of the earth's field. The vertical component is cancelled by large rectangular Helmholtz type compensating coils which can be seen in the photograph on the frontispiece. These coils are five feet by sixteen feet and consist of twenty-seven turns of no.16 wire. Powered by a Variac across the 110 V line, the resulting current is rectified by a selenium full wave rectifier in parallel with a 3000 micro-farad condenser bank. The current through the compensating coils is adjusted until a dip needle placed near the center of the instrument is horizontal. The vertical component of the earth's field varies slightly along the instrument, probably due to the presence of steel beams in the ceiling and/or the floor. These slight variations can be shown to be of second order, and no attempt was made to compensate for them.

Vacuum Equipment

The entire spectrometer tube was evacuated by means of a VMF-100 diffusion pump and a Cenco Megavac mechanical pump. The vacuum was measured by means of a McLeod gauge, and a vacuum of 10^{-5} mm Hg was obtained. At first, Octoil S pump fluid was used, but later a change was made to Dow 702 fluid. The latter proved to be much more stable and equally good.

Detectors

Geiger counters were the particle detectors used throughout this work. Figure 2.6 shows one of the tubes in detail. The large flange shown contains an "O" ring groove and is the means by which the tube is connected to the spectrometer proper. In order to utilize thinner windows, provision was made to refill the tubes without removing them from the spectrometer. Except for some of the earliest work, 0.25 mil mylar window material was used throughout and proved to be too fragile to withstand pressure differences of one atmosphere without serious distortion. Therefore the geiger tube filling system and the instrument are simultaneously evacuated. After evacuation, the geiger tube is filled from a large reservoir by means of a series of glass stopcocks. In this way the pressure difference across the window never exceeds that of the counting gas. This arrangement also permitted the refilling of individual geiger tubes without letting down the entire system. The counting gas used consisted of 90% Argon and 10% Ethyl alcohol at 10 cm Hg pressure. Plateaus of the order of 80-100 V were obtained after filling. In practice, these tubes had to be refilled after about a week, probably due to selective diffusion through the window. Constant refilling seemed to decrease the useful life of the counter, as evidenced by drifting counter characteristics. This was apparently due to the flexing of the mylar window under the 10 cm Hg pressure of counting gas, resulting in an increased diffusion rate. Occasional replacement of the windows rectified this problem.

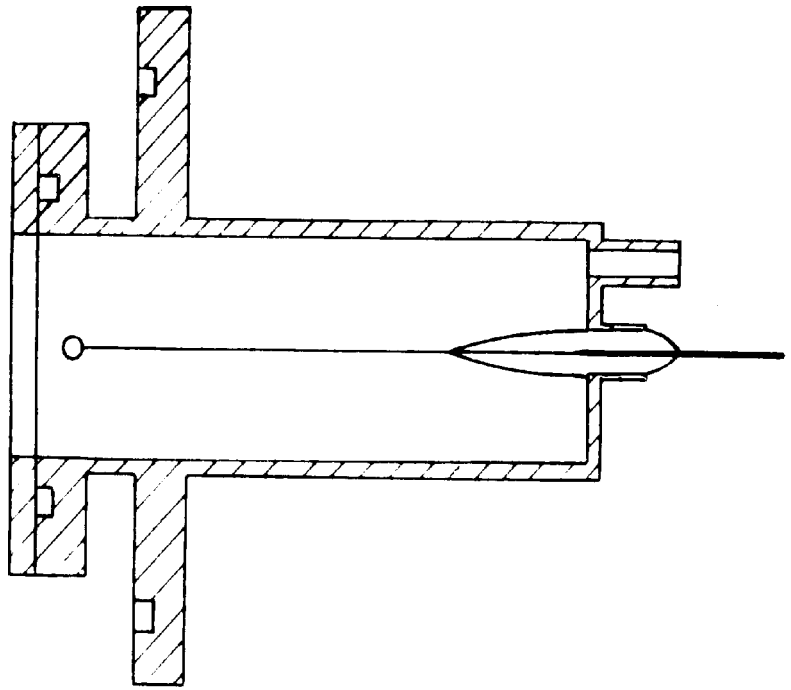


FIGURE 2.7 SKETCH OF GEIGER TUBE

CHAPTER III

THE ELECTRONICS

Introduction

In any work attempting to measure coincidences, the events recorded as coincident are a result of contributions from two types of phenomena. If N_T is the total number of coincidences detected, then

$$N_T = N_{real} + N_{acc.} \qquad (3.1)$$

where N_{real} is the contribution due to truly coincident events (in our case nuclear in origin or due to cosmic rays), and $N_{acc.}$ represents accidental coincidence counts caused by the detection of particles in the singles counters within a period of time, τ, short enough to be measured as coincidental by the circuitry.

If, in a two channel system, N_1 is the counting rate per unit time in channel no.1, and N_2 is the counting rate per unit time in channel no.2, the chance that a pulse from channel no.1 is accompanied by one from channel no.2 within $\pm \tau$ is

$$2 N_2 \tau$$

and the rate per unit time of accidental coincidences is

$$N_{acc.} = 2 N_2 N_1 \tau \qquad (3.2)$$

Equation (3.2) serves to define τ, which is generally referred to as the resolving time of the coincidence circuit, since it is the smallest time for which the circuit can resolve individual channel counts. The value of τ is determined by the individual "singles" pulse widths and by the point at which the output coincidence pulses are discriminated. So long as τ is stable, it can be computed from Equation (3.2) (if N_1 and N_2 are from completely independent sources), and once known, can be used to compute $N_{acc.}$. Consequently knowing τ, we can distinguish between real and

accidental coincidences by means of Equation (3.1). We shall now discuss certain of the restrictions on τ, and hence upon the circuitry which determine it.

Let us examine a little more fully the case of the detection of electrons of selected energy in each channel of a coincidence system. In this case

$$N_1 = N\omega_1 e_1 f_1$$
$$N_2 = N\omega_2 e_2 f_2 \qquad (3.3)$$

where N is the source strength, ω is the solid angle subtended by the counter expressed as a fraction, e is the efficiency of detection ($\sim 100\%$ for electrons and geiger tubes), and f is a factor lumping together source thickness, window thickness, possible conversion coefficients, etc. Hence

$$N_{acc.} = 2\tau N^2 \omega_1 \omega_2 e_1 e_2 f_1 f_2 \qquad (3.4)$$

The number of real coincidences $N_{1,2}$ will be

$$N_{1,2} = N\omega_1\omega_2 e_1 e_2 f_1 f_2 \qquad (3.5)$$

It is noted that $N_{acc.}$ varies as N^2, whereas $N_{1,2}$ is linear with N. Therefore, there is, in any experiment, an upper limit to the source strength N beyond which it is impossible to measure $N_{1,2}$, due to the fact that $N_{acc.}$ becomes $\gg N_{1,2}$, and statistical uncertainty in $N_{acc.}$ washes out any certainty in the value of $N_{1,2}$. Similarly this source strength can not be too weak, or the time required to obtain $N_{1,2}$ with any good statistics becomes prohibitively long.

If one assigns the operating condition that

$$N_{1,2} \approx N_{acc.}$$

then

$$N\omega_{1}\omega_{2}{}_{eff}{}_{1}{}_{eff}{}_{2} \approx 2N^{2}\tau\omega_{1}\omega_{2}{}_{eff}{}_{1}{}_{eff}{}_{2}$$

from which

$$2\tau N \approx 1$$

Thus the smaller the value of τ, the larger N can be.

In using geiger tubes, a lower limit exists for τ. This lower limit is set by the nature of the geiger type of discharge. If an ionizing particle enters a geiger tube, a time lag exists between the entrance of the particle and the build-up of the Townsend discharge. This time lag is not fixed, but can be up to 0.1 microseconds, and limits τ to a lower value of about 0.25 microseconds. Thus, 0.25 microseconds represents an optimum resolving time for the detection of coincidences with geiger tubes.

During the course of this work, two separate systems of electronics were utilized. Throughout the lining up and the work on Hf^{181}, a very simple system was used. This proved inconveniently unstable over the long periods of time needed to collect data, and it was finally discarded in favor of a more sophisticated instrumentation. The two schemes are described below.

First Electronics System

The first electronic scheme used in this work is block diagrammed in Figure 3.1. Cathode followers are located at the geiger tube and drive the ten feet or so of coaxial cable connecting them to the scaling circuit.

The scalers used are IDL, Model 161, scale of 256, with a slightly modified pulse forming stage. Ordinarily this model scaler has an input consisting of an RC differentiating network feeding into a "single shot" multivibrator, which puts out a negative pulse of about three microseconds duration and thirty volts amplitude for each input pulse. It is this pulse which fires the first scaling stage. Built into the scaler is a provision for simultaneously removing the pulse at this point. In the scalers used

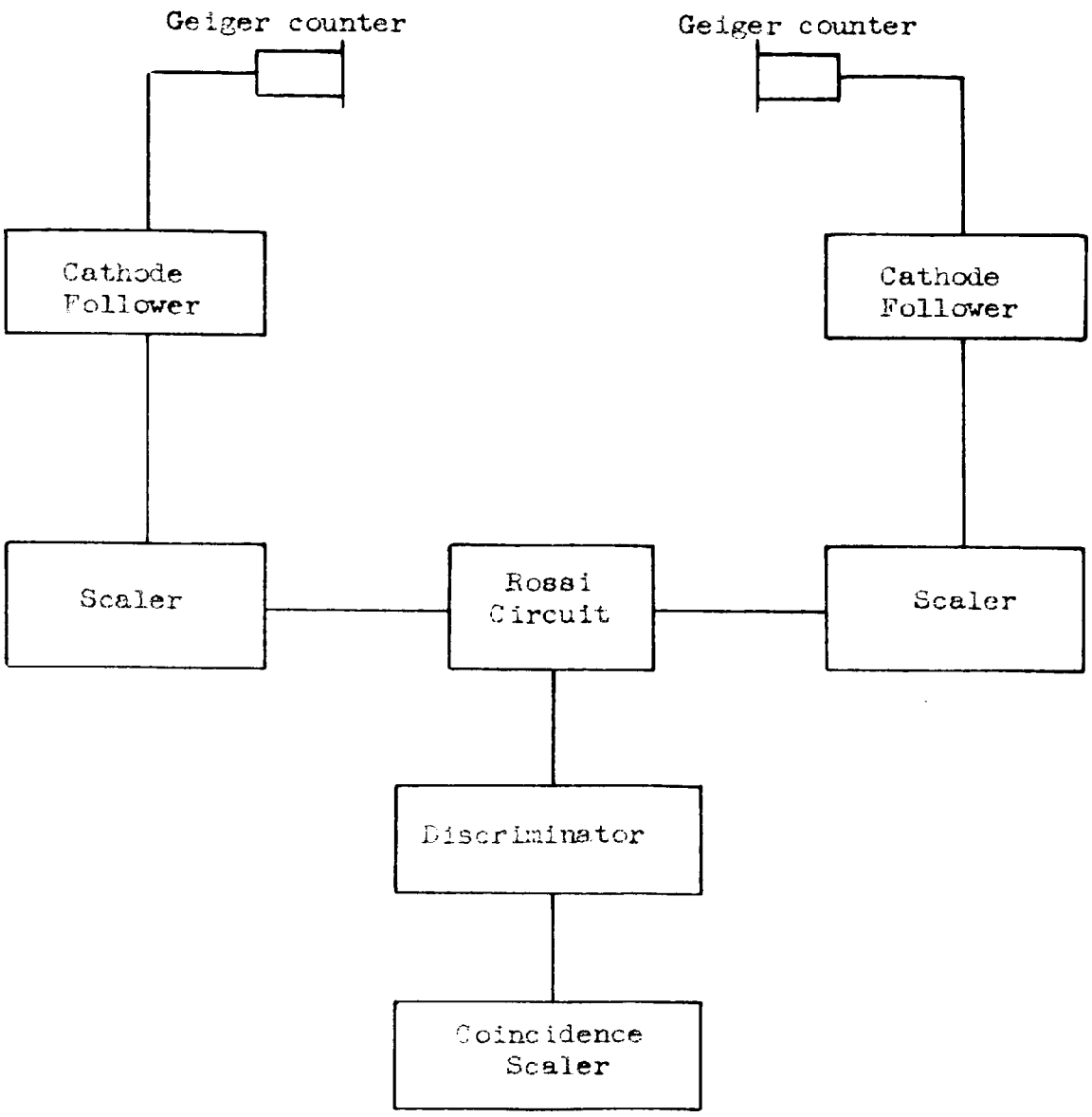


FIGURE 3.1 FIRST ELECTRONIC SYSTEM

in this work, the grid-plate coupling condenser between the two tubes of the multivibrator has been reduced in value. Since this condenser in conjunction with certain resistors effectively determines the pulse width put out, the effect of reducing its value is to shorten this width. This shortened pulse is still sufficient to trigger the scaling stages, and it is also used as the input pulse to the coincidence circuit.

The coincidence circuit is a standard pentode Rossi type consisting of four 6AC7's. Each side of the Rossi circuit consists of two 6AC7's in parallel, so as to provide greater stability. Power is supplied from the auxiliary power outlet of an A1 type amplifier, with an electronically regulated 285 V supply. Using this arrangement, the negative pulses from the scalers are highly differentiated and used as the Rossi input. A discrimination ratio of about 15:1 was attained, as measured on a Tektronix 511A oscilloscope. A drawing of the Rossi circuit is shown in Figure 3.2.

The output of the Rossi is fed into an Atomic Instrument Type 105 decade scaler. This scaler has a positive pulse discriminator in its input circuit and is very well regulated.

Using this arrangement, a resolving time of about 0.38 microseconds was set and used throughout all of the preliminary work. Some difficulty was encountered in maintaining a stable resolving time. The Rossi circuit used draws considerable current in the screen grids (the screen grid resistors have a dissipation value of one hundred and fifty watts) and this was probably part of the difficulty. Also, the pulse forming stage used is not well regulated in the model 161 scaler (gas tube regulation only), and thus, the pulse shapes were liable to change.

After the completion of the work done on Hafnium (during which period the resolving time was kept absolutely stable at 0.38 microseconds for a

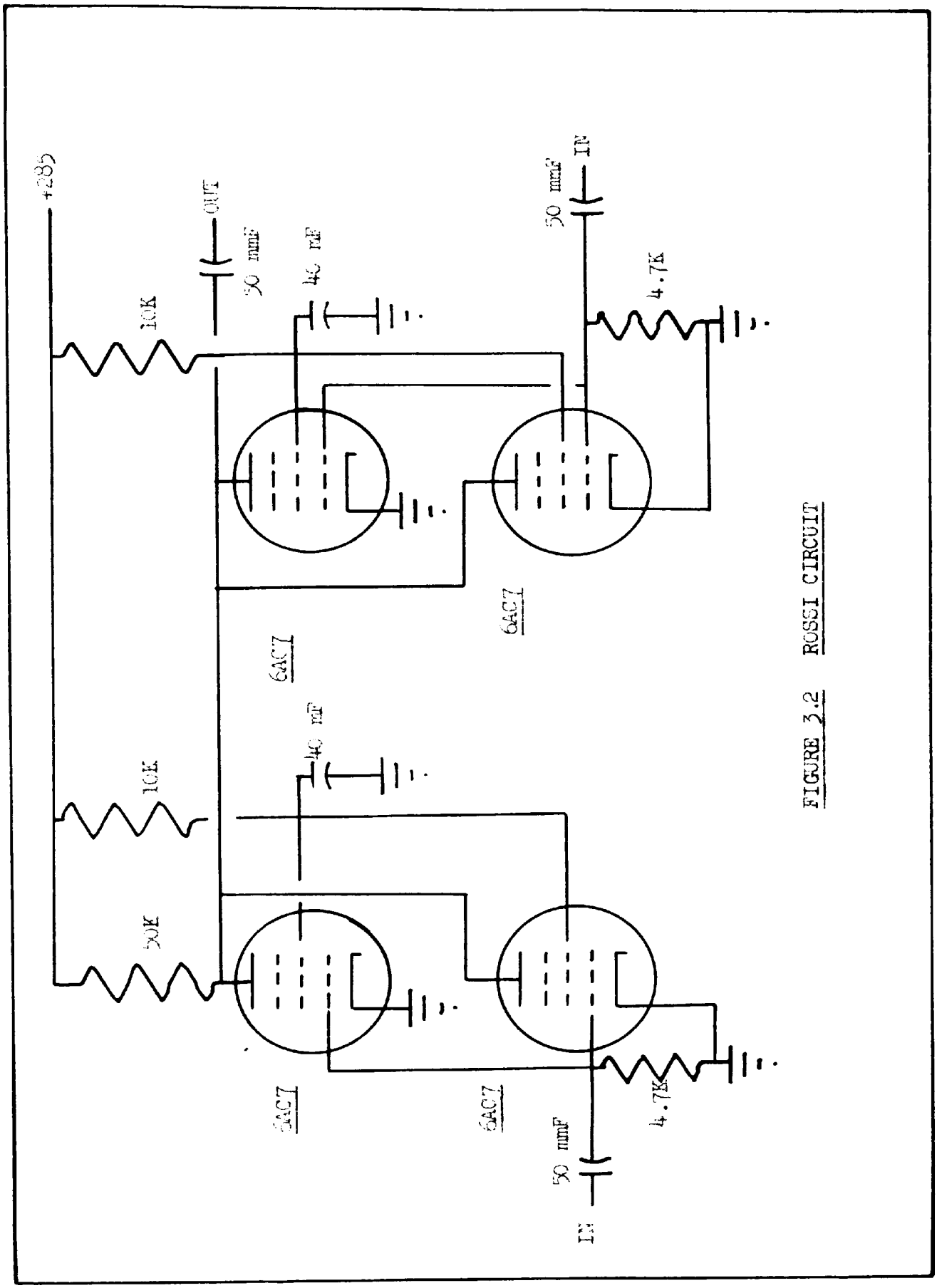


FIGURE 3.2 ROSSI CIRCUIT

period of two months), a drift in resolving time was again noted. Rather than repair the old system, it was decided to put in entirely new circuits.

Second Electronics System

The chief requirements of the new circuits were a different pulse forming stage for the single events (coincidence input) and a different coincidence circuit.

Available in the laboratory were two Atomic Instruments Type A1 amplifiers with associated discriminators and formed pulse outputs. These latter are electronically regulated and put out a well formed positive pulse of about 10 V amplitude, 0.1 microseconds rise and 0.5 microseconds width. Since our requirements were negative pulses of the same specifications (to trigger the Garwin type coincidence circuit decided upon), it was decided to use the A1's and modify their output. Actually, a simpler amplifier could have been used, since the uniformity of geiger pulses ($\sim$ 100%) at the counting rates used does not require the linearity of the A1.

As originally constructed, the A1's have a cathode follower output, preceded by a Schmidt type trigger stage to form the pulses. In order to change the polarity of the output, the cathode follower was changed to an invertor with a variable resistor in the plate circuit, and then a new cathode follower was installed. After inversion, the pulses showed positive overshoot, and so a diode clipper was also installed. The final conversion is shown in Figure 3.3.

This type of pulse forming provides certain other advantages. It is possible to shape the output pulses to some extent by means of the variable resistances R_1 and R_2. The Resistance R_1, being in the plate circuit of the invertor, allows some variation of pulse height. By means of R_2, it is possible to change the pulse width, since in addition to determining the amount of clipping, R_2 combined with C determines the time constant for the falling

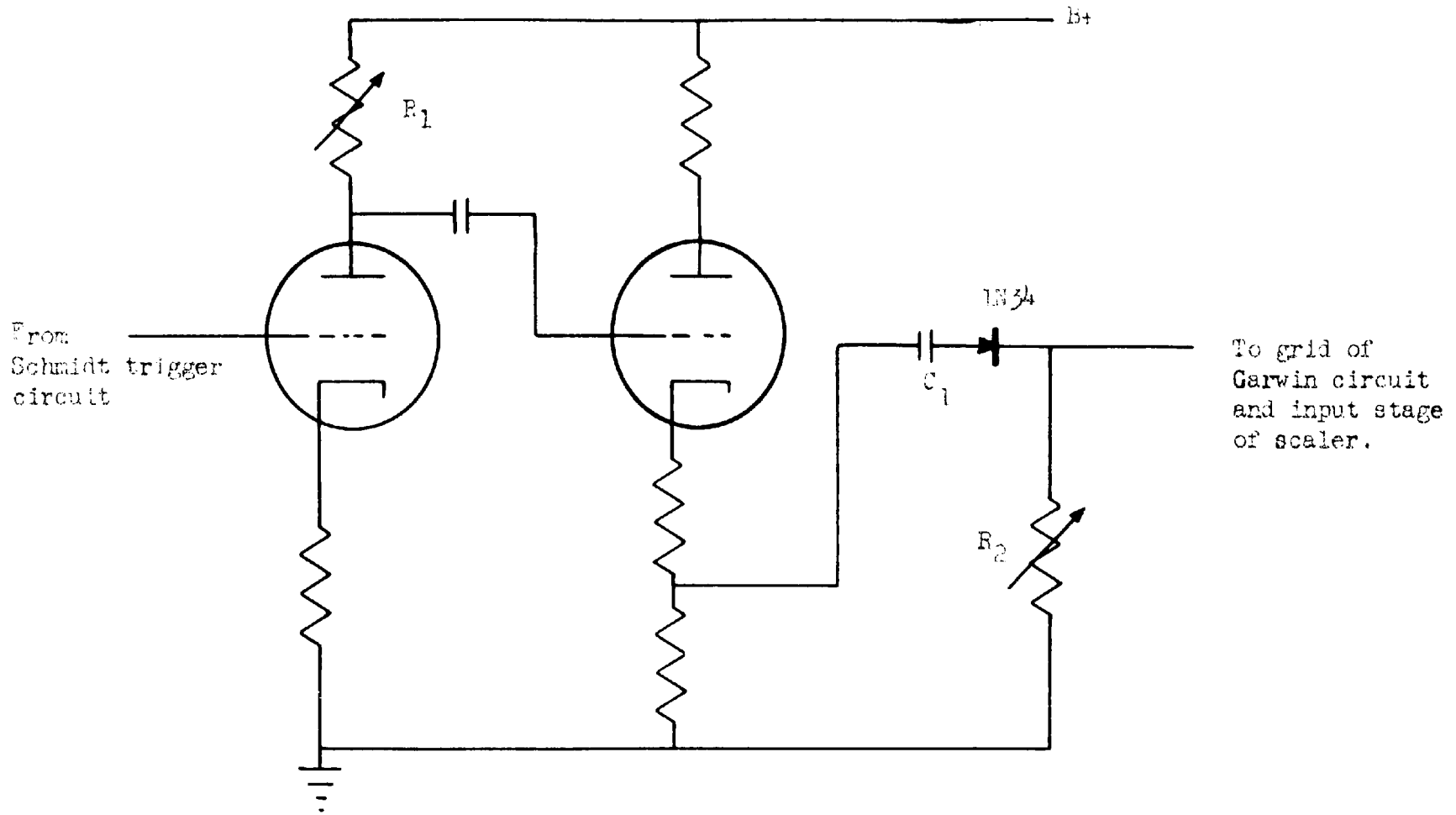
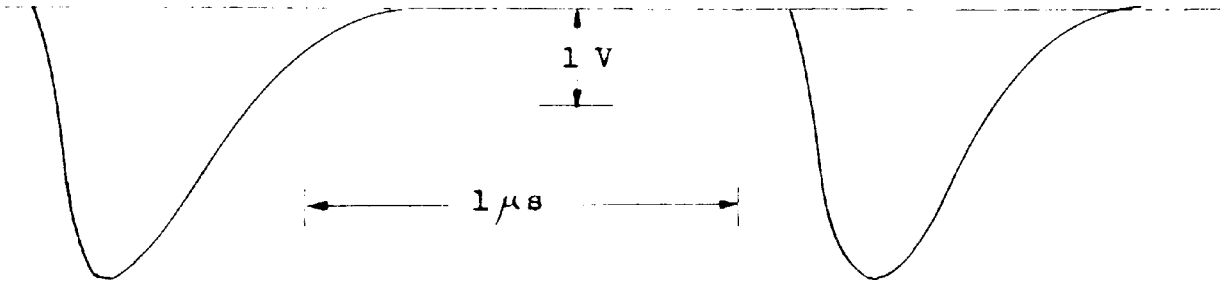


FIGURE 3.3 MODIFIED A1 OUTPUT

off of the negative output pulse. Thus the pulse height and rise are unaffected over a large range by changing R_2, but the pulse width can be varied in the fashion indicated below.



In practice, it proved possible, not only to match the output pulses by simple control knob adjustments while viewing them on an oscilloscope, but also to set them at any desired width to determine the resolving time. Below are shown typical pulses from each channel as plotted from the face of the Tektronix Type 511A oscilloscope.



These pulses were fed into a Garwin type coincidence circuit (45) shown in Figure 3.4. This is a simple triode Rossi circuit with a diode clamp. The diode does not affect the coincidence pulses from this circuit, but severely limits the amplitude of the singles output. This circuit was electronically regulated from the 285 V output of an Al and yielded a discrimination ratio of about 20:1.

The Garwin output was fed into the type 105 Atomic Instrument decade scaler previously mentioned, and its input discriminator was again utilized. A block diagram of this entire scheme is shown in Figure 3.5.

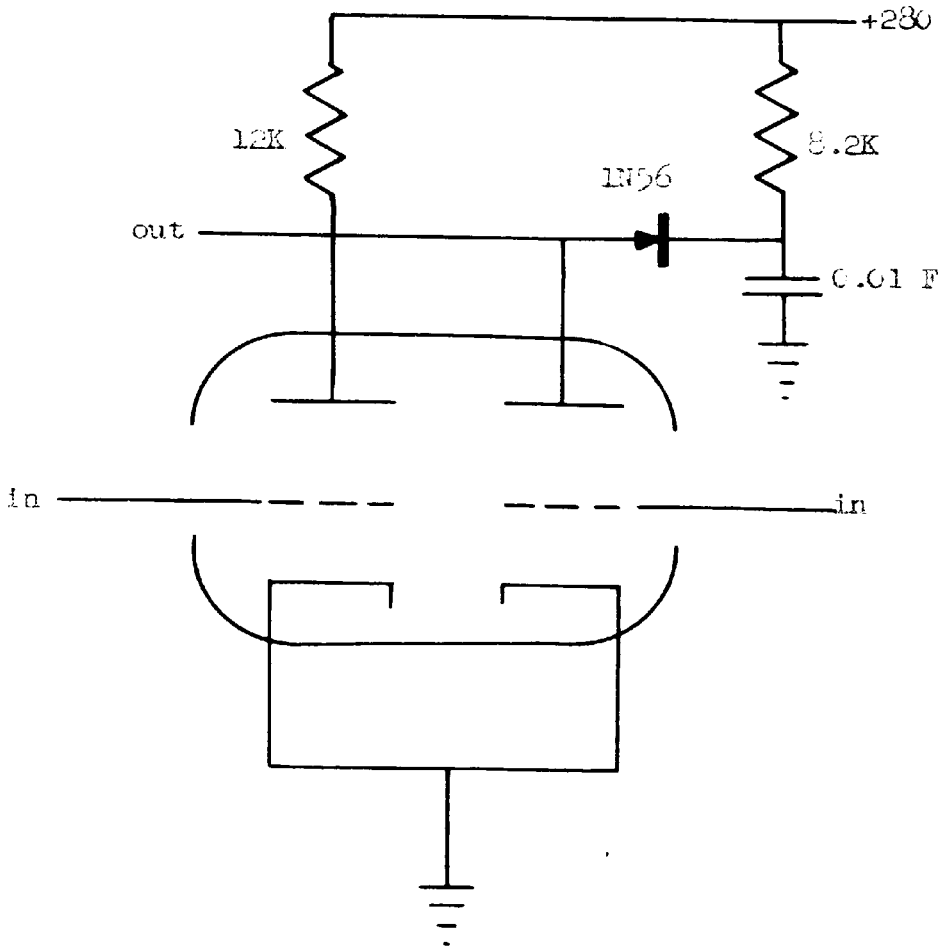


FIGURE 3.4 GARVIN CIRCUIT

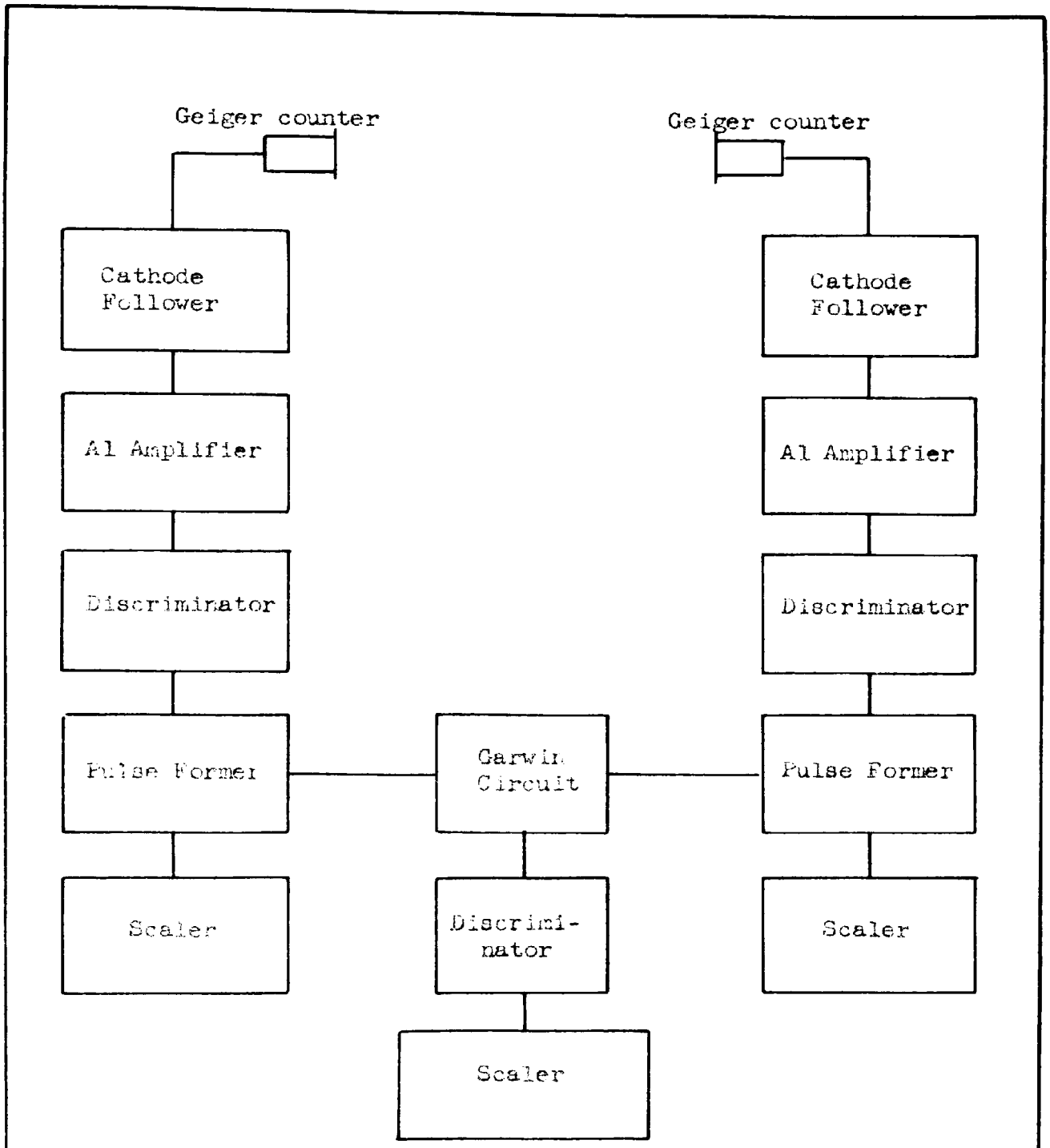


FIGURE 3.2 SECOND ELECTRONIC SYSTEM

Resolving times of the order of 0.25-0.30 microseconds were easily obtained, and for the work on $Eu^{152,154}$, a resolving time of 0.28 microseconds was used. As shown previously, this is about the lower limit for geiger inputs. The stability of the electronics was monitored by measuring the resolving time every two hours, during coincidence measurements, to a standard error of two percent. The stability proved quite satisfactory.

CHAPTER IV

PROPERTIES AND CALIBRATION OF THE THIN LENS SPECTROMETERS

If the focusing properties of a thin lens spectrometer are examined in first order, it is found that the relationship between source and detector distance with respect to the center of the coil behaves exactly according to a thin lens formula,

$$\frac{1}{p} + \frac{1}{q} = \frac{1}{f}$$

where

$$f = \frac{(\text{momentum})^2 \times \text{Const.}}{\int_{-\infty}^{\infty} H_z^2 \, dz}$$

and the z direction is along the spectrometer axis: hence the name "thin lens" spectrometer. These properties were first examined and confirmed by Klemperer (46), who constructed a lens spectrometer of this type and first used it to measure electron momenta. More thorough examinations of the properties of this type instrument were made by Deutsch, Elliot, and Evans (47), and by many others (48) (49) (50), who assumed the optimum condition of focus to be along the axis.

At a surprisingly later date, the focusing properties of the thin lens were reexamined, and the optimum condition of focus was found to be a ring in space rather than a point along the axis.

Ring Focus

The equations for the trajectory of an electron in the axial field of a thin lens spectrometer can not be solved and must be examined numerically.

Starting with the Lagrangian, in cylindrical coordinates, for an electron in an axially symmetric field (i.e. vector potential A_φ in the φ

direction only)

$$L = \frac{m}{2}\left[\dot{r}^2 + \left(r\dot{\varphi} + \frac{e}{mc}A_\circ\right)^2 + \dot{z}^2\right] - \frac{e^2}{2mc^2}A_\circ^2$$

the equations of motion can be easily shown to be

$$\begin{aligned}
\frac{d}{dt}(m\dot{r}) &= mr\dot{\varphi}^2 + \frac{e\dot{\varphi}}{c}\frac{\partial}{\partial r}(rA_\circ) \\
\frac{d}{dt}(m\dot{z}) &= \frac{er\dot{\varphi}}{c}\frac{\partial}{\partial z}(A_\circ) \qquad (4.1) \\
\frac{d}{dt}\left(mr^2\dot{\varphi} + \frac{erA_\circ}{c}\right) &= \frac{dp}{dt} = 0
\end{aligned}$$

where p, the canonical angular momentum, is a constant of the motion. The mass, m, though relativistic, is also constant since the particle velocity, v, is a constant of the motion. (i.e. A charged body undergoes a change of direction but not of energy in a magnetic field.) Substituting p into the first two equations (4.1) eliminates $\dot{\varphi}$, and if the independent variable is changed from t to z, recalling that

$$v^2 = \dot{r}^2 + (r\dot{\varphi})^2 + \dot{z}^2$$

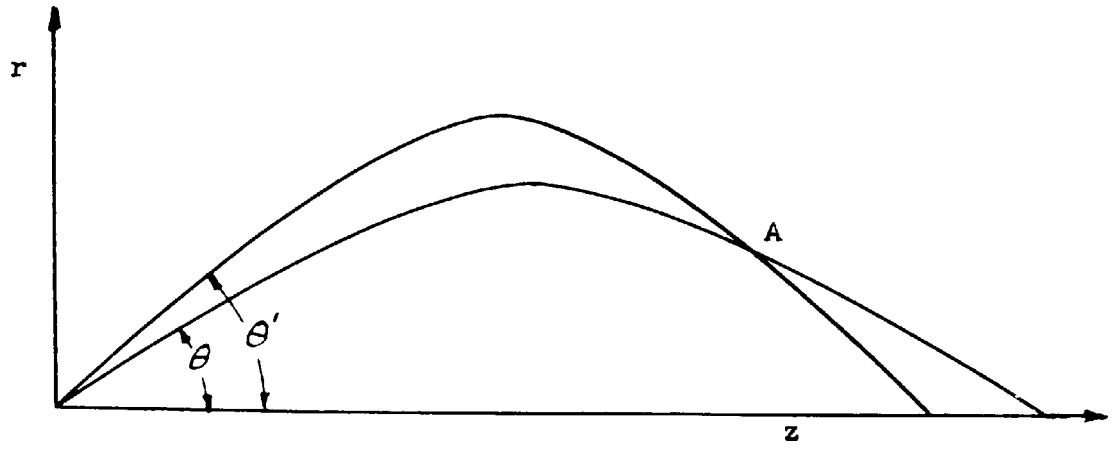
the three equations (4.1) become

$$r''\frac{(k^2 - A_\circ^2)}{1 + r'^2} - r'A_\circ\frac{\partial A_\circ}{\partial z} + A_\circ\frac{\partial A_\circ}{\partial r} = 0 \qquad (4.2)$$

where the prime denotes differentiation with respect to z, p has been allowed to go to zero, and k is mvc/e.

Equation (4.2) is the trajectory equation for an electron leaving a source on the axis in an axially symmetric magnetic field with no initial angular momentum. This equation has been numerically integrated by Keller et al.(51)for the case of the thin lens spectrometer.

Keller and his group have examined this equation for a whole range of electron momenta and for the cases of the source on the axis and slightly off the axis. One result of their data is shown in the sketch below.



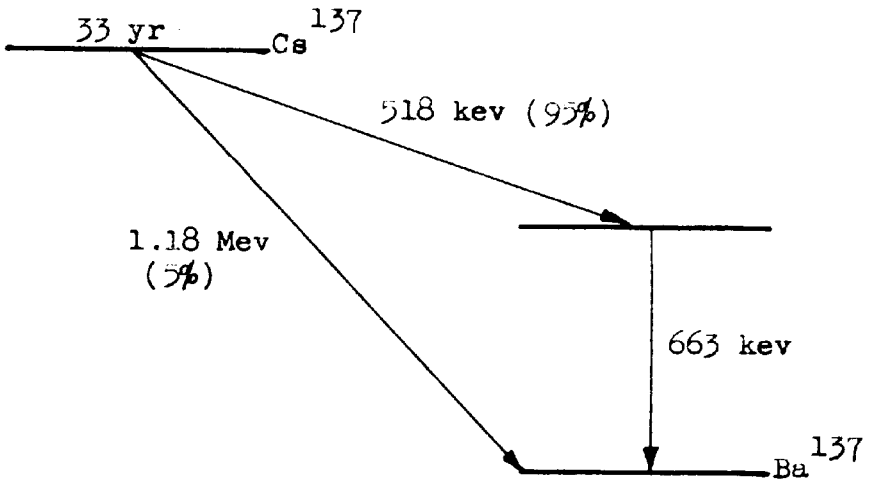
These curves represent the trajectories of two electrons of identical momentum, leaving a source on the axis at two angles θ and θ'. It will be noted that the trajectory of an electron leaving the source at the angle $\theta' > \theta$ crosses the trajectory of the electron leaving at the smaller angle, and intersects the axis closer to the source. This always occurs; the larger source angle paths always intersect the axis closer to the source and cross the trajectory of the smaller angle emission at a point in space A. Due to the axial symmetry, the points of intersection A, for a family of trajectories, form a surface in space. Any small piece, Δz, of this surface is a ring representing a small range of source angles. The effect of a larger source is to increase the "ring" area in space. Keller et al. showed that by means of proper baffles, one should be able to choose such a ring in space, and by doing so, to obtain a much more favorable transmission than would be possible for axial focusing. This result was confirmed experimentally by Pratt, Boley, and Nichols (52), who actually detected spatial rings by means of photographic film, and who, by proper baffles, improved their transmission by a factor of two over axial focusing.

Ring focusing is used in both of the component spectrometers of the instrument in this work. The actual size of the rings were determined by the previous work on the instrument of Bradley (43) (44).

Alignment and Resolution

While it should be theoretically possible to align a thin lens spectrometer purely from considerations of field shape and trajectory, in practice it is much simpler to do so experimentally. This was done here by placing a source with a pure conversion line in the spectrometer and adjusting the coils and baffles until maximum transmission and resolution occurred.

Throughout the lining up and calibration, the source used was Cs^{137}, whose decay scheme is shown below.



Cs^{137} has the following characteristics in its decay, which make it an ideal calibration and alignment element:

1) The K-conversion line of the 663 kev transition is known to high accuracy(53).
2) The K and L lines are separated from the 518 kev end-point continuous spectrum.
3) The 1.18 Mev end-point continuous spectrum contributes almost negligibly in the region of the conversion lines.
4) The 518 kev end-point continuous spectrum is well known and is forbidden. Hence, it is an excellent testing spectrum.
5) Cs^{137} can be obtained as a carrier free source.

6) The half life is thirty-three years, so that it is effectively a permanent laboratory source.

To align the coils, the K conversion line is focused onto the detector, and the coils are adjusted systematically by means of the adjusting screws until maximum transmission occurs. This is first done with the movable baffles wide open, so that they have no effect upon the line shape or transmission.

Then, when maximum transmission occurs for the open baffle setting, the movable baffles are brought closer together and begin to define an annular opening. This opening can be spatially adjusted by sliding the baffles back and forth together, along the z axis, until the point of ring focus is found, and the peak height for the conversion line is maximized. The coils are again adjusted for maximum transmission, and the whole process is repeated.

Since bringing the movable baffles closer together forms a smaller and smaller ring in space, the effect of this process is to increase the resolution with each cycle. The successive smaller annular openings transmit fewer electrons, but those which do pass the baffles more closely approximate a mono-energetic group due to the "ring focus" principle. This process was continued until the best resolution was obtained, compatible with a usable transmission. For purposes of alignment, and as a general lower limit, $\Delta p/p \approx 2\%$.

Figure 4.1 shows a family of curves of the Cs^{137} K and L conversion lines for various resolutions, adjusted to optimum alignment. The ordinate is counts per unit momentum interval per one hundred seconds, in arbitrary units, and the abscissa is coil current in arbitrary units ($\sim$ momentum).

The measurements labeling these curves designate the distance be-

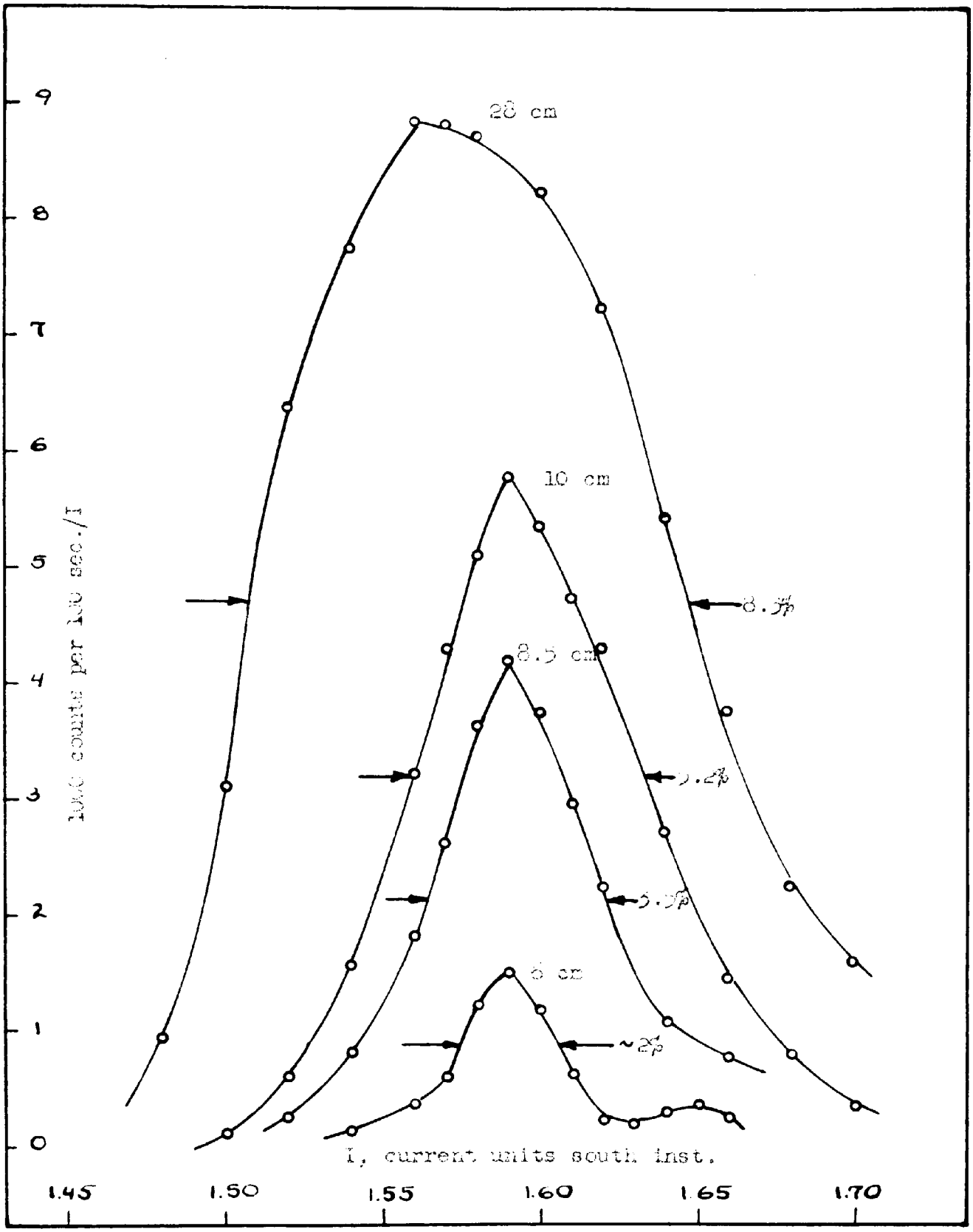


FIGURE 4.1 EFFECT OF BAFFLE SPACING ON RESOLUTION

tween measuring points outside the spectrometer chamber, and the actual baffle separation is about one centimeter less. It will be noticed that a great decrease in transmission occurs as the resolution is improved. Also, the K and L peaks are not separated until the best resolution is obtained.

There are several other factors limiting the resolution of a lens spectrometer which deserve mention at this time. These are, in addition to the finite opening of the ring focusing baffles, spherical aberration, source thickness, and source size.

The magnetic field due to the lens coils is not uniform throughout the radial range from the axis to the inside of the chamber. Therefore, electrons leaving the source at different angles will encounter different fields as they pass inside the coil and will be focused at different points. This corresponds to spherical aberration in geometric optics, and the effect is the same; a mono-energetic electron source appears spread out when measured. To a degree, this is connected with ring focusing, but it is a constant of the instrument, determined by the size and location of the angle defining baffle near the source, the chamber size, and the central scattering baffle. As mentioned previously, after the construction of this instrument, Hutchinson (44) was able to increase his resolution by increasing the size of the central ring baffle, thus narrowing the portion of the field available to detected electrons.

The ideal source for a thin lens spectrometer would be a point source on the axis. For practical purposes, this is not possible, and the effect of source size is to worsen resolution. Keller (51) showed mathematically that the effect of source size is to increase the ring focus area and cause overlap among momentum lines of different values. The size of source used will in general be a compromise between self-absorption,

specific activity, and allowably low counting rate. Dr. M. H. McGregor of this laboratory has shown that a source up to eight millimeters in diameter shows no appreciable deviation in resolution from a point source for an instrument of this type. This matter will be treated further in the section on coincidence resolution.

In general, any phenomena which tend to remove a portion of the energy from some of a set of mon-energetic electrons tends to cause a loss of resolution, due to the lower energy straggling of a measured line. Chief among the causes of energy loss is scattering within the source itself, or in any material covering the source (often used to prevent contamination of the spectrometer chamber). The thicker the source, the greater the low energy straggling, and in fact, at low energies, much actual loss of particles may occur due to complete self-absorption. The thinner the source and backing, the smaller this effect will be. In general, as in source size, a compromise must be made between what is desirable, and what is usable. This problem, too, will be discussed further in the section on coincidence measurement.

Calibration of the Beta Spectrometers

The momentum of an electron in nuclear spectrometry is usually expressed in terms of its magnetic rigidity in gauss-centimeters. This comes about since

$$p = He\rho \qquad (4.3)$$

where p is the momentum, ρ the radius of curvature of an electron in the uniform magnetic field H, and e the electron charge in e.m.u. Since e is a constant,

$$p' = \frac{p}{e} = H\rho \qquad (4.4)$$

where p' is the magnetic rigidity, and obviously $p' \sim p$. For a constant

field instrument, an absolute measurement of H combined with the measured radius of curvature serves to indicate the momentum, and has lead to the adoption of Hρ units of momentum.

In a thin lens spectrometer, H is non-uniform, and an indirect calibration is necessary. For an air core instrument such as this, the relationship between coil current and the field at any point is linear, so that a relation of the type,

$$p' = H\rho = kI \qquad (4.5)$$

(where I is coil current in terms of an arbitrary potentiometer reading) can be used. Thus it is only necessary to determine k, and a calibration of the instrument in terms of coil current will be established.

For both of the lens spectrometers used in this work, the K conversion line of Cs^{137} was used to determine k, and the line peak was used as the calibration point. Since the magnetic rigidity of these essentially mono-energetic electrons is very well measured to be 3381 gauss-centimeters (i.e. 623.8 kev = $E - E_K$), the calibration values were found from Equation (4.5).

$$k = \frac{H\rho}{I} = \frac{3381}{I} \qquad \frac{\text{gauss-centimeters}}{\text{current unit}}$$

The current unit is the arbitrary reading of the type K potentiometer across a shunt in series with the coil.

The values found for k in the two spectrometers used in this work are listed below, in Table III. In order to check the linearity of the current vs Hρ relationship, the 518 kev end-point beta spectrum of Cs^{137} was measured. This is a well known, once forbidden beta spectrum, of the "unique" type, which necessitates multiplying the Kurie plot by $a^{-1/2}$ in order to linearize the plot, where

$$a = (W_o - W)^2 + (W^2 - 1) \qquad (4.6)$$

TABLE III

CALIBRATION CONSTANTS OF THE THIN LENS SPECTROMETERS

	Current to focus Cs^{137} K-line	K in gauss-cm. per current unit
North Instrument	2.580	1310
South Instrument	1.590	2126

Figure 4.2 shows the beta spectrum and the separated K and L conversion lines. Figure 4.3 shows the Kurie plot. The correct end-point plus the linearity of the corrected Kurie plot serve to verify the $p' \sim I$ relationship. The deviation from linearity of the corrected Kurie plot at $\sim 1.4\ mc^2$ is due to absorption by the mica counter window used in this work.

The figures illustrating this check process were taken with the south instrument, but this entire procedure was followed for both beta spectrometers. From time to time, the linearity and calibration were reverified. through the use of well known conversion peaks. A few months after final assembly, the calibration constant was found to have drifted to a somewhat different value, at which it remained stable. Similar phenomena have been noted with other spectrometers of this design at this laboratory, and is probably due to mechanical sag of the instrument. This accounts for the difference in peak position between the value recorded above and Figure 4.3. The former figure is the stable value.

Correction Factors

1. Finite Resolving Power and Momentum Spectra

In order to obtain a Kurie plot, one must first determine the momentum spectrum of the emitted particles. To obtain the momentum spectrum

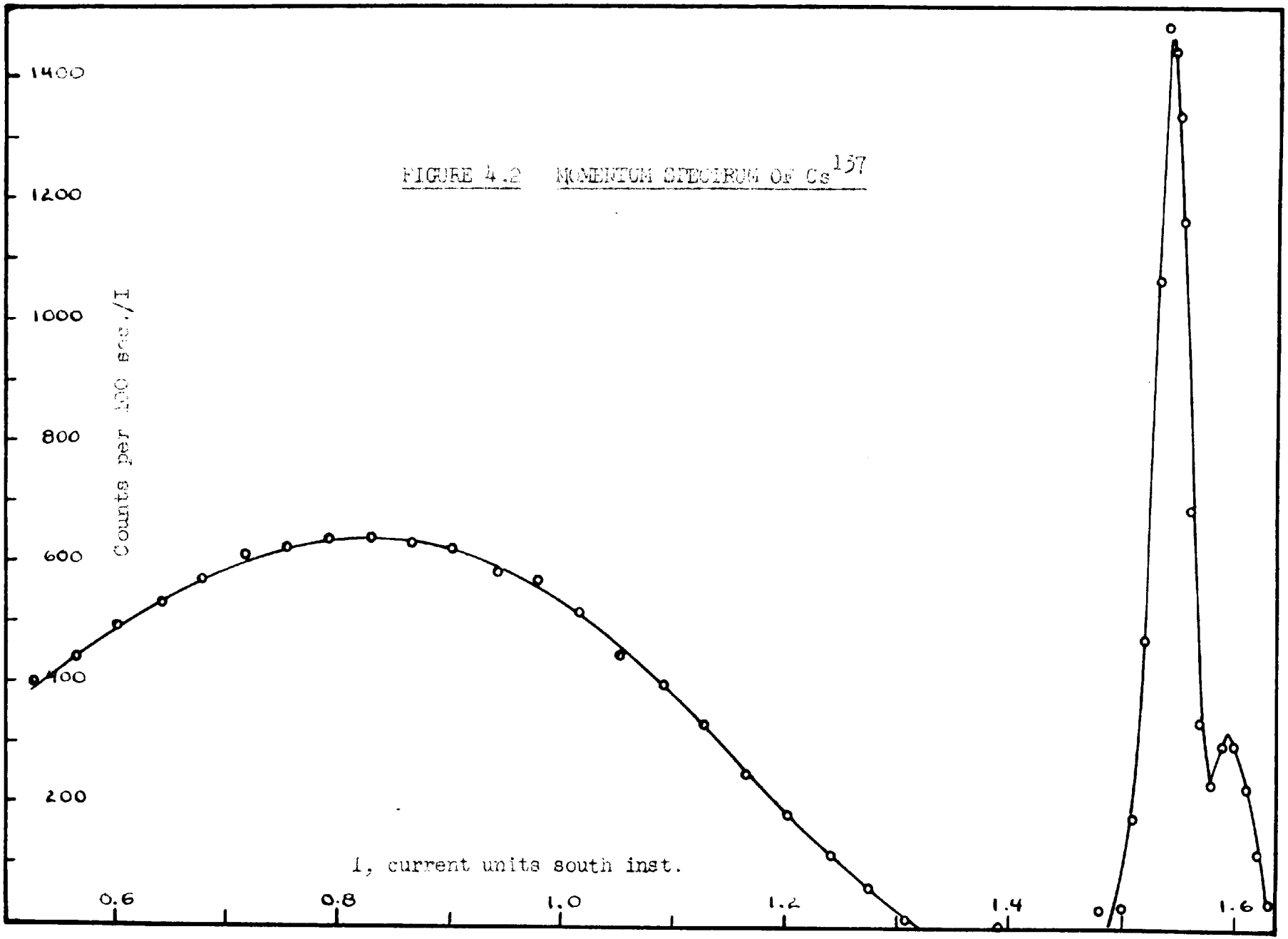


FIGURE 4.2 MOMENTUM SPECTRUM OF Cs^{137}

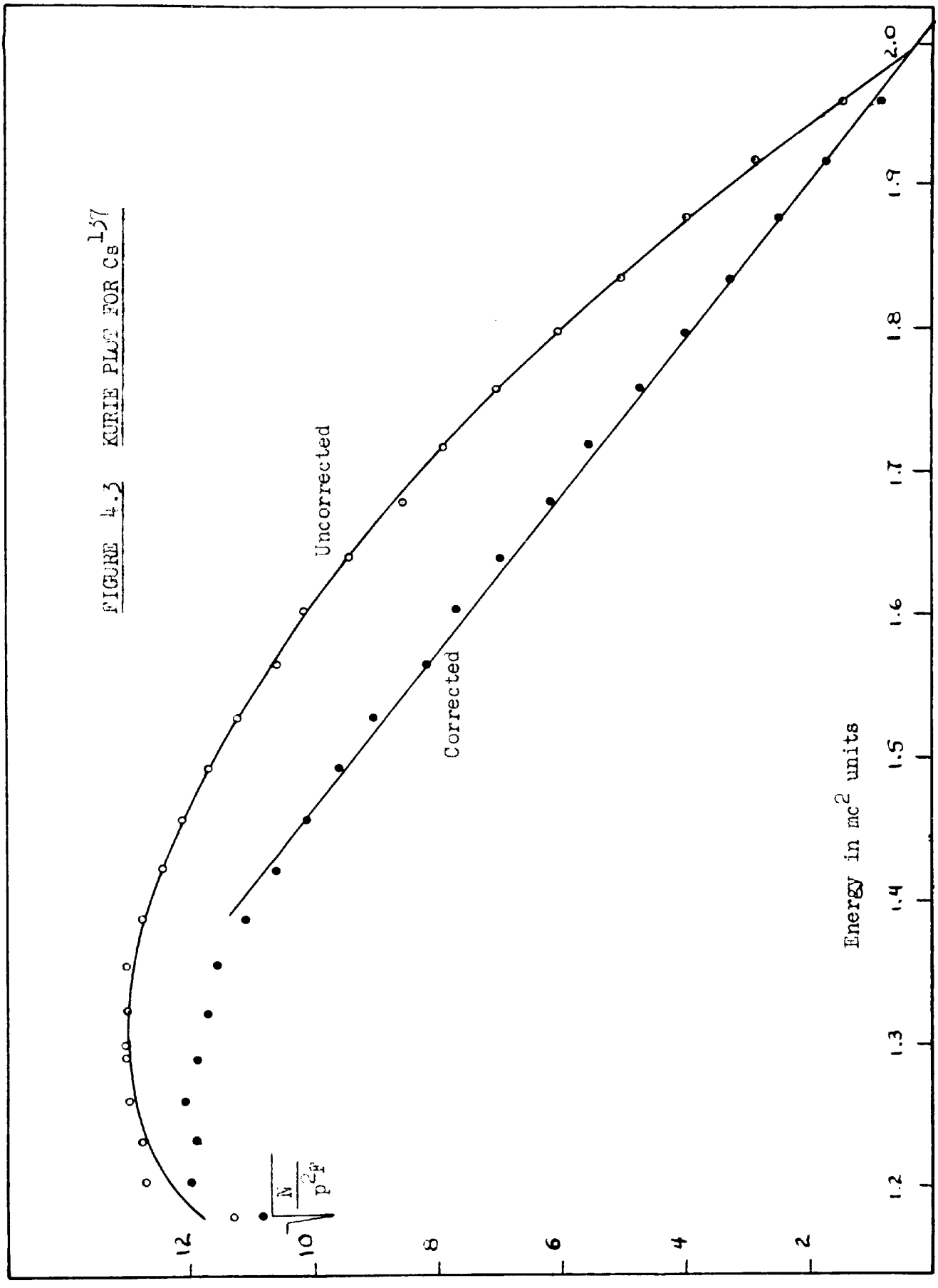
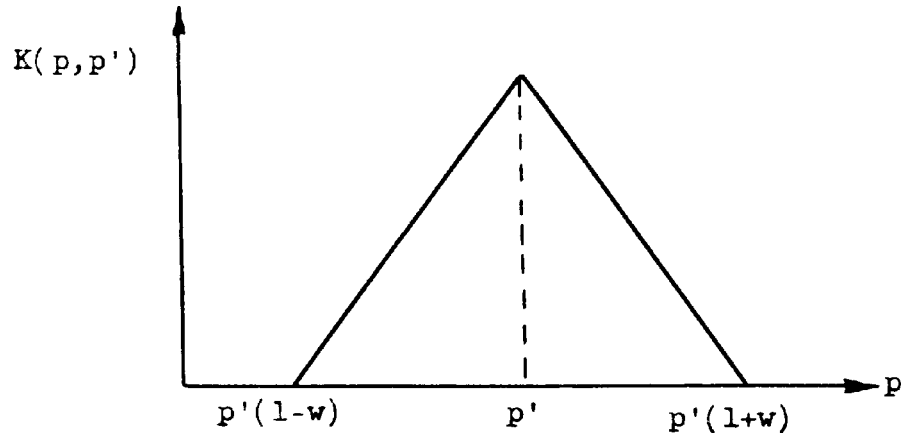


FIGURE 4.3 KURIE PLOT FOR Cs^{137}

one usually plots N(p) (particles per unit momentum per unit time) vs p (momentum), or numbers linearly proportional to these quantities. The counting rate of the detector, n(p), is not the same thing as N(p), due to the finite resolution of the thin lens spectrometer. Thus some relationship must be drawn between them.

The line shape of a pure conversion peak may be very well approximated by an isoceles triangle. Call the shape of the triangle K(p,p'), where p' is the momentum of the conversion line electrons, and p is the momentum corresponding to some current value in the coil. This is shown below.



where W is the resolution (= $\Delta p/p$ at half height) and is a constant of the instrument, as is t, the transmission. Now

$$K(p,p') = t\left(1 - \frac{1}{W}\left|\frac{p}{p'} - 1\right|\right) \qquad \left|\frac{p}{p'} - 1\right| < W$$

$$= 0 \qquad \left|\frac{p}{p'} - 1\right| > W$$

Then

$$n(p) = \int_{-\infty}^{\infty} K(p,p')N(p')dp' \qquad (4.7)$$

Equation (4.7) can be solved approximately by several methods (44) (54), with the result that, to order W^2 (54)

$$N(p) = \frac{1}{Wt}\left[\frac{n(p)}{p} + \frac{W^2}{12}\left(\frac{2n(p)}{p} + 4\frac{dn}{dp} + p\frac{d^2n}{dp^2}\right)\right]$$

Since $W \sim 2\%$, terms higher than W can be ignored, and the well-known result

$$N(p) = \frac{n(p)}{Wtp} \qquad (4.8)$$

is obtained. Since W and t are constants and $p \sim I$, then

$$N(p) \sim \frac{n(p)}{I} \qquad (4.9)$$

and a momentum spectrum results when $n(p)/I$ is plotted vs I.

In general, the dropping of terms of order > W is valid, and it is only in the case of very poor resolution that a correction need be made. In the only case in this work where such a correction would be warranted, the information desired makes it unnecessary (i.e. the coincidence spectra of the 0.7 Mev end-point beta spectrum of Eu^{152}).

2. Radioactive Decay

In the case where the element under study has a half-life of the same order as the time required to take the necessary data, a correction must be made for the radioactive decay. This is the well-known decay law

$$n = n_o e^{-.693t/T} \qquad (4.10)$$

where n_o is the original counting rate, n the counting rate after the time t, and T is the half-life. This correction has been applied wherever necessary.

3. Window Thickness and Efficiency

Throughout the data taking, 0.25 mil milar material was used, which has a cut-off at $\sim$ 10 kev and does not begin to cause any real counting loss until $\sim$ 110 kev. In general, this will not affect any of the measurements quoted here, and for coincidence work at low energies, ratios will be used which eliminate this factor.

The counters used here can be considered one hundred percent efficient for electrons.

4. Corrections for Counter Dead Time

The counters used in this work have a dead time of the order of two hundred microseconds, and any particles entering them within this period would not be counted. The correction for this type of loss is (55)

$$R = R'/(1-R't_o)$$

where R' is the observed counting rate, R the true counting rate, and t_o is the dead time. Dead time losses were not appreciable in this work.

CHAPTER V

THE THIN LENS COINCIDENCE SPECTROMETER

The use of two thin lens spectrometers in coincidence (henceforth referred to as the thin lens coincidence spectrometer) presents certain characteristics and imposes certain limitations upon the uses of the instrument, not normally encountered in the component spectrometers proper. It is, therefore, worthwhile to discuss these characteristics in some detail.

Coupling

The geometric arrangement of the component spectrometers is such that the individual fields from the separate coils couple with each other. That is to say, when one of the spectrometers is set so as to focus electrons of a certain momentum upon its detector, and the other spectrometer is then turned on, the field of the latter may add to or subtract from the field of the former, so that electrons of a different momentum will be focused. It is this phenomena which we shall refer to as coupling.

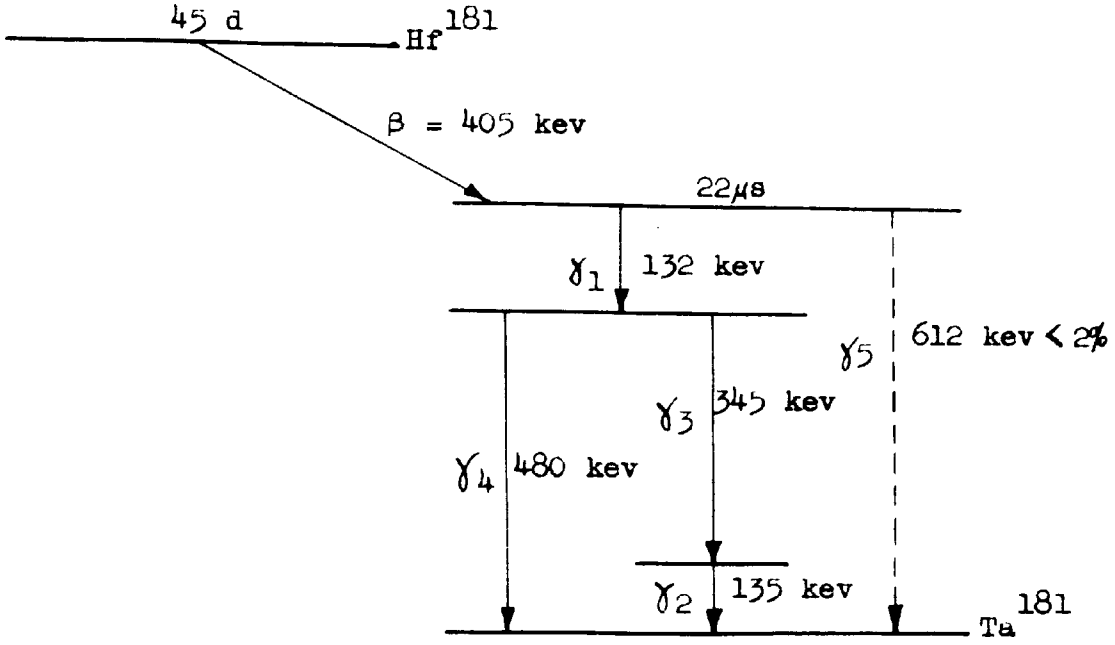
The coupling between the component instruments used here was $\sim 1\%$. It was compensated experimentally in the following manner. The desired current setting was made in the north instrument (for example) with the south instrument off. Then the south instrument was turned on, and the current in the north instrument was readjusted until its original counting rate was reestablished. This had to be done for both instruments before taking data and was quite simple in practice.

After the construction of this instrument, we learned of the existence of similar thin lens coincidence spectrometers in Canada and in the U.S.S.R. The former instrument had $\sim 6\%$ coupling, and the details of the latter are unknown to us (56) (57).

Coincidence Resolution

The first coincidence work done on this instrument concerned the spectrum

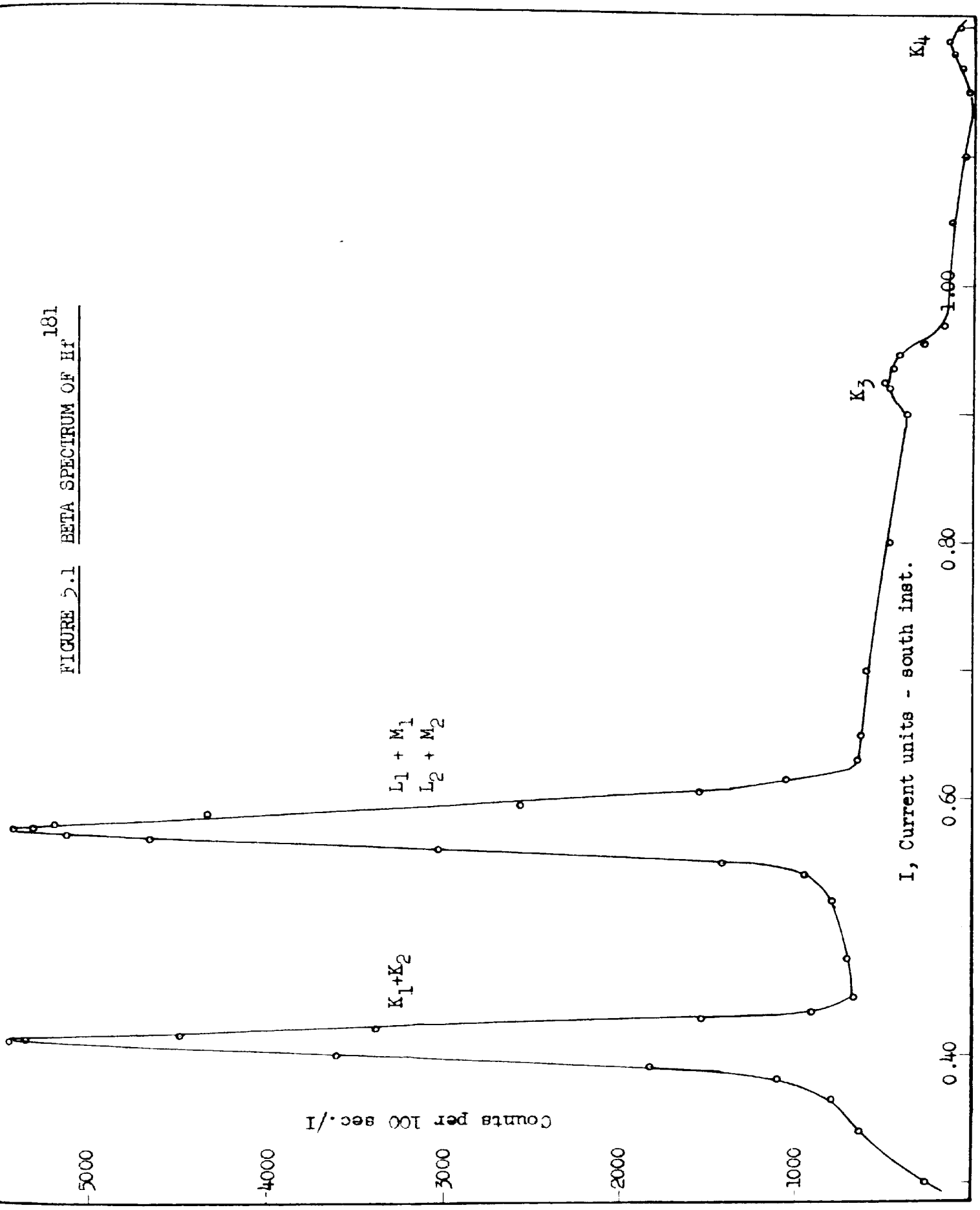
of Hf^{181}. The decay of Hf^{181} was first described in detail by Cork (58), and Wiedenbeck and Chu (59), who assigned a decay scheme of the following form to it.



The beta spectrum of this element is as shown in Figure 5.1, with the conversion peaks labeled. The resolution $\approx 2.5\%$.

Coincidence data was run with the coincidence spectrometer by focusing one lens spectrometer on the K_1K_2 peak and sweeping across the L_1L_2 peak with the other. Then the K_1K_2 peak was swept across with the fixed spectrometer as before. The results of these runs are shown in Figures 5.2 and 5.3. The solid curves represent the coincidence peaks, while the dotted curves represent the conversion lines which were swept across. Due to the twenty-two microseconds excited state, these coincidence peaks are independent of the beta spectrum. The coincidence data is normalized to the fixed peak (i.e. number of coincidences per fixed peak count). No correction is made here for window thickness, counting rate, etc., since the measurements are relative. This work served as a recheck of a portion of Shreffler's work (37), and confirmed that the γ 1 and γ 2 are in cascade.

FIGURE 5.1 BETA SPECTRUM OF Hf^{181}



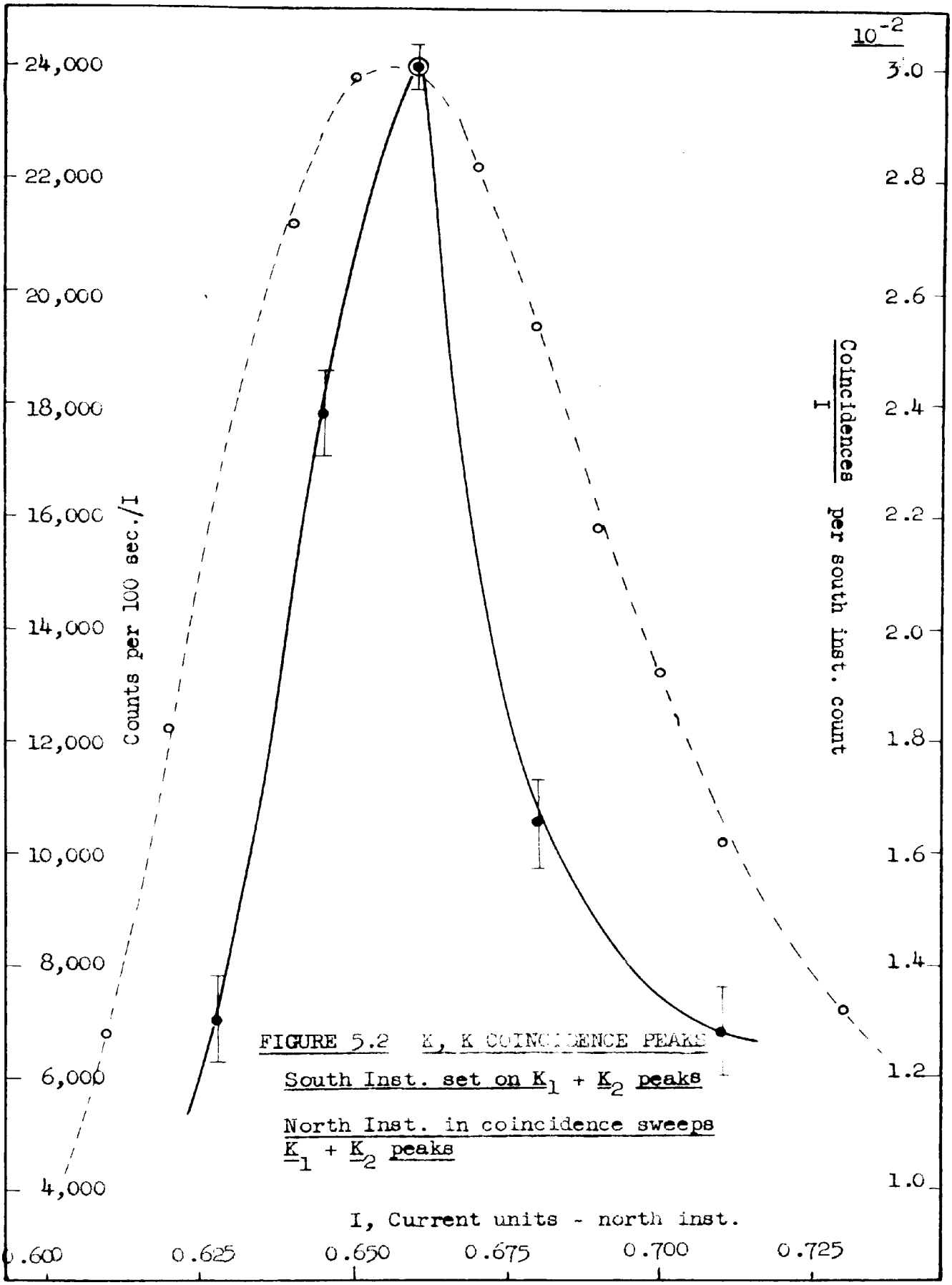


FIGURE 5.2 K_1, K_2 COINCIDENCE PEAKS

South Inst. set on $K_1 + K_2$ peaks

North Inst. in coincidence sweeps $K_1 + K_2$ peaks

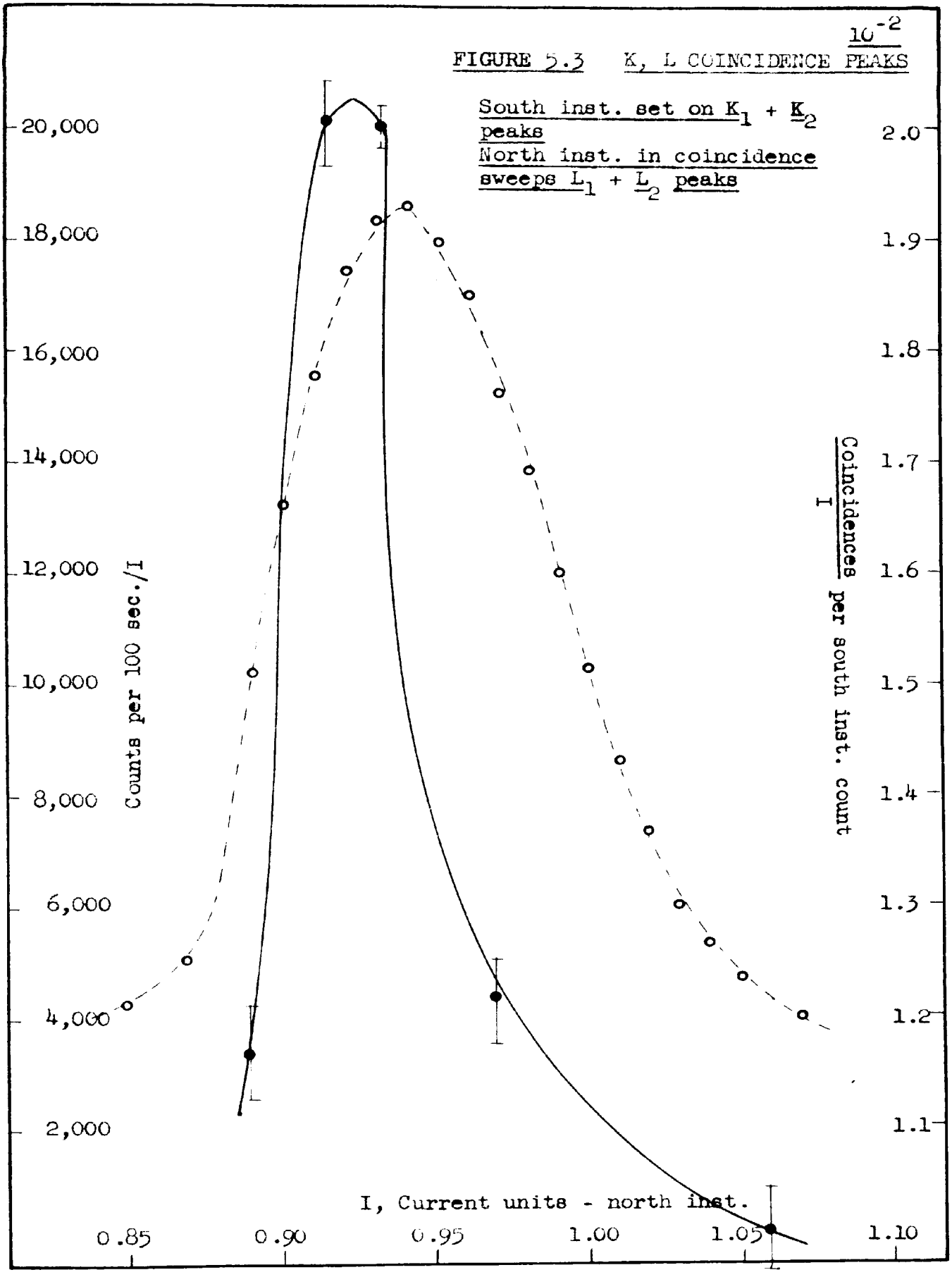


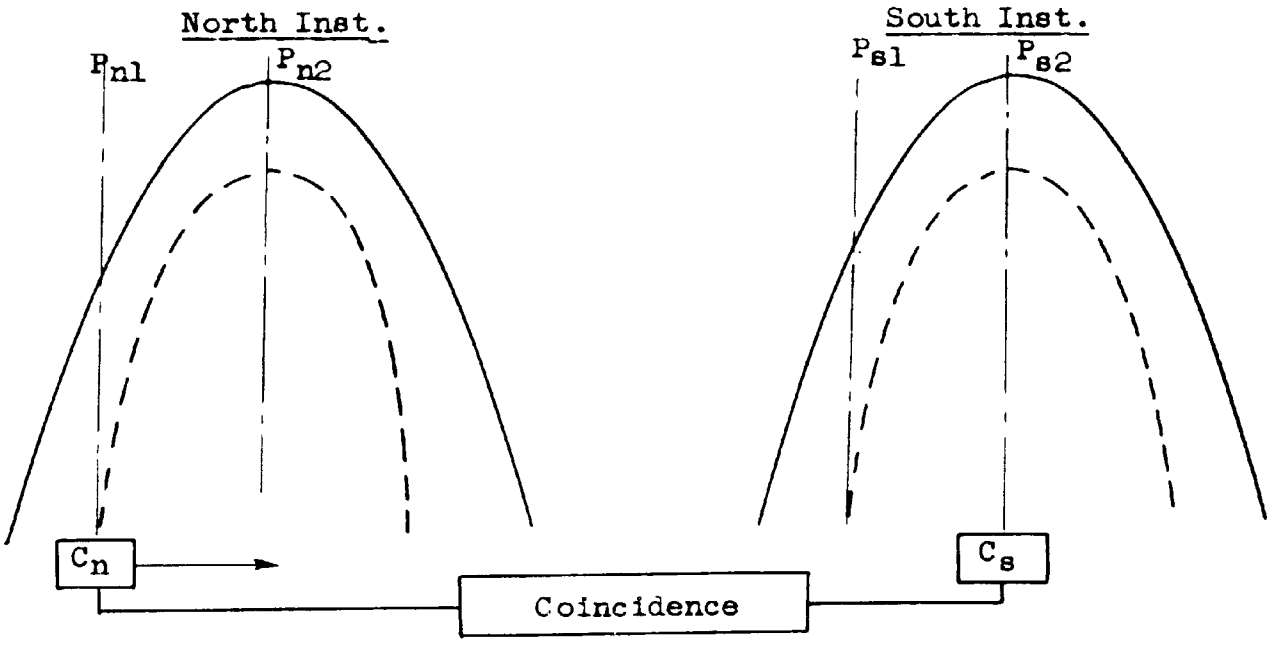
FIGURE 5.3 K, L COINCIDENCE PEAKS

The most striking thing about the coincidence peaks with respect to the normal momenta peaks is the greatly improved resolution (> a factor of two in Figures 5.2 and 5.3). This is not entirely unexpected, since Fowler and Shreffler noticed a similar phenomena in their work. An explanation can be offered in terms of 1) source size and 2) source thickness.

1) Unfortunately the argument concerning the effect of source size on coincidence narrowing is largely intuitive, since one can not integrate the equations of motion of the electron paths. (After considerable effort, Keller et al. (51) were able to predict resolution, but not line shape.)

Figure 5.4 shows the effect of source size on resolution, using the Cs^{137} K and L peaks. Both sources had about the same total activity and differed only in size, one being four millimeters across, the other twenty millimeters. Sources as large as twenty millimeters were never used in data taking, and some of the abnormality of its line shape may be due to scattering; the important feature, however, is its relative broadening.

Keeping this in mind, let us examine the manner in which coincidence data is usually taken. Shown below, schematically, are two peaks, repre-



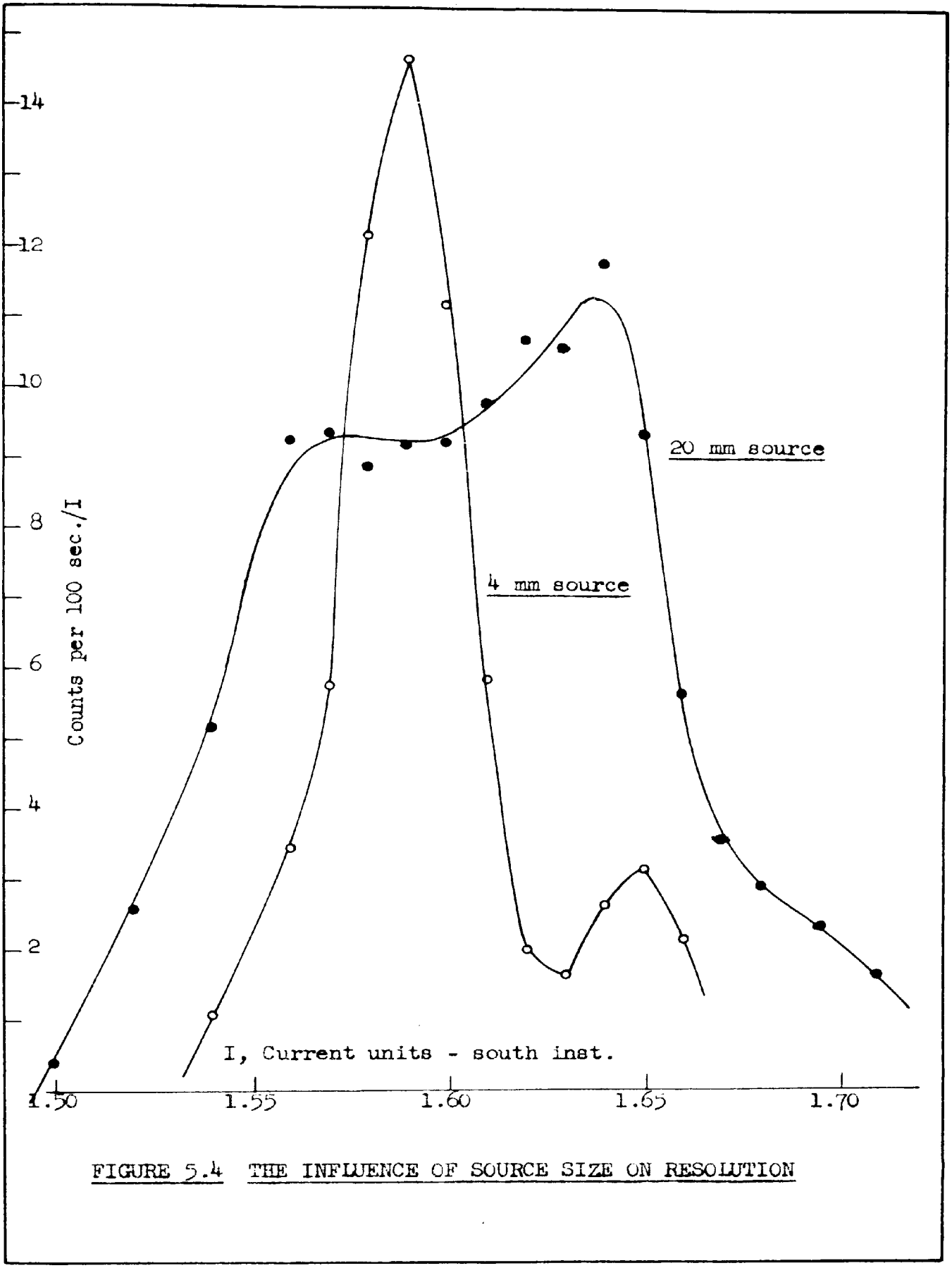


FIGURE 5.4 THE INFLUENCE OF SOURCE SIZE ON RESOLUTION

senting coincident conversion electrons, as seen by the individual spectrometers. The dotted peak is a coincidence peak. C_s represents the position of the fixed counter on point P_{s2} of the spectrum as seen by the south instrument. Actually one should now integrate over the contribution of each infinitesimal portion of the source to the individual line shapes. Since this can not be done by the means available, let us assume that the outer parts of the source contribute most to the wings of the individual peaks, and that the central portion of the peak contains contributions from the central (on axis) portions of the source as implied by Figure 5.4. This being the case (remembering that true coincidences can only come from the same nucleus), the counter C_s will be more likely to detect true coincidences with C_n when the latter is at position P_{n2} than at P_{n1}, simply because the coincident electron will be more likely to be there. (Relatively more coincidences would be expected with C_s at P_{s1}.)

The total result of this effect will lead to a narrowing of the coincident peak as shown by the dotted curve. The magnitude of the narrowing will, of course, depend upon the original resolution of the individual spectrometers, with greater narrowing to be expected for finer resolution. With poorer individual resolution, each detector would see more of the line, and one would expect less narrowing. Fowler (36) and Shreffler (37) have actually performed the integration over the contribution of various parts of the source to coincidences, for the case of a 180° spectrometer, and find the effect mentioned above. Though the trajectories are quite different, similar effects would be expected in the case of the thin lens coincidence spectrometer.

2) Source thickness also contributes to the narrowing of the coincidence peak. A true coincidence comes about only from events originating in the same nucleus. In order to be recorded as counts by the individual

detector, the electrons must, between them, traverse the entire source. Hence a fairly large number of electrons might be expected to be scattered. The effect of scattering is to broaden the individual peaks by the shifting of electrons to lower energy (ignoring self-absorption).

Coincidence scanning would be expected to reject a portion of the scattered electrons and bring about narrowing in this fashion. The likeliest case one would expect to encounter would be where both electrons are scattered somewhat. Let us say they are scattered to positions P_{nl} and P_{sl} in the sketch above. In that case, while C_n might see the electron at P_{nl}, C_s would not detect the electron at P_{sl}. This argument leads to a rejection of a portion of the scattered electrons and hence a narrowing of the coincidence peak.

Source thickness will be discussed in greater detail in the section concerning the limitations of the thin lens coincidence spectrometer.

The Hf^{181} coincidence peaks were run with the movable baffles wide open, in order to receive as many singles counts as possible. While a large number of coincidences are rejected, for the reasons stated above, the improvement in counting rate was sufficient to warrant this practice.

Coincidence Data and Corrections

Throughout this work, coincidences are always considered with respect to a fixed point. Thus all measurements are relative. As an example, the Hf^{181} coincidence data plotted in Figures 5.2 and 5.3 represent the number of coincidences at the "scanning" detector, divided by the number of counts at the "fixed point" counter.

All of the work on $Eu^{152,154}$, concerning the coincidences between peaks, was done by computing the number of coincidences per fixed point count. This was done at the peak and on either side of it (where measurable), and then the data was compared with the fixed peak interchanged.

In each case, a coincidence should be indicated, if existent. In the case of the coincidence beta spectrum, the method is obvious from examination of the Kurie plot.

The only correction, other than accidentals, to the true coincidence counts would be the correction due to large air showers caused by cosmic rays. Due to the small counter volume and large counter separation, one would expect the effect to be small. This phenomena was measured over a two day period, and a total of two coincidence counts were recorded. This was the same as the number of accidentals to be expected from the individual counter background counts. Thus no correction for cosmic ray effects were thought necessary.

Limitations of the Thin Lens Coincidence Spectrometer

Some discussion of the limitations of the instrument constructed and used in this work seems warranted at this point.

The solid angle of the individual spectrometers is rather limited (~0.3%). Since the true coincidence rate depends on the solid angle squared (Equation 3.5), this severely limits the rate at which data can be taken. Combined with effects due to the source, which are described below, this makes the taking of data a tedious process. An example may be furnished from the Hf^{181} case.

South Instrument	North Instrument	Total Coincidences	Time
27,713 x 256 counts	21,741 x 256 counts	2004 counts	33,600S

These are extremely favorable data, measured at an optimum point. There are few conversion lines as strong as the Hf^{181} K and L lines due to the 134 and 136 kev gamma rays. In general, data taking is much slower than this, and over twenty-four hours may be required to obtain 15% statistics.

One might expect that by going to stronger sources, and using a faster

detecting device (such as scintillation detectors), the taking of data might be hastened. This would be true only in certain special cases where highly active sources, with ideal conversion lines, could be put into a suitable form to constitute a usable source.

In the work done with this instrument, the activity and chemical or physical form of the sources seem to be the limiting factors. Unless the source can be put into such chemical form as to permit precipitation in an extremely thin source, or so fine as to be evaporated from a suspension, self-absorption in the source will prohibit the taking of data. In the course of this work several elements had to be rejected, either because of insufficient activity, or because a thin enough source could not be made. In addition, the requirement of thinness limited the total activity of the source; in many cases it became necessary to dilute the source to make it thinner. For this reason, it seems unlikely that going to faster detectors in order to use stronger sources would prove worthwhile. While the increased total activity would be expected to decrease the time necessary for taking data, unless the specific activity were extremely high, it is likely that the added thickness of the material would actually decrease the coincidence rate.

As an example, Professor J. M. Cork of this university made available to the author a quantity of Ir^{192}. This source was highly active, but in the form of a metallic powder. Since iridium has about the same chemistry as platinum, it is almost impossible to put into solution. Its boiling point is $> 4500°F$ so it could not be deposited by vaporizing, and the individual grains were too large to permit convenient precipitating from suspension. The latter was tried, but due to self-absorption, the source proved too weak (coincidence-wise) to use.

Unless an active source with good conversion lines can be obtained, which is capable of being made into a thin source, it will prove extremely difficult to collect data with a thin lens coincidence spectrometer.

Uses

Once the limitations upon the source have been met, the thin lens coincidence spectrometer is excellent for certain types of work.

Where suitable conversion lines exist, good resolution gamma-gamma coincidences can be done. Also unambiguous beta-gamma coincidences can be measured, and in fact, the coincidence beta spectra may be plotted to determine the end-point of the beta involved.

It is possible to do unambiguous delayed coincidence measurements (56) to determine the lifetime of isomeric states. In this case, the use of scintillation counting techniques might be advantageous to measure lifetimes $< .25$ microseconds, even if considerations of source strength would not warrant it.

Using an instrument of this type, it should be possible, in certain cases, to measure the ratio of K-L conversion coefficients of gamma rays whose peaks are obscured by other lines. Suppose we have three gamma rays, $\gamma_1\gamma_2\gamma_3$, where γ_1 and γ_2 are in coincidence, but neither is in coincidence with γ_3. Further let us assume that the K and L peaks of γ_1 and γ_3 overlap. Then if coincidences are measured between the K and L lines of γ_1, and say, the K line of γ_2, the coincidence rates will be, for the two K lines

$$n_{K1,K2} = N\omega_N\omega_S\alpha_{K1}\alpha_{K2}f_2 \qquad (5.1)$$

and

$$n_2 = N\omega_N\alpha_{K2}f_2 \qquad ((5.2)$$

where N is the source strength, n_2 is the single counting rate for γ_2,

ω_N is the solid angle for the instrument measuring n_2, ω_S is the solid angle for the other instrument, α_{K1} AND α_{K2} are the respective K conversion coefficients, and f_2 is some factor lumping counter efficiency, etc. Then

$$\frac{n_{K1K2}}{n_2} = \alpha_{K1}\omega_S \qquad (5.3)$$

Similarly:

$$\frac{n_{L1K2}}{n_2} = \alpha_{L1}\omega_S \qquad (5.4)$$

Ignoring any considerations of momentum spectra (i.e. division by I)

$$\frac{\text{Equation } (5.3)}{\text{Equation } (5.4)} = \frac{\alpha_{KL}}{\alpha_{L1}}$$

from which the multipolarity of an obscured gamma ray might be measured.

CHAPTER VI

THE DECAY OF Eu^{152} AND Eu^{154}

Natural europium contains two isotopes, Eu^{151} (47.77%) and Eu^{153} (52.23%), which when subject to thermal neutron bombardment go to Eu^{152} and Eu^{154} respectively, by (n,γ) reaction. Eu^{152} decays with two lifetimes. There is a 9.2 hour decay, which has been examined by Tyler (62) and Hill (63), and which seems fairly well understood. In addition, Eu^{152} exhibits a second lifetime of the order of years, as does Eu^{154}. These lifetimes have been examined mass spectrographically, and by other means, with results ranging from five to sixteen years (64) (65) (66). The lifetimes are listed below according to experimenter.

TABLE IV

HALF-LIFE MEASUREMENTS FOR Eu^{152} AND Eu^{154}

Experimenter	Eu^{152}	Eu^{154}
Hayden, Reynolds and Inghram	5.3 yrs.	5.4 yrs.
Karaker, Hayden and Inghram	13 ± 2 yrs.	16 ± 4 yrs.
Lockett and Thomas*	12.4 ± 0 4 yrs (?)	7.5 (?) yrs.

The radioactivity of the long-lived $Eu^{152,154}$ was first examined by Cork, Shreffler, and Fowler (67), who noted many of the conversion electrons by means of a 180° spectrometer. A careful examination of the momentum spectrum was made by Shull (68), using a magnetic double focusing spectrometer of excellent resolution. Fowler also examined the $Eu^{152,154}$ decay by measuring coincidences between conversion lines using the instru-

*The isotopic assignment of the 12.4 year half-life is not completely certain; the 7.5 year figure is fairly uncertain as to magnitude.

ment previously described (36). He found that coincidences existed between the 123 kev and 344 kev, and the 244 and 122 kev lines. Considerable additional work was done by Cork's group, accurately measuring the line energies and proposing decay schemes (69) (70). In addition, Shavtvalov (57) noted coincidences between the ~0.7 Mev end-point beta spectrum and a conversion line he assigned to the 336 kev gamma ray; also Katz (71) made certain isotopic assignments to the gamma rays in disagreement with the coincidence work of Fowler (i.e. 123 kev to mass 154, and 344 to mass 152).

Up until the present writing, the state of the $Eu^{152,154}$ long-lived decay may be summarized by saying that while at least two beta decays were known to occur from the mixture, and at least ten gamma rays had been noted, no sound decay scheme existed. The gamma energies usually assigned are, in kev, 122, 123, 244.3, 336.4, 344, 720, 778, 964, 1086, and 1116. In addition, Shull finds a 412 line, and, by means of a photo source, a 1402 line. In the present work, the beta decay was examined, conversion lines measured, and coincidences sought between conversion lines and conversion lines, conversion lines and beta spectra, and between the gamma rays.

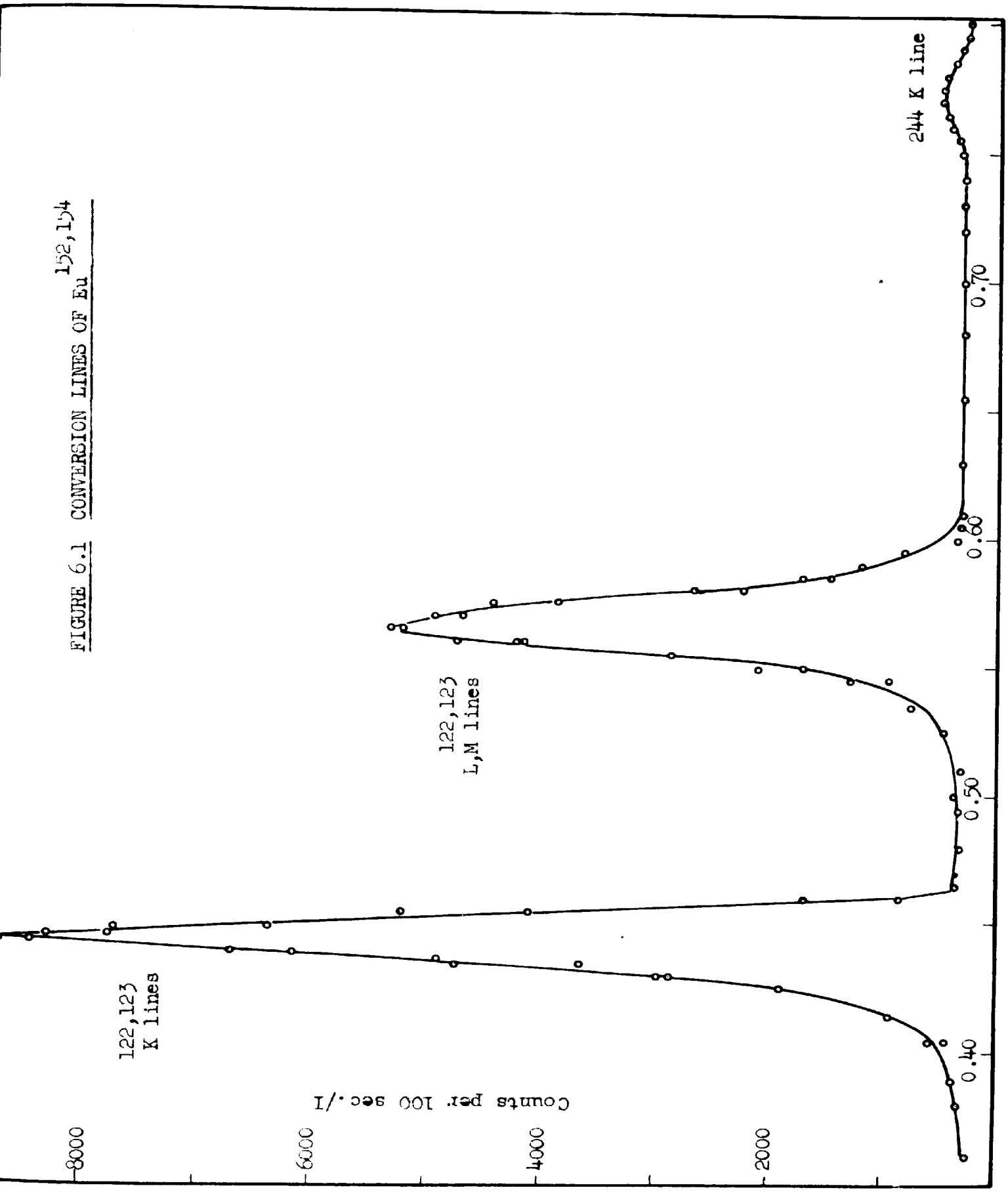
Source Preparation

The $Eu^{152,154}$ used in this work was kindly provided by Professor J. M. Cork of this university, and is the remaining portion of the material used by Shull, Fowler, and Cork. Hence it is at least five years old, and the 9.2 hour lifetime may be considered to have completely decayed.

This europium was in the form of an oxide powder, which was put into solution by dissolving in distilled water, made acid by a drop of HCl. (Europium is not appreciably soluable in non-acid solution.)

The sources used in this work were prepared by evaporating the $Eu^{152,154}$ solution thus obtained onto a double layer of zapon backing (~0.034 mg/cm^2), and then covering the source with a similar zapon sheet to prevent contami-

FIGURE 6.1 CONVERSION LINES OF $^{152,154}Eu$



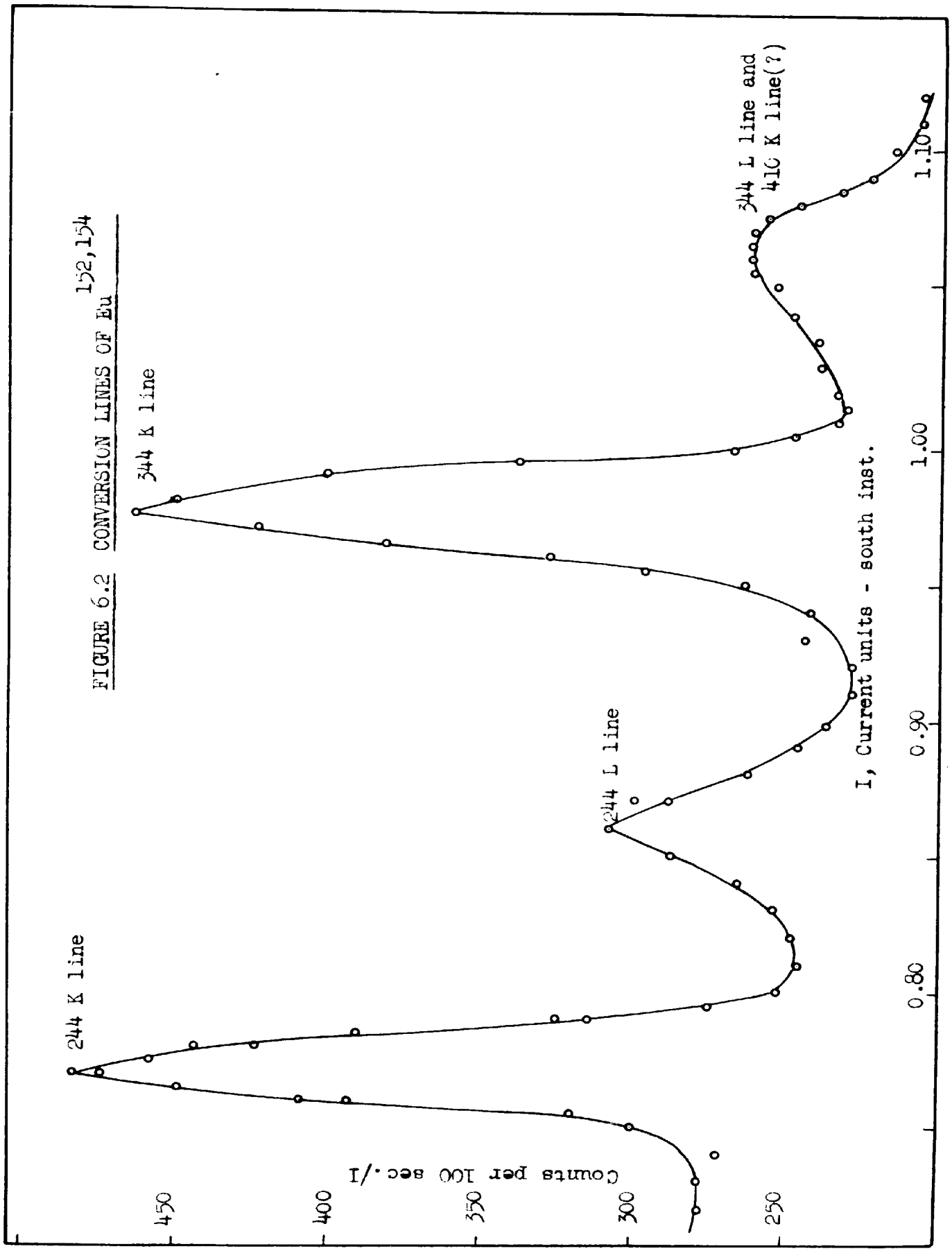


FIGURE 6.2 CONVERSION LINES OF $^{152,154}Eu$

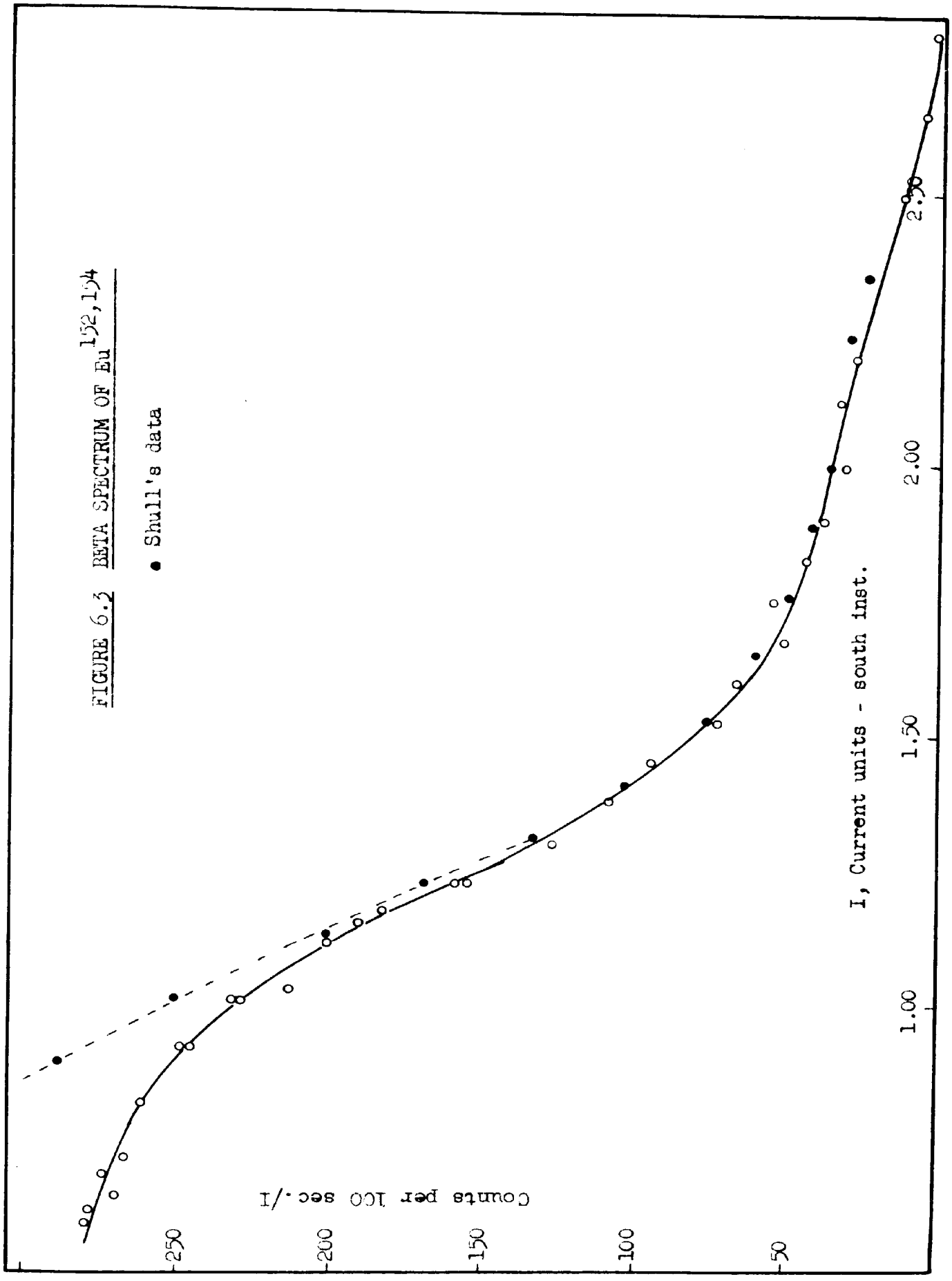


FIGURE 6.3 BETA SPECTRUM OF $Eu^{152,154}$

nation of the tube. Evaporation of the source was accomplished under a heat lamp while being manually rocked, in order to obtain as thin a source as possible. Two sources were prepared: a weaker source ~ 1 cm. in diameter, which was used to determine the momentum spectrum, and a strong thin source ~ 1.7 cm. in diameter used for coincidence work.

Beta Spectrum

The beta spectrum of the $Eu^{152,154}$ mixture was measured using the south instrument. The resolution was 2.2%, as determined by the K line of Cs^{137}.

Figure 6.1 shows the partial momentum spectrum with the conversion lines identified, Figure 6.2 shows just the smaller amplitude conversion lines, and Figure 6.3 the beta spectrum alone. Due to the large differences in peak height, it is necessary to break up the plot in this fashion. The 244 K-peak is included in Figure 6.1 to illustrate the relative heights.

Included in the beta spectrum shown in Figure 6.3 are a series of points normalized from Shull's data. It will be noted that the lower energy beta spectrum seems to have decayed considerably. This indicates that the relative lifetimes as represented by 5.3 and 5.4 year half-life estimates are probably in error. With this in mind, a careful examination of the 244 and 344 kev conversion peaks was made, in order to compare their areas with Shull's data. In this fashion, it was hoped that some information might be obtained as to which beta decay they accompanied. No attempt was made to do this for the 122 and 123 lines due to the large amount of scattering "tail" in Shull's data. Unfortunately the higher energy peaks do not appear to be completely defined in this work, and possibly due to this and to scattering in some of Shull's peaks, no real conclusions could be drawn. Final conclusions are left to the coincidence

work.

The values found for the peaks shown are listed on the drawings, and agree with the previously measured values within the uncertainty of this work. For the only clean lines, the values of 244.0 kev and 344.3 kev were found. (Cork et al. find values of 244.3 kev and 343.8 kev respectively.)

Figure 6.4 shows the Kurie plot for the beta spectrum. The high energy end-point is 1.45 ± 0.05 Mev. This is somewhat lower than the previously measured value of 1.575 ± .15 (Shull) and 1.58 (Hill and Shepherd (63)). The lower energy end-point is measured here as 700 ± 30 kev, again lower than previous values. Furthermore, there appears to be the possibility of a weak lower energy line. This last beta decay must be classified as doubtful, since a second Kurie plot subtraction leads to vastly enlarged errors, and in addition, the region over which it is measured contains many conversion lines, with the accompanying possibility of scattering. In order to minimize this scattering, the beta spectrum has been plotted in this region exclusively from points close to the high energy edge of conversion lines. This third beta spectrum has an end-point of 330 ± 100 kev.

Coincidences between the Beta Spectra and the Conversion Lines

In order to take coincidence measurements, the weaker source used in the preceding work was replaced with the stronger one described above.

No coincidences were observed between either the 122 and the 123 L peaks and the continuous beta background due to the 0.7 and 1.4 Mev end-point betas. The L conversion peak was used rather than the K in order to reduce self-absorption of the lower energy K peak electrons. (This practice was followed throughout for these lines.) This is in agreement with the work of Shavtvalov (57).

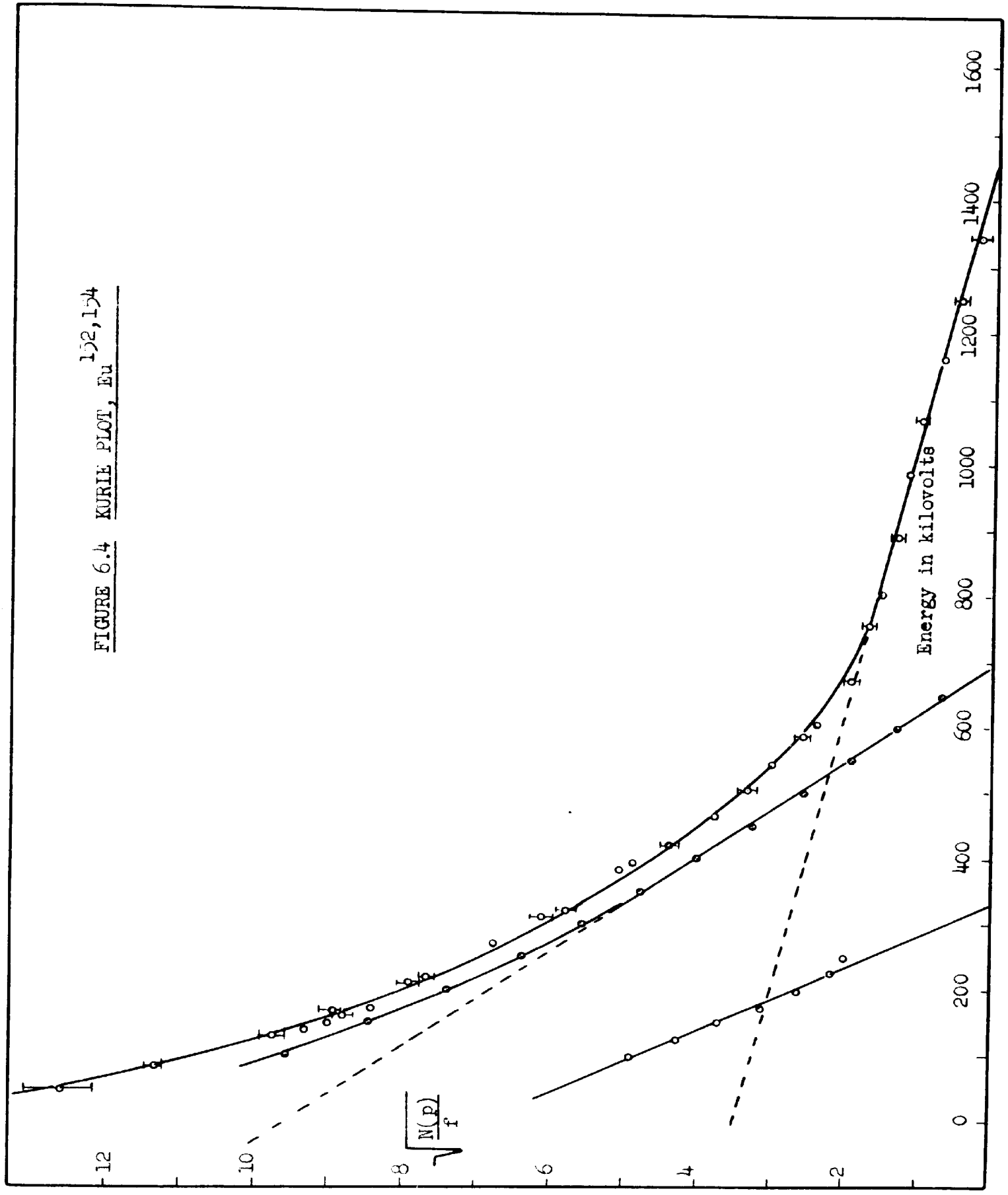


FIGURE 6.4 KURIE PLOT, $Eu^{152,154}$

No coincidences were found between the 244 K line and the beta background, due to either of the two higher energy end-point beta spectra.

Coincidences were found between the 344 kev K conversion peak and the continuous beta spectrum of 0.7 Mev end-point. The beta spectrum was plotted by coincidence measurements and is shown in Figure 6.5. While the uncertainties in the individual points are large, the result appears unambiguous. The coincidence rate for this data was rather slow, and running times up to 62,000 seconds were required for each point. Figure 6.6 shows the Kurie plot for this spectrum. The end-point is ~700 kev. For a beta spectrum of this type, taken with the baffles wide open, a resolution correction would normally be made. The correction for resolution would be small, and since the beta component involved is unambiguous, no correction has been made.

Shavtvalov found similar beta-gamma coincidences, which he assigned to a 336 kev gamma ray. A careful examination of the data of Shull (available at this university) shows no evidence at all that any such line is converted with reasonable intensity. Such a line would appear as a hump on the low energy edge of the 344 K-conversion peak in Figure 6.2, if it were at all intense. Therefore the beta-gamma coincidence assignment is made as described above, to the 344 kev line.

It is not possible to measure coincidences with the lowest energy end-point beta spectrum, since the conversion lines would overlap it at the resolution used.

Coincidences between Conversion Peaks

In agreement with Fowler (36) and Katz (71), no coincidences were noted between the 122 and 123 kev K or L conversion peaks, or between the 244 and 344 K conversion peaks. In agreement with both authors, coincidences were found between the K conversion peaks of the 122 or 123

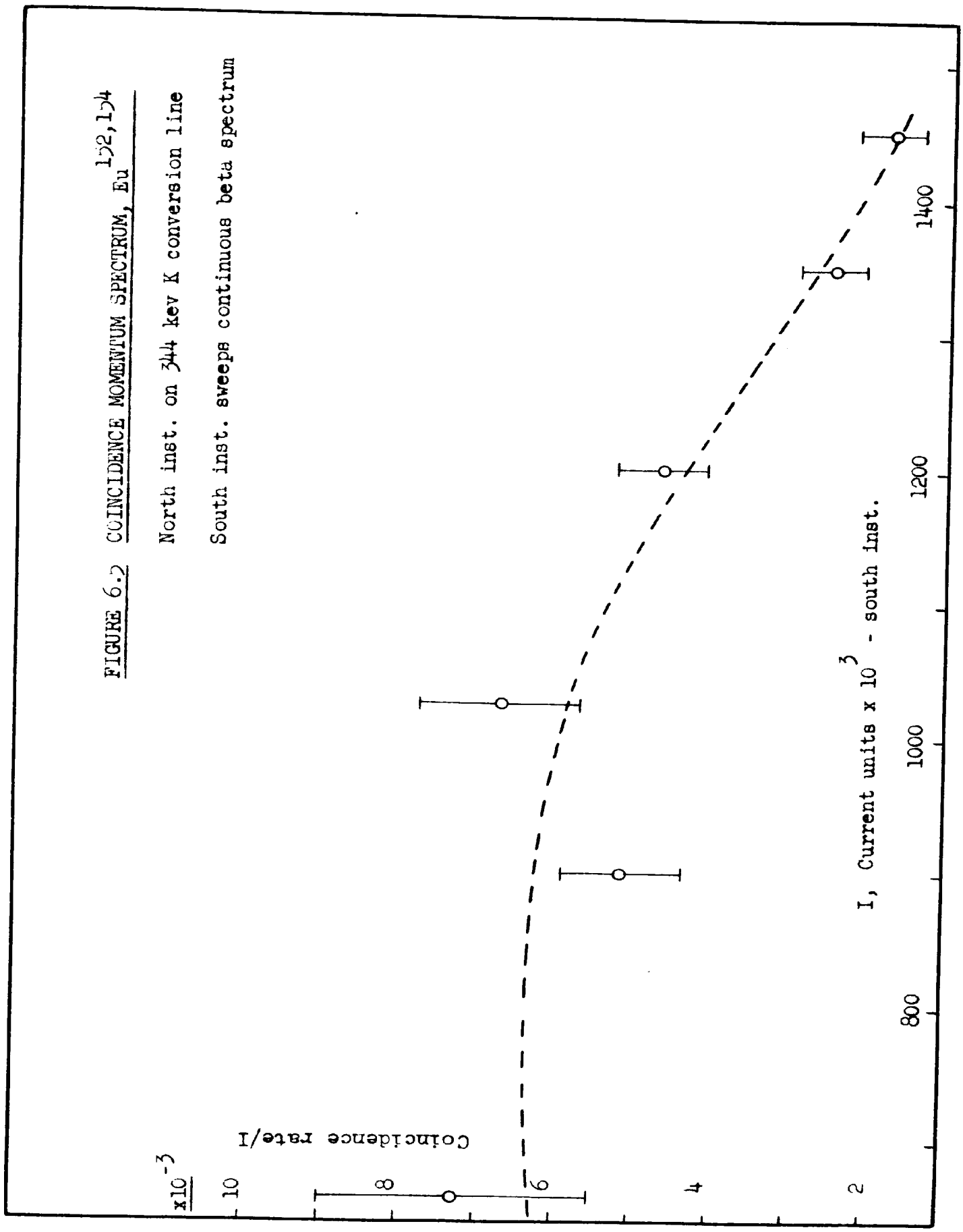


FIGURE 6.2 COINCIDENCE MOMENTUM SPECTRUM, $Eu^{152,154}$

North inst. on 344 kev K conversion line

South inst. sweeps continuous beta spectrum

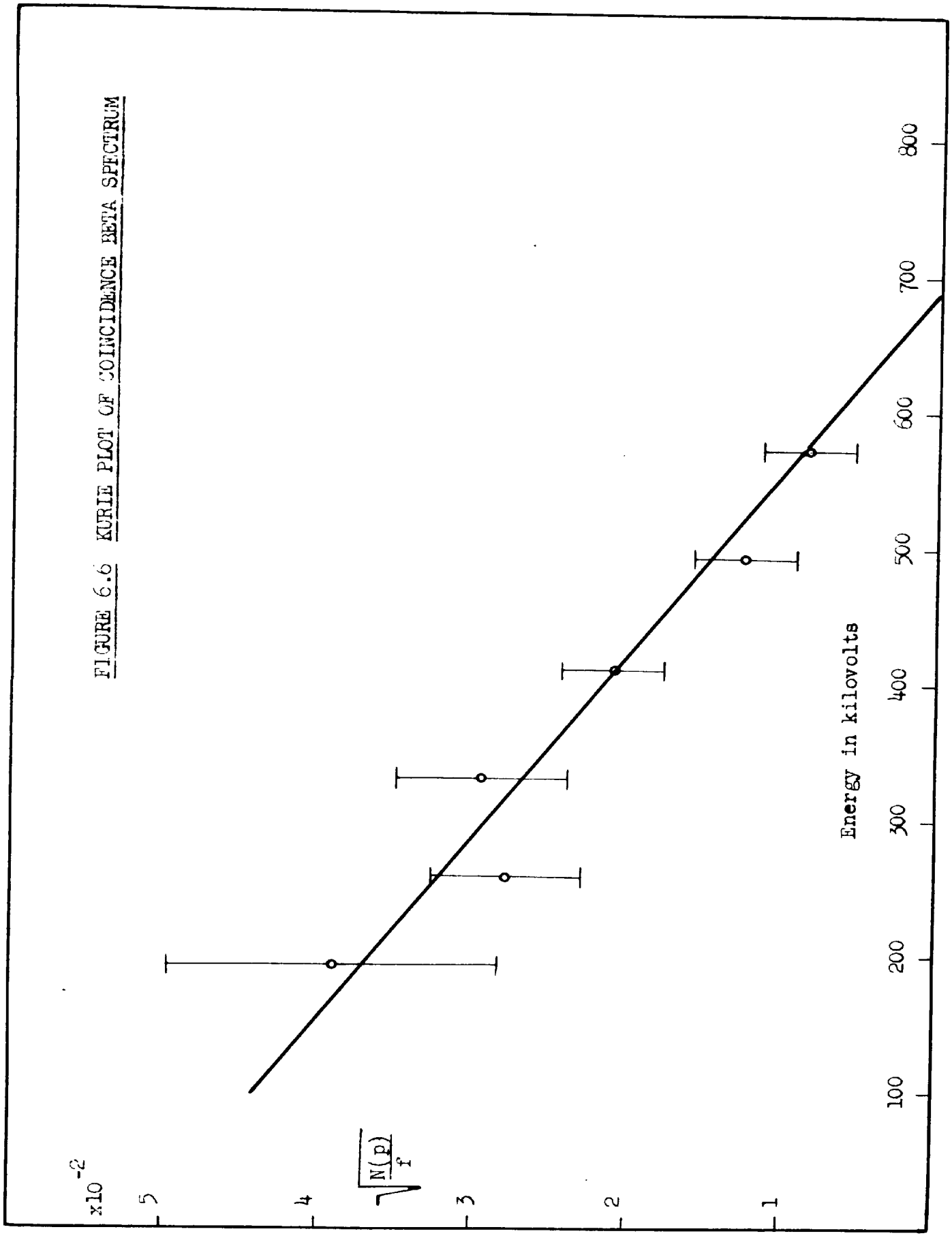


FIGURE 6.6 KURIE PLOT OF COINCIDENCE BETA SPECTRUM

kev (unresolved) gamma and the 244 kev K conversion line.

Coincidences were not found between the unresolved 122+123 kev gamma ray L peaks and the K peak of the 344 line. This is in agreement with Katz and Lu (below), but is in disagreement with Fowler.

These conversion line coincidence results were obtained by noting, in all cases, the differences between peak and background rates for both peaks in the manner previously described.

The results may be summarized as follows:

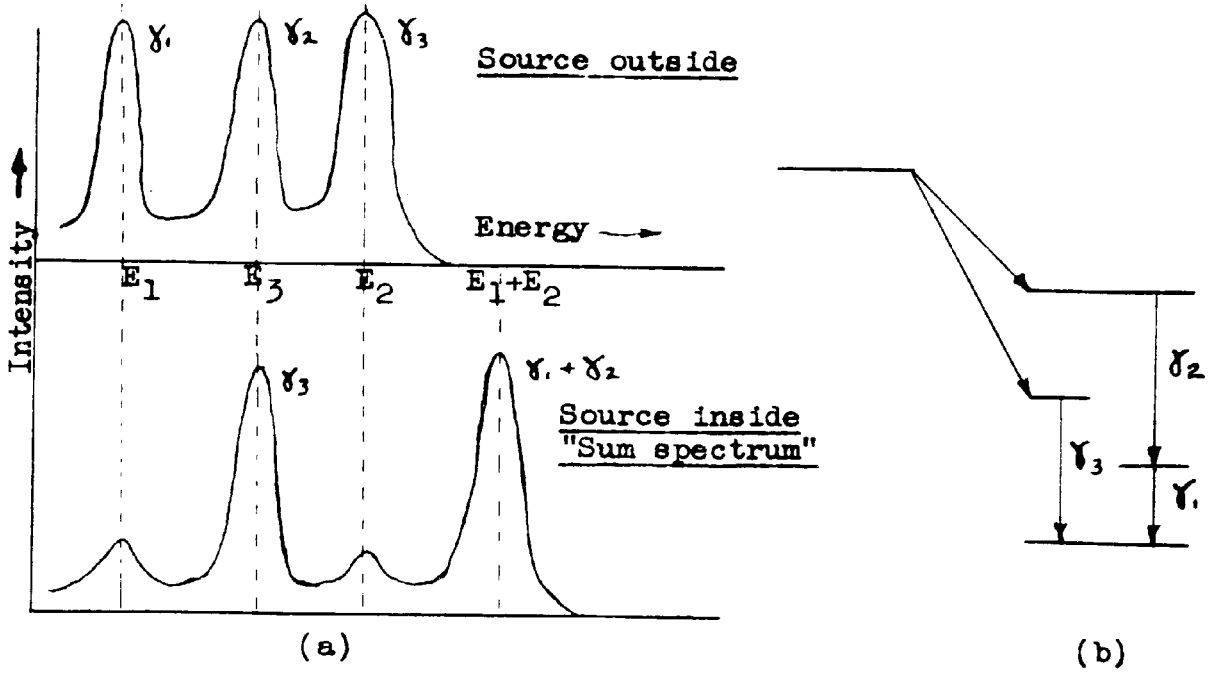
1. The 122 or 123 kev gamma ray is in coincidence with the 244 kev gamma ray.
2. The 344 kev gamma ray is in coincidence with the continuous beta spectrum which has an 0.7 Mev end-point.
3. No other coincidences between the beta spectrum and conversion lines are found.
4. No other coincidences between conversion lines are found.

The Gamma-Gamma Coincidences

The gamma coincidence spectrum of $Eu^{152,154}$ has been run by Mr. Daniel Lu of this university, using the crystal summing technique, which Professor M. L. Wiedenbeck and he developed (73).

The crystal summing technique is a method of doing double, triple, and higher coincidences by means of a scintillation detector and only one channel. The scintillation crystal (thallium activated sodium iodide, in this case) has a small hole drilled into it. The normal gamma spectrum of the source being studied is first run in the usual fashion. Then the source is inserted into the hole in the crystal, and the spectrum is re-run. In this case, the crystal subtends an angle of essentially 4π with respect to the source, and gamma rays which are emitted simultaneously are recorded as peaks whose energy is equal to the sum of the individual energies

of the gamma rays. Thus on comparing the spectra for the source outside the crystal and the source inside, peaks which are in coincidence will have disappeared in the latter case, and peaks represented by their energy sum will have appeared. An illustrative case is shown below.



where (a) is the two spectra, and (b) the hypothetical decay scheme which they represent. Despite the 4π solid angle, the crystal is not one hundred percent efficient, so that residual γ_1 and γ_2 peaks appear in the "source inside" or "sum" spectrum. Experience with the particular crystal used here has shown that when a peak is in coincidence with another of ~100 kev or less, it will completely disappear in the "sum" spectrum. This is because the absorption efficiency of the crystal is about one hundred percent for the lower energies. For higher energies, a small residual peak is noted, as in the case illustrated. Note that in the scheme above, γ_3 at energy E_3, not being coincident with another gamma ray, is unaffected by the change of source position. In the case of K-capture or high internal conversion coefficient, this method detects not only the X-ray when the source is outside the crystal, but coincidences with the X-ray when it is inside the crystal.

Figure 6.7 shows the gamma ray spectrum of $Eu^{152,154}$ with the source outside and inside the crystal. Resolution is ≈ 9% at 700 kev. The ordinate is counts per unit time in arbitrary units, and the abscissa, also in arbitrary units, is pulse height (~ energy). The principle gamma ray peaks and the sum peaks are identified.

Examination of Figure 6.7 yields the following results:

1. Part of the 122 or 123 kev peak (unresolved) is in coincidence with an X-ray.
2. Part of the 122 and 123 kev peak is <u>not</u> in coincidence with an X-ray; hence one is in coincidence with an X-ray, and the other is not, or vice versa.
3. The 244 kev transition appears to be in coincidence with an X-ray. (It disappears completely in the "inside" spectrum, and hence must be in coincidence with something of <u>low</u> energy.)
4. The 244 kev gamma ray is in coincidence with 122 or 123 kev gamma ray.
5. The 344 kev gamma ray is not in coincidence with anything (i.e. it is unchanged in the two spectra).
6. A gamma ray is seen ≈ 410 kev, but if any coincidences with it occur, they are obscured by other peaks.
7. A 720 kev peak occurs in the normal spectrum, but any possible coincidences with lower energy gamma rays are obscured by other peaks in the sum spectrum.
8. A large sum peak appears in the sum spectrum at ≈ 1140 kev. It will be noted that 720 + 122 or 123 + 244 + 47 ≈ 1140, and that 964 + 122 or 123 + 47 is also ≈ 1140. In these sums, 47 kev is the K-X-ray energy of samarium.


FIGURE 6.7 CRYSTAL SUMMING DATA
FOR ^{152,154}Eu
OUTSIDE
INSIDE
PULSE HEIGHT
X-rays
two X-rays
b.B.S
22 B.I 23
10 B.I
122 or 23 + X-ray
22 B.I 23 keV
10 20.8
244 keV
344 keV
410 keV
720 keV
778 keV
964 keV
1085 B.I 16 keV
415 keV
1085 + 122 or 123 + X-ray
415 keV + X-ray
415 keV + 22 or 123 keV

9. A 778 kev line occurs, but it is not in coincidence with anything.

10. A 964 kev line is seen in the normal spectrum. Its partial disappearance in the sum spectrum assures that it is in coincidence with something. The broadening at the low energy base of the 1140 kev sum peak indicates that it is probably in coincidence with an X-ray. (Also see 8 above.)

11. The 1086 and 1116 kev peaks are seen in the normal spectrum, but are unresolved.

12. Sum peaks equal to 1086 plus two X-rays, and to 1086 plus 122 or 123 plus an X-ray are seen.

13. A 1415 peak is seen in the normal spectrum.

14. Sum peaks equal to 1415 plus an X-ray, and to 1415 plus 122 or 123 are seen. No peak equal to 1415 plus 122 or 123 plus an X-ray is seen. Hence 1415 is in coincidence with 122 or 123 or its conversion X-ray, but not with a K-capture X-ray.

Isotopic Assignments

The following isotopic assignments are made by Katz and Lee (71) and shall be adhered to in constructing the decay schemes: the 344, 244, and 122 kev gamma rays belong to the isotope of mass 152; the 1116 and 123 kev gamma rays belong to the isotope of mass 154. This is confirmed by the coincidence measurements made here and by information received privately from E. L. Church (74). Katz's results are based on enriched isotopes, and Church's upon the relative intensity of conversion lines from bombarded and from fission product sources. Church also finds that the 123 line is internally converted in Gadolinium. In addition, Hill and Shepherd (63) find no positrons from the $Eu^{152,154}$ mixture to one part in four thousand.

This information, combined with the data described above, allows decay schemes to be drawn for Eu^{152} and Eu^{154}.

Decay Scheme of Eu^{152}

The decay scheme for Eu^{152} is shown in Figure 6.8. The 122 and 244 kev gamma rays are known to belong to the isotope of mass 152. Hence the 244 kev transition must be in coincidence with the 122 and not the 123 kev transition. Since neither the 122 or the 244 kev gammas are in coincidence with the beta decay, and since they are in coincidence with an X-ray, they are assigned to the K-capture branch of the 152 isotope. The quadruple coincidence of 720, 244, and 122 kev gamma rays with the X-ray place them in the position shown. The energy fit of the 964 kev gamma ray, combined with its coincidence with the 122 or 123 kev gamma ray and an X-ray, fit it into the scheme as drawn. Intensity considerations lead to the relative placement of the 122, 244, and 720 kev lines. The 1086 kev gamma ray's position is demonstrated by the triple coincidences of 1086 plus 122 plus an X-ray, and 1086 plus two X-rays. (The latter comes about from the high conversion rate of the 122 kev transition.)

The beta decay branch is as indicated because the coincidence of the 344 kev gamma ray and the 0.7 Mev end-point beta spectrum has been established, and no other coincidence with the 344 kev gamma ray is seen. The dotted transition between the beta spectrum of end-point 300 kev and the 410 kev gamma ray is tentatively proposed because of the energy fit.

The spectrum of the 9.2 hour Eu^{152} has been included in Figure 6.8 for the sake of completeness (27).

Decay Scheme of Eu^{154}

The decay scheme for Eu^{154} is shown in Figure 6.9. The coincidence of the 123 and 1415 kev gamma rays has been demonstrated. However, no coincidences between the 123 kev gamma ray and either an X-ray or the

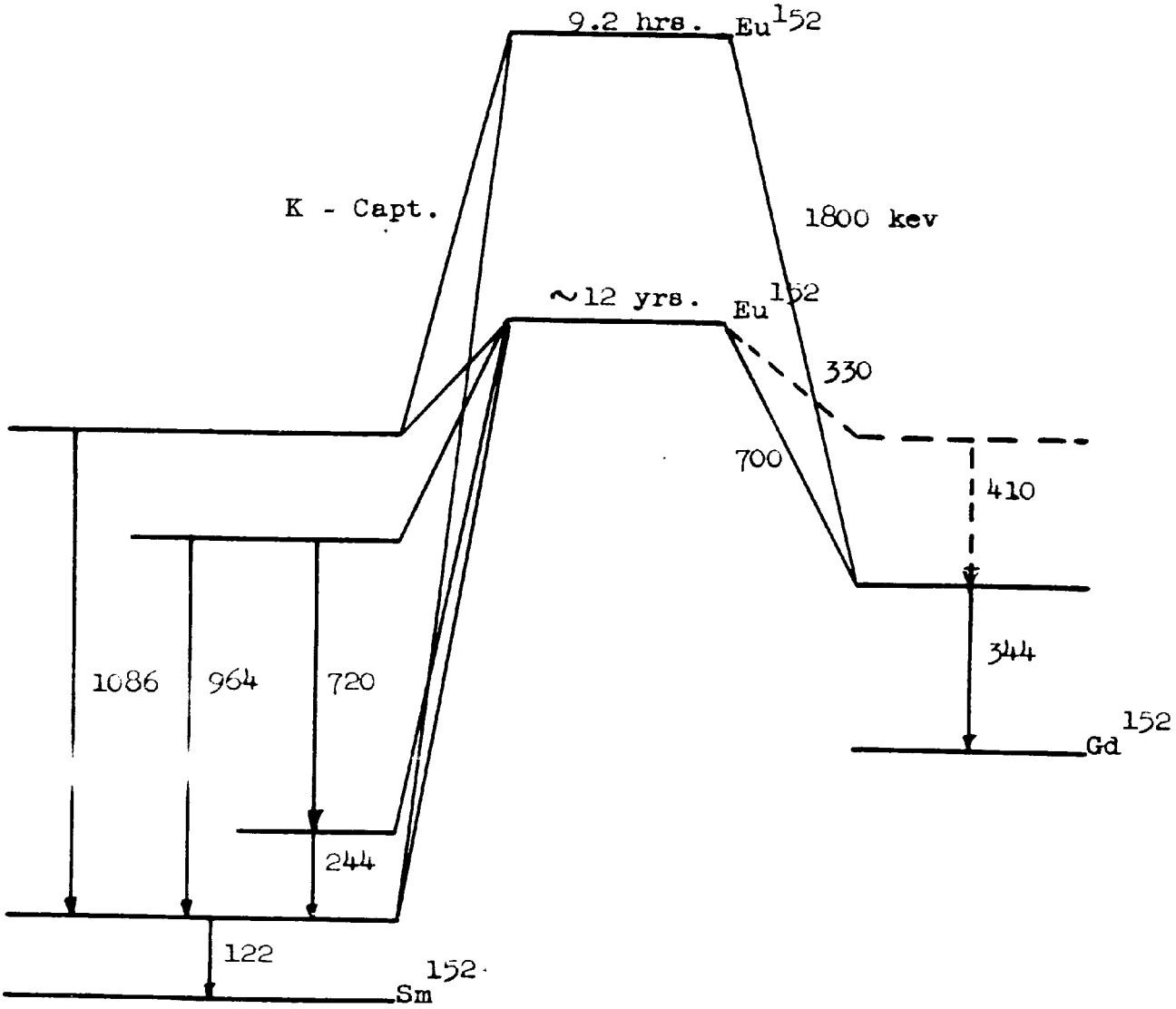


FIGURE 6.8 DECAY SCHEME OF Eu^{152}

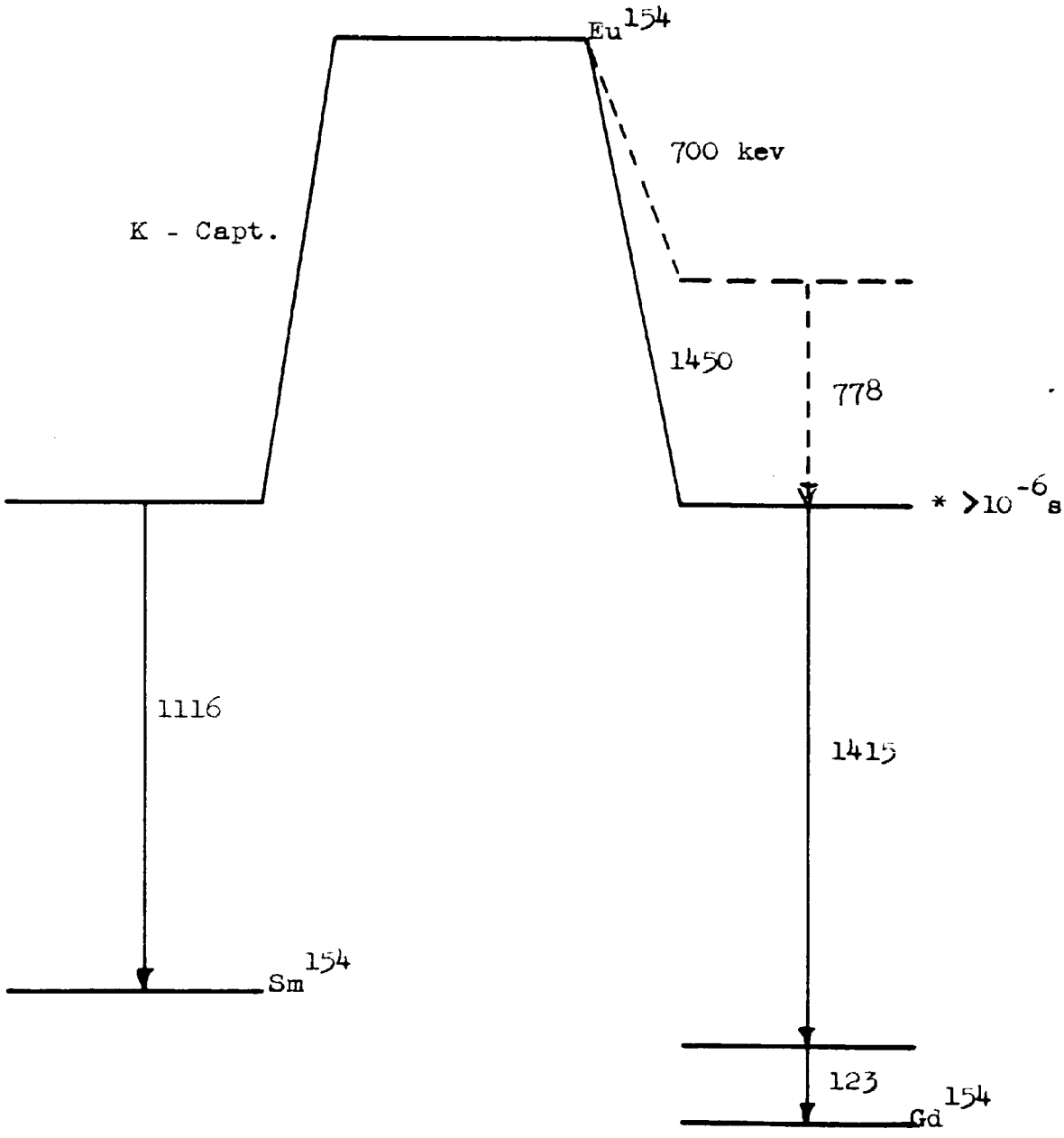


FIGURE 6.9 DECAY SCHEME OF Eu^{154}

continuous beta spectrum exists. Since the 123 kev gamma ray is converted in $Gd^{154}(73)$, the beta decay branch is constructed as shown with the delay indicated. The dotted transition is made purely on the basis of energy fit, and represents the possibility that the beta spectrum of 0.7 Mev end-point actually consists of two spectra of almost identical end-points, one occurring in Eu^{152}, the other in Eu^{154}. Both the 778 and 410 kev gamma transitions are dotted in this work. They have been seen only by Cork, Shull, and ourselves using the same source material, and could be due to contamination caused by other rare earths.

Although no coincidences between the 1116 kev gamma ray and an X-ray are seen, they would be obscured by the large 1140 kev sum peak. This gamma ray is known to belong to the isotope of mass 154 (70) and does not fit into the beta decay branch. Hence it must result from K-capture in Eu^{154}.

Results

The decay schemes of Eu^{152} and Eu^{154} have been demonstrated.

BIBLIOGRAPHY

1. H. Becqueral, Comptes Rendus, 122, 501, 689 (1896).

2. F. O. Giesel, Ann. Phys. Chem., 69, 834 (1899).

3. S. Meyer and E. von Schweidler, Phys. Zeit., 1, 90 (1899).

4. E. Rutherford, Phil. Mag., 5, 177 (1903).

5. N. Bohr, H. A. Kramers, and J. C. Slater, Zeits. Phys., 24, 69 (1924).

6. C. D. Ellis and W. A. Wooster, Proc. Royal Soc., A117, 109 (1927).

7. W. Pauli, Michigan Summer Symposium on Modern Physics. (unpublished notes) (1934).

8. H. R. Crane, Rev. Mod. Phys., 20, 278 (1948).

9. C. W. Sherwin, Phys. Rev., 71, 1299 (1949).

10. F. Reines and C. L. Cowan, jr., Phys. Rev., 92, 830 (1953).

11. E. Fermi, Zeits. f. Phys., 88, 161 (1934).

12. A. H. Spees and C. Zahn, Phys. Rev., 58, 861 (1940).

13. P. A. M. Dirac, Quantum Mechanics, 2nd ed., Oxford University Press, London, 1935.

14. C. D. Anderson, Phys Rev., 41, 405 (1932); 43, 491 (1933).

15. H. Yukawa and S. Sakata, Proc. Phys. Math. Soc. of Japan, 18, 128 (1936).

16. L. Alvarez, Phys. Rev., 53, 213 (1938); 54, 486 (1938).

17. F. Soddy, Nature, 99, 414, 433 (1917).

18. O. Hahn, Chem. Berichte, 54, 1134 (1921).

19. B. V. Kerchatov, I. Kurchatov, L. Myssohski, and L. Roussenow, Comptes Rendus, 200, 1201 (1935).

20. E. Amaldi, O. d'Agostino, E. Fermi, B. Pontecorvo, and E. Segre, Ricerci Scientifica, 61, 581 (1935).

21. E. Rutherford, Phil. Mag., 34, 153 (1917).

22. C. D. Ellis, Proc. Royal Soc., A99, 261 (1921).

23. O von Baeyer, O. Hahn, and L. Meitner, Phys. Zeits., 12, 273 (1911); 13, 264 (1912).

24. E. J. Konopinski and L. M. Langer, Ann. Rev. Nuc. Sci., 2, 261 (1953)

25. F. Kurie, J. Richardson, and H. Paxton, Phys. Rev., 49, 368 (1936).

26. M. Goldhaber and R. D. Hill, Rev. Mod. Phys., 24, 179 (1952).

27. S. M. Hollander, I. Perlman, and G. T. Seaborg, Rev. Mod. Phys., 25, 469 (1953).

28. M. Goldhaber and A. W. Sunyar, Phys. Rev., 83, 906 (1951).

29. M. E. Rose, G. H. Goertzel, and J. Perry, K-Shell Internal Conversion Coefficients; Revised Tables, Oak Ridge National Laboratory Report ORNL-1023 (unpublished).

30. I. M. Blatt and V. F. Weisskopf, Theoretical Nuclear Physics, John Wiley and Sons, New York, 1952, p.618.

31. D. Lu. Private communication.

32. N. Feather, Proc. Camb. Phil. Soc., 34, 599 (1930).

33. J. W. M. DuMond, Rev. Sci. Instr., 18, 626 (1947).

34. R. L. Walker and B. D. McDaniel, Phys. Rev., 74, 315 (1948).

35. N. Feather, J. Kyles, and R. Pringle, Proc. Phys. Soc. London, 61, 466 (1948).

36. C. Fowler, thesis, University of Michigan (1949).

37. R. Shreffler, thesis, University of Michigan (1949).

38. R. Katz, R. D. Hill, and M. Goldhaber, Phys. Rev., 78, 9 (1950).

39. M. K. Wiedenbeck and D. C. Lu.- Private communication.

40. G. Breit and I. I. Rabi , Phys. Rev., 38, 2082 (1931).

41. D. R. Hamilton, Phys. Rev., 58, 122 (1940).

42. H. Frauenfelder, Ann. Rev. Nuc. Sci., 2, 129 (1953).

43. G. A. Bradley, thesis, University of Michigan (1952).

44. D. R. Hutchinson, thesis, University of Michigan (1953).

45. R. L. Garwin, Rev. Sci. Instr., 21, 569 (1950).

46. O. Klemperer, Lond. Phil. Mag., 20, 545 (1935).

47. M. Deutsch, L. G. Elliot, and R. D. Evans, Rev. Sci. Instr., 15, 178 (1944).

48. K. Siegbahn, Phil. Mag., 37, 162 (1946).

49. Ea A. Quade and D. Halliday, Rev. Sci. Instr., 19, 234 (1948).

50. E. N. Jensen, L. J. Laslett, and W. W. Pratt, Phys. Rev., 75, 450; 76, 430 (1949).

51. J. M. Keller, E. Koenigsberg, and A. Pashin, Rev. Sci. Instr., 21, 713 (1950).

52. W. W. Pratt, F. I. Boley, and R. T. Nibhols, Rev. Sci. Instr., 22, 92 (1951).

53. L. M. Langer and R. D. Moffat, Phys: Rev., 78, 74 (1950).

54. M. H. MacGregor, thesis, University of Michigan (1953).

55. L. J. Rainwater and C. S. Wu, Nucleonics, 1, 60 (1947).

56. R. E. Bell and R. L. Graham, Phys. Rev., 86, 212 (1952).

57. L. J. Shavtvalov, J. Exp. Theor. Phys. U.S.S.R., 21, 1123 (1950).

58. J. M. Cork, R. Shreffler, and C. Fowler, Phys. Rev., 72, 1200 (1947).

59. K. Y. Chu and M. K. Wiedenbeck, Phys. Rev., 75, 226 (1949).

60. C. Y. Fan, Phys. Rev., 87, 252 (1952).

61. F. K. McCowan, Phys. Rev., 93, 471 (1954).

62. A. W. Tyler, Phys. Rev., 56, 125 (1939).

63. J. M. Hill and L. R. Shepherd, Proc. Phys. Soc. (London) 63A, 126 (1950).

64. R. J. Hayden, J. H. Reynolds, and M. G. Inghram, Phys. Rev., 75, 1500 (1949).

65. D. G. Karraker, R. J. Hayden, and M. G. Inghram, Phys. Rev., 87, 901 (1952).

66. E. E. Lockett and R. H. Thomas, Nucleonics, 11, no.3, p.14 (1953).

67. J. M. Cork, R. G. Shreffler, and C. M. Fowler, Phys. Rev., 72, 1209 (1947); 73, 78L (1948)

68. F. B. Shull, Phys. Rev., 74, 917 (1948).

69. J. M. Cork, H. B. Keller, W. C. Rutledge, and A. E. Stoddard, Phys. Rev., 77, 848 (1950)

70. H. B. Keller and J. M. Cork, Phys. Rev., 84, 1019 (1951).

71. R. Katz and M. R. Lee, Phys. Rev., 85, 1038 (1952).

72. S. A. Moszkowski, Phys. Rev., 82, 35 (1951).

73. M. K. Wiedenbeck and D. C. Lu.-Private communication to appear as a letter in Physical Review of April 15, 1954.

74. E. L. Church, Argonne National Laboratories.-Private communication.

75. E. J. Konopinski, Rev. Mod. Phys., 15, 209 (1943).